Title

Immune Perturbations of Macrophages, Monocytes, and Myeloid Progenitors with Chronic Alcohol Drinking

Author

Lewis, Sloan

Publication Date

2021

UNIVERSITY OF CALIFORNIA,
IRVINE

Immune Perturbations of Macrophages, Monocytes, and Myeloid Progenitors with Chronic Alcohol Drinking

DISSERTATION

submitted in partial satisfaction of the requirements
for the degree of

DOCTOR OF PHILOSOPHY

In Biological Sciences

by

Sloan Alexandra Lewis

Dissertation Committee:
Professor Ilhem Messaoudi, Chair
Professor Melissa Lodoen
Professor Andrea J. Tenner
Professor Marcelo Wood
Assistant Professor Kai Kessenbrock

2021

DEDICATION

To my parents,
Scott and Tracy
who instilled in me the belief that my dreams were possible,
and worked every day to make sure this was true

"Celebrate what you've accomplished, but raise the bar a little higher every time you succeed"

-Mia Hamm

TABLE OF CONTENTS

LIST OF FIGURES

ACKNOWLEDGEMENTS

There are many people who deserve recognition for the successful completion of this dissertation. Firstly, a big thanks to my PhD advisor and mentor for the last four years, Dr. Ilhem Messaoudi. You pushed me to be a better scientist and taught me many lessons about being a mentor and leader. To the past and present members of the Messaoudi Lab, thank you for being a fun and motivating group to be around. Andrea, thank you for your support and guidance when I was beginning my PhD journey and providing an example of the kind of scientist I wanted to become. Brianna, thank you for being a constant source of help and positivity over the years and for your patient and understanding presence for many stressful experiments. Suhas, thank you for patiently teaching me much of what I know; your dedication and excitement for science motivated me every day to push myself physically and mentally further to do the best science I could. Nicholas, my lab brother, I can't imagine doing the PhD journey without you with me at every step, and I will miss your constant and sometimes annoyingly insightful questions and comments that have made me a better scientist.

To my committee members, Dr. Melissa Lodoen, Dr. Andrea Tenner, Dr. Marcelo Wood, and Dr. Kai Kessenbrock, some of you watched me through this whole journey and some were more recent additions, but I am grateful to all of you for the support and guidance on this project. This work would not have been possible without some amazing collaborators. Dr. Kathy Grant and her team at the Oregon National Primate Research Center made collecting samples an easy process and helped me understand the importance of our model. Dr. Helen Goodridge who gave guidance on experiment design and protocols for

Chapter 3. Dr. Liz Kovacs who was a co-mentor for my F31 and took me under her wing and made me feel welcome at alcohol research meetings.

To all of the friends I have made at UCI, Bridget, Morgan, Andrew, and everyone else who has been there for me along the way, thank you for making this experience fun and for understanding me in ways only other graduate students could. I hope we stay in touch as we move forward through our careers. To my friends who have stood by me for many years, Amanda, George, Amy, Shannon, David, and many others, thank you for your loyalty and for our past and future adventures. To Steve, my best friend and partner in life, your unwavering confidence in me pushes me to be the best version of myself and your love sustains me. And to our pups, Scruffy and Sunny, thank you for the cuddles, kisses, and wagging tails that make any day better.

None of this would have been possible without the support of my entire family. My siblings, Trevor and Piper, are the best lifelong friends anyone could ask for and make me laugh more than anyone else. My grandparents, Susan, John, and Marlene, have built me up for my entire life and I strive to continue to make them proud. Finally, to my parents Scott and Tracy, thank you for everything you have done for me. None of this would have been possible without you and I am so grateful to have you both in my life.

CURRICULUM VITAE

Sloan Alexandra Lewis
Department of Molecular Biology and Biochemistry
Institute for Immunology
University of California, Irvine

EDUCATION

University of California, Irvine 2017-2021
Irvine, CA
Ph.D. Biological Sciences
Advisor: Dr. Ilhem Messaoudi

University of California, Santa Barbara 2012-2016
Santa Barbara, CA
B.S. Biochemistry and Molecular Biology

RESEARCH EXPERIENCE

Ph.D. Research, Messaoudi Lab 2017-2021
University of California, Irvine
- Extracellular vesicle-bound miRNA as biomarkers of alcohol consumption
- The effects of chronic alcohol consumption on circulating and tissue resident innate immune cells
- Alcohol's effect on myelopoiesis and bone marrow progenitors
- Impact of alcohol use on the host immune response to SARS-CoV-2 infection
- Aging and peripheral immune responses during severe COVID-19

Undergraduate Research, Rothman Lab 2014-2016
University of California, Santa Barbara
- Fluorescent Sensor Design using CRISPR/Cas9 Genome Editing

HONORS AND AWARDS

Society for Leukocyte Biology Presidential Award	2021
Achievement Rewards for College Scientists (ARCS) Scholar	2019-2021
UCI Immunology Fair 2nd place Oral Presentation	December 2020
Ruth L. Kirschstein National Research Service Award- F31	2020-2022
Robert Warner Award for Outstanding Achievement	May 2020
UC Irvine NIH Immunology Training Grant (T32) Award	2019-2020
Society for Leukocyte Biology Travel Award	2019
Gordon Research Conference Travel Award	2019
UCSB University Honors Program	2012-2016
UCSB Dean's Honors	2013
Major Distinction: Molecular, Cellular, Developmental Biology	2016
Undergraduate Research Grant Award	2015-2016
Team Captain, UCSB Rowing	2015-2016

MANUSCRIPTS (UNPUBLISHED)

Lewis SA, et al. "The effects of chronic alcohol drinking on host immune response to SARS-CoV-2 in the lung" (*In preparation*).

Lewis SA, et al. "Chronic alcohol drinking disrupts monocyte production and function from progenitors in the bone marrow niche in non-human primates" (*In preparation*).

Lewis SA, Doratt B, Sureshchandra S, Pan T, Gonzalez SW, Shen W, Grant KA, Messaoudi I, "Profiling of extracellular vesicle-bound miRNA to identify candidate biomarkers of chronic alcohol drinking in non-human primates" (*Accepted ACER 12/10/2021*).

Lewis SA, Doratt B, Sureshchandra S, Jankeel A, Newman N, Shen W, Grant KA, Messaoudi I, "Ethanol Drinking Induces Non-Specific Inflammation and Functional Defects in Alveolar Macrophages" (*Revisions submitted 10/25/2021*).

Sureshchandra S and **Lewis SA**, Doratt B, Jankeel A, Ibraim IC, Messaoudi I, "Single cell profiling of T and B cell repertoires following SARS-CoV-2 mRNA vaccine" (*Accepted JCI Insight*).

PUBLICATIONS

Lewis SA, Sureshchandra S, Zulu MZ, Doratt B, Jankeel A, Ibraim IC, Pinski AN, Rhoades NS, Curtis M, Jiang X, Tifrea D, Zaldivar F, Shen W, Edwards RA, Chow D, Cooper D, Amin A, Messaoudi I. "Differential dynamics of peripheral immune responses to acute SARS-CoV-2 infection in older adults". *Nature Aging*. 2021 Oct; DO 10.1038/s43587-021-00127-2.

Lewis SA, Sureshchandra S, Doratt B, Jimenez VA, Stull C, Grant KA, Messaoudi I. "Transcriptional, Epigenetic, and Functional Reprogramming of Monocytes From Non-Human Primates Following Chronic Alcohol Drinking". *Front Immunol*. 2021 Aug; PMID: 34489976.

McMahan RH, Afshar M, Amedee AM, Bishehsari F, Carr RM, Coleman LG, Herrnreiter CJ, **Lewis SA**, Mandrekar P, McCullough RL, Morris NL, Vasiliou V, Wang HJ, Yeligar SM, Choudhry MA, Kovacs EJ. "Summary of the 2019 alcohol and immunology research interest group (AIRIG) meeting: Alcohol-mediated mechanisms of multiple organ injury". *Alcohol*. 2020 Sep; PMID: 32353591.

Barr T and **Lewis SA**, Sureshchandra S, Doratt B, Grant KA, Messaoudi I, "Chronic ethanol consumption alters lamina propria leukocyte response to stimulation in a region-dependent manner". *FASEB J*. 2019 Jun; PMID: 30897342.

SKILLS

Techniques	Bioinformatics
Cell culture and stimulation	R
Multi-parameter Flow Cytometry	UNIX
Luminex Assays	RNA-Seq Analysis
ELISA	ATAC-Seq Analysis
Flow Sorting	ChIP-Seq Analysis
ATAC-Seq/scATAC-Seq	scRNA-Seq Analysis
ChIP-Seq	Data Integration Methods
RNA-Seq/scRNA-Seq	scATAC-Seq Analysis
BSL3 certified	

RESEARCH PRESENTATIONS

Lewis SA, (July 2021). scRNA-Seq and functional profiling of alveolar macrophages with alcohol use. Oral presentation for the Presidential Award at the virtual Society for Leukocyte Biology annual meeting.

Lewis SA, (April 2021). Impact of chronic alcohol consumption on the lung immune landscape with implications for susceptibility to viral infections. Oral presentation for the annual Alcohol and Immunology Research Interest Group (AIRIG) online.

Lewis SA, Sureshchandra S, Messaoudi I. (April 2021). Integrative scRNA-Seq, epigenetic, and functional profiling of the myeloid compartment in non-human primates following chronic alcohol consumption. Poster presentation at the online Cold Spring Harbor Laboratory Meeting on Systems Immunology.

Lewis SA, Gong Y, Sureshchandra S, Kessenbrock K, Shen W, Messaoudi I. (September 2020). Mapping Myeloid Cell Fates Following In Vivo Chronic Alcohol Consumption. Poster presentation at the online 2020 Center for Multiscale Cell Fate Research Annual Poster Competition.

Lewis SA, Sureshchandra S, Doratt B, Stull C, Grant KA, Messaoudi I. (November 2019). Impact of Chronic Alcohol Consumption on the Functional and Epigenetic Landscapes of Monocytes and their progenitors. Oral presentation given at the Alcohol and Immunology Research Interest Group (AIRIG) and poster presented at the Society for Leukocyte Biology Meeting in Boston, Massachusetts.

Lewis SA, Sureshchandra S, Stull C, Grant KA, Messaoudi I. (June 2019). Transcriptional profiling of monocytes to elucidate mechanisms behind heightened pro-inflammatory response to LPS stimulation with chronic heavy alcohol consumption. Poster presented at Immunology LA in Los Angeles, CA.

Lewis SA, Barr T, Sureshchandra S, Doratt B, Grant K A, Messaoudi I. (March 2019). Chronic alcohol consumption alters lamina propria leukocyte response to

stimulation in a region-dependent manner. Poster presented at Gordon Research Conference: Alcohol-induced end organ diseases in Ventura, CA.

Lewis SA, Rothman J. (June 2016). Fluorescent sensor design using CRISPR/Cas9 genome editing. Poster presented at the undergraduate research symposium at the University of California, Santa Barbara.

CERTIFICATE COURSES

Communication Skills for Academics	Spring 2020
Industry Insights for STEM Scientists	Spring 2021

SOCIETY MEMBERSHIPS

American Association of Immunologists
Society for Leukocyte Biology

TEACHING/LEADERSHIP EXPERIENCE

Student Seminar Leader, UCI 2020-2021
Preliminary Exam Mentor, UCI Spring 2019, 2020
Teaching Assistant, UCI Fall 2018
- Immunology with hematology, M121
- Microbiology Lab, M118L

Undergraduate/Graduate Student Mentor, UCI 2018-2021
- Brianna Doratt (Undergrad/Masters, 2018-2021)
- Sungjun Beck (Rotation Student, 2020)
- Alexander Moshensky (Rotation Student, 2021)

WORK EXPERIENCE

Bay Area Women's Sport Initiative
Athlete Team Leader 2016-2017

ABSTRACT OF THE DISSERTATION

Immune Perturbations of Macrophages, Monocytes, and Myeloid Progenitors with Chronic Alcohol Drinking

by

Sloan Alexandra Lewis

Doctor of Philosophy in Biological Sciences

University of California, Irvine, 2021

Professor Ilhem Messaoudi, Chair

Chronic alcohol drinking adversely affects human health and is a significant risk factor for numerous conditions including cardiac and liver disease, cancer, and sepsis. Furthermore, patients who consume alcohol chronically have increased susceptibility to viral and bacterial infections, suggesting compromised immune function. Studies to date have shown a disproportionate effect of alcohol on innate immune cells, notably monocytes and tissue resident macrophages, but the mechanisms by which chronic alcohol consumption leads to immune cell dysfunction remains poorly understood. Moreover, whether alcohol and its metabolic products are acting on immune cells in the periphery or on their progenitor cells in the bone marrow has yet to be investigated. This work aims to address the broad hypothesis that **chronic alcohol drinking perturbs the epigenetic, transcriptomic, and functional landscapes of macrophages, monocytes, and their progenitor cells in the bone marrow**. To that end, we utilized a non-human primate model of chronic alcohol self-administration, which is both physiologically relevant and accurately recapitulates human drinking behavior. After 12 months of daily alcohol drinking, we profiled three major cell populations from these animals: tissue-resident macrophages from

the alveolar space, monocytes from the blood, and progenitor cells from the bone marrow. For each of these populations, we integrated large scale epigenomic and transcriptional data with cell-type relevant functional assays to explore alcohol-induced perturbations of immune function and the mechanisms behind them.

In alveolar macrophages, we show increased baseline activation transcriptionally and epigenetically with alcohol, poising the cells towards heightened inflammatory responses to lipopolysaccharide (LPS) and respiratory syncytial virus (RSV). This was accompanied by increased ROS production but decreased ability to phagocytose bacteria. scRNA-Seq revealed oxidative stress and oxidative phosphorylation signatures, which was coupled with increased mitochondrial activation. These findings show reprogramming of the alveolar macrophages towards heightened inflammation and stress coupled with reduced functional capabilities with alcohol, which could lead to reduced ability of these cells to identify and clear infections. This may explain the increased susceptibility of patients who chronically consume alcohol to respiratory pathogens.

Frequency of blood monocytes were increased in circulation with alcohol and showed a similar phenotype of hyper-inflammatory protein response to LPS. This was also complemented epigenetically with increased chromatin accessibility of loci encoding cytokine response genes at baseline state, suggesting alcohol is priming these cells for the inflammatory response. Moreover, similarly to alveolar macrophages, scRNA-Seq of monocytes revealed shifts towards oxidative stress and *HIF1A* induction indicating a broad impact of alcohol and its metabolites on circulating and tissue resident cells. As monocytes are short-lived cells in the blood, we determined that this hyper-inflammatory phenotype

persisted after a one-month abstinence period from alcohol suggesting bone marrow progenitor involvement.

Indeed, CD14+ cells in the bone marrow broadly expressed markers of stress and inflammation with alcohol. Assessment of the function of CD34+ progenitors suggested skewing of colony differentiation towards granulocyte/monocyte colonies and increased production of hyper-inflammatory monocytes in culture. scRNA-Seq of the CD34+ cells showed increased inflammatory markers in myeloid lineage subsets and broad signatures of oxidative stress with alcohol. Taken together, these data suggest an impact of alcohol on myeloid cell production and function at multiple levels: in the bone marrow, in circulation, and in the lung.

INTRODUCTION

The development, maintenance and lifetime functioning of the immune system to combat invading pathogens is a complex and critical process for life. Immunity has often been thought of as a weighted scale sitting in perfect balance. Tipping too far in one direction can lead to hyper-inflammation and often autoimmunity where the body begins to recognize and respond to its own cells as foreign. Conversely, tipping in the opposite direction can lead to tolerance or the inability to respond efficiently to microbial infection. With that in mind, there are a number of factors, both genetic and environmental, that shift this delicate balance one way or another. This body of work focuses on an environmental factor, chronic alcohol drinking, and its impact of immunity.

Long-term, heavy alcohol drinking has negative consequences on human health and immunity.

Producing and consuming alcoholic beverages is a historic tradition extending across cultures and continents that continues today. Alcohol drinking is widespread in the United States where 85.6% of people over 18 years old report having drank alcohol at some point in their lifetimes (1). Moreover, 25.8% and 6.3% of people over the age of 18 engage in binge drinking (male, >5 drinks; female, >4 drinks in 2 hours) and heavy alcohol use (male, >14 drinks; female, >7 drinks per week), respectively (1). These types of excessive and risky drinking behaviors contribute to the over 95,000 alcohol-related deaths annually in the United States alone, making it the third-leading preventable cause of death (2). While some studies have shown that moderate drinking has positive effects on health and immunity (3, 4), long term heavy drinking is known to have severe consequences on the human body. These include increased incidence of cardiac disease (5, 6), certain types of cancer (7-10),

liver cirrhosis (11), sepsis (12) as well as detrimental effects on anti-microbial responses (4, 13). Specifically, heavy alcohol drinking has been linked to higher susceptibility to bacterial and viral infections including pneumonia and tuberculosis (14, 15), hepatitis C virus, and HIV (16, 17). This impaired pathogen response coupled with reduced wound healing and tissue recovery (18, 19) strongly suggest immune dysfunction with alcohol drinking.

There are two major branches of the immune system: innate and adaptive (20). The innate immune cells including granulocytes, monocytes, and macrophages are the first responders to a new pathogen (20). These cells recognize pathogens, send out signals to initiate the adaptive response, resolve inflammation, and heal tissues. Once the response is initiated, the antigen-specific responses generated by cells of the adaptive arm (T and B lymphocytes) is activated to clear the pathogen and results in immunological memory for future infections (20). Theories have emerged in recent years suggesting the concept of trained immunity, where innate immune cells are also able to have a type of memory response to a secondary infection (21-23).

The body of work on alcohol and immunity has pointed to a disproportionate effect of alcohol on innate immune cells, specifically monocytes and macrophages (13, 24, 25). The balance of inflammatory and resolving functions of these cells is critically important for both host defense and tissue homeostasis. However, a major limitation in studying the effects of alcohol drinking on immunity has been the lack of an animal model that accurately models human physiology and drinking behavior.

Recapitulating human drinking behavior using non-human primates.

In vitro studies with human monocytes or cell lines, and in vivo rodent models of acute or chronic drinking have provided valuable insights, but they have significant

limitations. While some human studies have used monocytes from individuals engaged in chronic alcohol consumption, most studies use samples from healthy donors or transformed human macrophage cell lines treated in vitro with concentrated doses of ethanol. Alternatively, rodent models are complicated by forced gavage feeding or access to liquid only ethanol diets that introduce stress and other factors into the experiment. Moreover, these studies are often short-term and utilize high doses to induce liver damage (26-32). Therefore, they do not fully capture the chronicity of human alcohol drinking and add organ damage as a confounding factor. Ultimately, studying the effects of alcohol drinking on human patients would be the gold standard, however, many factors make this challenging. Most individuals with alcohol use disorders also engage in chronic smoking, use of recreational or illicit drugs, exhibit nutritional deficiencies, and have significant organ damage when they are recruited into studies (33). These factors make it challenging to identify the effects of alcohol drinking versus those of these other harmful activities on immune function. Additionally, it is extremely difficult to discern how much alcohol is consumed as self-reporting is unreliable. Therefore, there is a pressing need to perform immunological studies in animal models that accurately mirror the behavioral and metabolic complexity of human drinking. Nonhuman primates (NHPs) are a critically important animal model of alcohol drinking due to: 1) genetic and physiological similarity to humans; 2) propensity to consume alcohol voluntarily (34, 35); 3) similarity of alcohol absorption and metabolism to humans (36); and 4) real-time recording of alcohol intake under controlled conditions while avoiding complications of gastric tube insertion or gavage feeding (37). The use of NHPs allows for the investigation of chronic alcohol drinking on immunity in an

outbred species while maintaining proper control over housing conditions, nutritional status and precise recording of ethanol intake.

Using this innovative model, we can begin to answer some questions that have previously remained elusive:

1. How does alcohol drinking alter the function of monocytes and macrophages that contributes to increased infection susceptibility?
2. What are the transcriptomic and epigenomic mechanisms behind these functional changes?
3. Are the alcohol-mediated defects in monocytes occurring in the periphery or on monocyte progenitor cells in the bone marrow?

The following dissertation aims to answer these questions and contribute to basic and translational research into alcohol drinking and human health.

Alcohol drinking disrupts the function of tissue resident macrophages in the lung.

Tissue-resident macrophages are specialized populations of cells that are either embryonically derived or re-populated from circulating monocytes (38-41). They have unique epigenetic, transcriptional, and functional programs that make them efficient in their environments (42). It is well appreciated that disruptions to the functioning of these cells can have devastating consequences on host defense (40, 41, 43-45). A number of the bacterial and viral infections where alcohol drinking is linked to increased susceptibility are respiratory including respiratory syncytial virus (RSV) (46, 47), community-acquired pneumonia (15, 48, 49), and tuberculosis (50, 51). Alcohol drinking is also a risk factor for acute respiratory distress syndrome (ARDS) (52, 53) and can increase the risk of admission

to intensive care unit (ICU) in patients with pneumonia (15, 46, 52, 54). These observations make the dominant lung immune cell and resident macrophage population in the alveolar space, the alveolar macrophage, of significant interest. Perturbations of alveolar macrophages either directly or indirectly with alcohol drinking could affect pathogen recognition, response, and recovery in the lung. In fact, many studies have attempted to understand how alcohol and its metabolites may be affecting the functional and metabolic properties of alveolar macrophages (55). These studies have broadly pointed to alcohol-induced oxidative stress contributing to reduced phagocytic function (55-59). Whether this happens with alcohol drinking in non-human primates and how it could compromise defense responses to pathogens in the lung have yet to be determined. Mechanistically, the alcohol-induced changes to the transcriptional and epigenetic landscapes of these cells also remains elusive.

Alcohol drinking disrupts the function of blood monocytes.

Populations of resident macrophages, especially under conditions of inflammation, infection, or injury, are re-populated by circulating blood monocytes. These monocytes circulate throughout the body and search for signs of infection or inflammation, until they are recruited to a tissue, extravasate in, and differentiate into macrophages (60, 61). Monocytes themselves can respond to pathogens in the blood or elsewhere but phagocytic and other effector functions are increased in macrophages (60, 62). Arguably, as alcohol is ingested and absorbed into the bloodstream in the stomach and upper intestine, cells in circulation would see alcohol and its metabolic products well before it made it to tissues (63, 64). Additionally, as blood is easier to obtain than other tissue samples, monocytes are easier to study in humans. Accordingly, the effects of alcohol drinking on monocyte populations

have been investigated by many laboratories. A majority of the findings suggest that there is a discrepancy between acute and chronic alcohol exposure on monocyte inflammatory responses to bacterial agonists (13). While acute exposure leads to a dampening of inflammatory responses (65-69), chronic exposure leads to exacerbated responses (66, 70, 71). The epigenetic and transcriptomic mechanisms behind heightened inflammatory responses with chronic alcohol drinking in a relevant model have yet to be elucidated.

Tracing alcohol-induced changes in blood monocytes to their bone marrow progenitors.

The clear impacts of alcohol drinking on monocyte epigenetics and function accompanied by the fact that monocytes are short-lived cells in the blood point to an effect of alcohol on monocyte progenitors. Monocytes are constantly repopulated from bone marrow progenitor cells (72-74). The bone marrow compartment is also a site of monocyte storage from which they can be released for emergency myelopoiesis (75). The effects of alcohol drinking on myelopoiesis have not been well-studied thus far, however there are known disruptions to hematopoiesis noted in patients with alcohol use disorders (76-78). These along with studies in rodents showing altered granulopoiesis in response to bacterial infection with alcohol (79, 80) suggest the effects of alcohol drinking may extend to the bone marrow niche. Alcohol-induced effects on bone marrow progenitors that lead to altered differentiation states and production of functionally and epigenetically altered monocytes is a critically needed research area.

Goals and scope of the dissertation

Broadly, this work aims to address the effects of long-term alcohol drinking on macrophages, monocytes, and bone marrow progenitors in NHP. The function of these cell

populations under homeostatic and defense response conditions is critically important to the maintenance of balance in the immune system. Further, alcohol-induced reprogramming of these populations can have drastic effects on their function. This dissertation suggests a connection between these reprogramming events and host defense, with the hopeful goal of identifying mechanisms by which alcohol drinking leads to compromised immunity in patients.

CHAPTER 1:

Ethanol Drinking Induces Non-Specific Inflammation and Functional Defects in Alveolar Macrophages

Sloan A. Lewis[1,2], Brianna Doratt[1,2], Suhas Sureshchandra[1,2], Allen Jankeel[1], Natali Newman[3], Weining Shen[4], Kathleen A. Grant[3], Ilhem Messaoudi[1, 2, 5]

[1] Department of Molecular Biology and Biochemistry, University of California, Irvine, CA, USA
[2] Institute for Immunology, University of California, Irvine, CA, USA
[3] Oregon National Primate Research Center, Oregon Health and Science University, Beaverton, OR, USA
[4] Department of Statistics, University of California, Irvine CA, USA
[5] Center for Virus Research, University of California, Irvine, CA, USA

This manuscript was resubmitted after revisions to the American Journal of Respiratory Cell and Molecular Biology on 10/25/21

ABSTRACT

Chronic alcohol drinking is associated with increased susceptibility to viral and bacterial respiratory pathogens. In this study, we utilize a rhesus macaque model of voluntary ethanol self-administration to study the effects of long-term alcohol drinking on the lung. We report a heightened activation and inflammatory state in alveolar macrophages (AM) obtained from ethanol (EtOH) drinking animals that is accompanied by increased chromatin accessibility in intergenic regions that regulate inflammatory genes and contain binding motifs for transcription factors AP-1, IRF8, and NFKB p-65. In line with these transcriptional and epigenetic changes at basal state, AM from ethanol drinking animals generate elevated inflammatory mediator responses to LPS and respiratory syncytial virus (RSV). However, transcriptional analysis revealed an inefficient induction of IFN-γ and IFN-β signaling pathway genes with EtOH in response to RSV, suggesting disruption in anti-microbial defenses. Correspondingly, AM from EtOH drinking animals exhibited increased cytosolic reactive oxygen species (ROS) and decreased ability to phagocytose bacteria. Moreover, bulk RNA and ATAC sequencing data revealed reduced expression and chromatin accessibility of loci associated with tissue repair and maintenance with chronic EtOH drinking. Similarly, analysis of scRNA-Seq data revealed shifts in cell states from tissue maintenance to pathogen response with EtOH that may be mediated by altered differentiation trajectories. Finally, chronic EtOH drinking was associated with increased oxidative stress and metabolic shifts towards oxidative phosphorylation coupled with increased activated mitochondria. Collectively, these data provide novel insight into mechanisms by which chronic EtOH drinking increases susceptibility to infection in patients with alcohol use disorders.

INTRODUCTION

Alcohol use is prevalent in the United States with over 50% of people 18 years or older reporting alcohol consumption (National Survey on Drug Use and Health 2019). Amongst these individuals, 25% report binge drinking and 6.3% report heavy drinking. Long term heavy drinking is associated with numerous adverse health outcomes, including increased incidence of cardiac disease (5, 6), certain types of cancer (7-10), liver cirrhosis (11), and sepsis (12), making it the third leading preventable cause of death in the United States (2). Of importance, chronic heavy alcohol drinking compromises lung health and immunity leading to increased susceptibility to both bacterial and viral pulmonary infections (46), notably respiratory syncytial virus (RSV), (47) community-acquired pneumonia (15, 48, 49), and tuberculosis (50, 51). Alcohol use is also a risk factor for acute respiratory distress syndrome (ARDS) (52, 53) and can increase the risk of admission to intensive care unit (ICU) in patients with pneumonia (15, 46, 52, 54). While the mechanisms underlying increased vulnerability and severity of pulmonary infections with chronic alcohol consumption have yet to be fully elucidated, studies using rodent models as well as *in vitro* cell cultures have identified defects in the beating of the ciliated epithelium (81-83) as well as impaired epithelial barrier function (84, 85) as major risk factors. Moreover, these studies report significant defects in both the innate and adaptive branches of the immune system (46), especially within alveolar macrophages (AM), the first line of defense in the lung (86). Specifically, prolonged alcohol exposure has been shown to increase the release of TGF-β but reduce chemokine production (CCL3) from AM needed to recruit immune cells into the lung (87-91). Additionally, alcohol exposure disrupts the ability of AM to clear both microbes and dying cells to reduce damage to tissue (92, 93) potentially due to oxidative stress (94). The

molecular basis for altered macrophage metabolism and function in the lung with alcohol is yet to be determined.

Lung-resident macrophages can be categorized into interstitial and alveolar with interstitial macrophages primarily residing within the tissue while alveolar macrophages are predominantly found within the lumen of the alveoli (95-100). Studies in mice have revealed that lung macrophages are derived from yolk sac and fetal liver as well as from bone marrow monocytes (101, 102). It is believed that embryonically derived macrophage populations have a self-renewal capacity and are functionally distinct from the monocyte-derived macrophages populations, however, whether this is true in humans is still unanswered (95). Recent studies have uncovered enormous heterogeneity in lung macrophage populations, but the mechanisms by which environmental factors or inflammatory settings alter the ability of these cells to clear pathogens and repair tissue remain poorly understood.

In this study, we use bronchoalveolar lavage (BAL) samples collected from rhesus macaques that voluntarily self-administered ethanol (EtOH) or an isocaloric solution for 12 months to examine the alcohol-induced epigenetic and transcriptomic changes that are coupled to altered macrophage function. While AM from EtOH drinking animals generate a heightened inflammatory response to bacterial and viral pathogens, they have a dampened antiviral transcriptional response to RSV and exhibit reduced phagocytosis of bacterial particles compared to AM from control animals. These functional defects were accompanied with epigenetic alterations at baseline where genomic regions associated with activation and degranulation processes were more accessible, but those associated with tissue maintenance and cell migration were more closed relative to AM from control animals.

Finally, scRNA-Seq analysis revealed shifts towards heightened inflammation and oxidative stress and away from tissue repair in AM from EtOH group relative to controls.

METHODS AND MATERIALS

See the data supplement for detailed methods

Animal studies and sample collection:

These studies used blood and bronchoalveolar lavage (BAL) samples from 11 female and 8 male rhesus macaques (average age 5.68 yrs; 9 controls and 10 chronic heavy drinkers). BAL cells were obtained after 12 months of daily drinking and cryopreserved until they could be analyzed as a batch. Cohort information is outlined in **Supp. Table 1.1**.

Flow cytometry analysis:

BAL cells were stained with the indicated surface antibodies, acquired with an Attune NxT Flow Cytometer and analyzed using FlowJo software.

Monocyte/Macrophage Stimulation Assays:

$6.5x10^4$ FACS sorted CD206+ cells from the BAL were cultured with or without 100 ng/mL LPS or RSV at an MOI of 5 for 16 hours. Supernatants from stimulated AM were measured using a 31-plex panel of indicated factors.

Bulk RNA-Seq library preparation and data analysis

Libraries from PBMC RNA were generated using the TruSeq Stranded RNA LT kit. Libraries from purified CD14+ monocytes RNA were generated using the NEBnext Ultra II Directional RNA Library Prep Kit. Libraries were multiplexed and sequenced on the NovaSeq platform. RNA-Seq reads were quality checked and trimmed and aligned to *Macaca mulatta* genome (8.0.1). Read counts were normalized using RPKM method. Differentially expressed

genes (DEG) were identified using edgeR (103) (**Supp. Table 1.5**). Functional enrichment of DEG was performed using Metascape (104).

ATAC-Seq library preparation and data analysis:

AM were subjected to nuclei isolation, transposition, and amplification for ATAC-Seq. Libraries were multiplexed and sequenced to a depth of 50 million 100bp paired reads. Reads were quality checked, trimmed, and aligned to the *Macaca Mulatta* genome (8.0.1). Mitochondrial reads and PCR duplicate artifacts were removed. Samples from each group were concatenated and accessible chromatin peaks were called using Homer's *findPeaks* function (105) (FDR<0.05) and differential peak analysis was performed using Homer's *getDifferentialPeaks* function ($P < 0.01$) (**Supp. Table 1.5**).

10X 3' scRNA-Seq library preparation and analysis

Cells were loaded onto 10X Chromium Controller. cDNA amplification and library preparation (10X v3.1 chemistry) were performed according to manufacturer protocol and sequenced on a NovaSeq S4 to a depth of >30,000 reads/cell. Sequencing reads were aligned to the *Macaca mulatta* (8.0.1) reference genome using cellranger v3.1 (10X Genomics). Quality control steps were performed prior to downstream analysis with *Seurat* v3.2.2 *(106)*, where cells with fewer than 200 unique features (ambient RNA) and cells with greater than 20% mitochondrial content (dying cells) were removed. Pseudotime trajectory of the AM/monocytes was reconstructed using Slingshot (107). Differential expression analysis was performed using MAST under default settings in *Seurat*. Gene signatures and pathways from KEGG (https://www.genome.jp/kegg/pathway.html) (**Supp. Table 1.4**) were compared using *Seurat's AddModuleScore* function.

Macrophage functional assays

Mitochondrial membrane potential, intracellular ROS, and phagocytosis were measured using MitoTracker Red CMXRos, CellRox Deep Red Reagent, and pHrodo Red S.*aureus* BioParticles, respectively (Thermo Fisher/Invitrogen, Waltham, MA).

Statistical Analysis:

All statistical analyses were conducted in GraphPad Prism 7.

RESULTS:

Chronic EtOH drinking alters surface activation and chemokine receptor expression on monocyte and macrophage populations in the lung

Chronic heavy alcohol drinking has been shown cause activation and hyper-inflammation in monocytes in the blood (108) and macrophages in the spleen (24). The alveolar space in the lung is home to a large population of tissue-resident macrophages and infiltrating monocytes that are the first responders to respiratory infections. Given that patients with alcohol use disorders have increased susceptibility to respiratory pathogens, we used a multipronged approach to uncover the pleiotropic impact of chronic heavy drinking on the transcriptional, epigenetic, and functional landscape of the alveolar macrophages (AM). We collected bronchial alveolar lavage (BAL) samples from male and female rhesus macaques that either consumed EtOH or an isocaloric solution daily for 12 months (**Figure 1.1A and Supp. Table 1.1**). We first determined the impact of chronic EtOH on the phenotype of AM by profiling cell surface markers using flow cytometry (n=6 control, 8 EtOH). Based on previous studies (109-111), we identified alveolar macrophages (AM) as CD206+CD169+, interstitial macrophages (IM) as CD206+CD169-, and infiltrating monocytes as CD206-CD169-CD14+HLA-DR+ (**Figure 1.1B**). AM were further subdivided based on expression of CD163 (**Figure 1.1B**). No significant differences in frequencies of these major macrophage/monocyte populations were observed with EtOH. (**Figure 1.1C**). Examination of surface activation markers and chemokine receptors revealed higher expression of CD40, CCR7, HLA-DR, CD86, CD163, and CD11C on AM compared to IM or monocytes (**Figure 1.1D**). IM and monocytes, however, had higher expression of CCR2, CX3CR1, and CCR5

compared to AM (**Figure 1.1D**). Interestingly, chronic EtOH drinking led to heightened activation of the CD163lo AM subset as indicated by increased expression of CD40 (corrected p=0.07) (**Figure 1.1E**). To determine whether EtOH dose impacted the expression of surface markers, we performed correlation analyses of median fluorescence intensities (MFI) with the 12-month average dose of EtOH. Average daily EtOH drinking positively correlated with CD40, CX3CR1 and CCR7 expression on AM (**Figure 1.1F**) and with CCR5 and CCR2 expression on monocytes and IMs (**Figure 1.1F**). CD11c expression negatively correlated with EtOH dose in monocytes and AMs while CD86 expression positively correlated with EtOH dose in the CD163lo AM population (**Figure 1.1F**). Therefore, while EtOH drinking does not result in major subset redistribution, it impacts the activation status of AM and chemokine receptors associated with lung trafficking on monocytes in a dose-dependent manner.

Chronic EtOH is associated with downregulation of genes important for wound healing and upregulation of genes important for activation and degranulation in AM

We have previously reported a disruption of transcriptional programs of both peripheral monocytes and splenic macrophages with chronic alcohol drinking (24, 25, 108). Therefore, we next examined transcriptional rewiring of lung-resident alveolar macrophages. AM were purified from control and EtOH animals (n=3/group) and bulk RNA sequencing performed (**Figure 1.1A**). EtOH drinking explained the most variability in baseline transcriptional profiles in AMs (**Figure 1.2A**). Differential analysis revealed 24 genes to be upregulated with EtOH (**Figure 1.2B**) including *CTSG, SNAP25*, *MYO3A* and *HEBP2* which are all associated with granulocyte activation and degranulation (**Figure 1.2C**). EtOH drinking was also

associated with 195 downregulated DEG, notably *CLEC1B*, which is associated with an anti-inflammatory macrophage phenotype (**Figure 1.2A**) (112). Functional enrichment showed that the downregulated DEG mapped significantly to gene ontology (GO) terms "response to wounding" (*CLEC1B, NRP1, PTK2,* and *PRKACB*), "cell morphogenesis" (*MYO7A, PLCGG1*), and "vasculature development" (*HMGA2*, *ACTA2*) pathways (**Figure 1.2D and 1.2E**). These observations indicate that chronic EtOH drinking skews AM away from tissue maintenance and repair and towards an inflammatory transcriptional state.

Chronic EtOH drinking results in opened promoter regions at CTSG and SNAP25 genes involved in degranulation and activation in AM

To assess whether baseline transcriptional changes in the AM could be due to epigenetic changes, we performed ATAC-Seq on purified AM from control and ETOH animals (n=3/group). Although the relative distribution of open promoter and distal regions was comparable between groups (**Figure 1.3A**), several differentially accessible regions were identified within the promoter and distal intergenic regions (**Figure 1.3B**). The 70 genes regulated by promoters that were more closed with EtOH enriched to GO terms associated with barrier function such as endothelium development (*CLDN3*, *CLDN5*) and T-helper cell differentiation (*FOXP1*) (**Figure 1.3C**). The 25 genes associated with promoters that were more accessible with EtOH mapped to GO term "regulation of hormone levels" (*CTSG*, *SNAP25*, and *MYO3A*) (**Figure 1.3C, D**). Intriguingly, expression of these 3 genes were also upregulated based on the bulk RNA-Seq analysis (**Figure 1.3D**).

Analysis of potential cis-regulatory mechanisms of regulation in the non-promoter regions was performed by first lifting the genomic regions from the macaque to human genomes

followed by enrichment using the GREAT database. This analysis revealed no significant enrichment of the regions that were less accessible with chronic EtOH; however, intergenic regions that were more accessible with chronic EtOH drinking significantly enriched to respiratory system development (*CTGF, EGFR, TGFBR2*) and regulation of response to external stimulus (*C1QB, CD180, CXCR4, IL21*) (**Figure 1.3E**). Finally, we performed transcription factor (TF) binding motif analysis on the distal intergenic differentially accessible regions (DAR), which showed higher likelihood of binding sites for TF that play a critical role in inflammation, notably AP-1, IRF8, and NFKB p-65 with chronic EtOH (**Figure 1.3F**). These observations indicate significant remodeling of the epigenetic landscape of AM with chronic EtOH drinking leading to cells poised toward inflammation and away from tissue repair and adaptive immune activation.

AM generate a heightened inflammatory response, but compromised interferon transcriptional response with chronic EtOH

Previous studies have reported an exaggerated inflammatory response by myeloid cells to LPS with chronic alcohol drinking (13, 24, 108, 113). Thus, we stimulated FACS purified AM with LPS (n=6/group) and determined immune mediator production by Luminex (**Supp. Figure 1.1A and Supp. Table 1.2**). As described for peripheral blood and splenic macrophages, AM from EtOH drinking animals mounted a hyper-inflammatory response as indicated by heightened production of cytokines (IL-6, TNFα) and chemokines (CXCL8, CXCL10, CCL2, CCL4) compared to control AM (**Supp. Figure 1.1A**). We next examined responses of AM to a respiratory pathogen. Purified AM were stimulated with respiratory syncytial virus (RSV) *ex vivo* (n=8/group) and antiviral responses were determined using

RNA-Seq and Luminex. In response to RSV stimulation, AM from control animals secreted several growth factors (BDNF, VEGF, PDGF, and FGF), a few chemokines (CCL5 and CXCL10) and canonical inflammatory marker IL-6 (**Figure 1.4A**). Despite comparable viral loads (**Supp. Figure 1.1B**), AM from EtOH exposed animals produced significantly increased amounts of additional cytokines (IL-1β, IL-12, IL-15, IFNβ, IL-7) as well as growth factors (GM-CSF, C-CSF) relative to their unstimulated condition (**Figure 1.4A**). AM from EtOH exposed animals also produced significantly higher levels of IL-6, IL-12 and TGFα relative to their control counterparts (**Figure 1.4B**). Moreover, significant positive correlations between IL-6, IL-12, and CCL5 concentration and EtOH dose was observed (**Figure 1.4C**).

In contrast to the immune mediator production profile, fewer DEG were detected in AM from the EtOH group compared to controls (516 DEG in control vs. 340 DEG in EtOH group) (**Figure 1.4D**). DEG upregulated in the control group alone enriched to regulation of innate immune response and negative regulation of immune processes (**Figure 1.4E**), whereas those upregulated in the EtOH group enriched to cell cycle and response to drug processes (**Figure 1.4E and Supp. Figure 1.1C**). Interestingly, gene signatures of cellular response to type I (IFNβ) and type II (IFNγ) interferons (*CCL18, IFI16, TLR2*, and *TLR3*) **(Figure 1.4F)** and regulation of innate immune processes (*CD80, CD86*, and *CCL2*) were upregulated only in control AM (**Supp. Figure 1.1D**). A significant number (297) of downregulated DEG from the control AM mapped to regulated exocytosis, cell morphogenesis, and response to wounding pathways (**Supp. Figure 1.1E**) such as *SIGLEC10, PTPN6*, and *SDC1* (**Supp. Figure 1.1F**). Next, the Chea3 database (114) was used to predict transcription factor (TF) regulation of the DEG. This analysis showed that genes upregulated only in control AM with RSV were regulated by phagocytosis and viral response associated TFs PLSCR1, SP100, and

IRF7, while genes upregulated in EtOH AM were regulated by inflammatory TF HMGA2 (**Supp. Figure 1.1G**). These observations indicate that chronic EtOH drinking results in a heightened inflammatory response coupled with compromised transcriptional responses to microbial pathogens.

scRNA-Seq profiling reveals significant changes in AM cell states with chronic EtOH

To investigate the impact of chronic EtOH on AM cell states, we performed scRNA-Seq on CD14+ purified cells from BAL samples obtained from control (n=3 females pooled, 4 males) and EtOH (n=3 females pooled, 2 males) animals (**Supp. Figure 1.2A**). Integration of replicates and further uniform manifold projection (UMAP) of clustering analysis revealed 11 clusters (**Figure 1.5A,B, and Supp. Figure 1.2B**). Expression of major macrophage/monocyte markers identified 10 AM clusters (AM 0, 1, 2, 3, 4, 5, 6, 8, 9, 10; expressing high levels of *MSR1, MARCO*, *FABP4, PPARG, MRC1, LTAH4*, and *CTSD*) and 1 monocyte cluster (7; expressing high levels of *FGL2, MS4A6A, and CCL17*) (**Supp. Figure 1.2C and Supp. Table 1.3**). To validate our identification of cluster 7 as monocyte cluster, we integrated single cell profiles of BAL macrophages with those of blood monocytes from the same female animals (108) (**Supp. Figure 1.3A**). We projected cells that clustered with the blood monocytes back onto the UMAP, which revealed that cluster 7 was the major monocyte subset with some monocyte infiltration in cluster 0 (**Supp. Figure 1.3B**).

The AM clusters were further defined based on their unique expression of genes and their functional implications (**Figure 1.5C and Supp. Figure 1.3C**). AM cluster 2 highly expressed genes associated with stress (*CD44, FOSB*) and cytokine responses (*PTPRC*). Clusters 3 and 4 had high expression of genes mapping to regulation of cell adhesion (*S100A10, LGALS3*) and

angiogenesis (*TGFBR3, GPNMB*), respectively. AM cluster 5 was characterized by high levels of cathepsin genes (*CTSB, CTSL, CTSG*) associated with bacterial response processes. Cluster 9 was enriched in transcripts important for proliferation (*STMN1, MKI67, TOP2A*) and cluster 10 with oxidative stress response (*LCN2*). AM cluster 8 was an anti-viral response cluster with high expression of *ISG15, IFIT1*, and *IRF7*. Cluster 6 genes mapped to sterol biosynthesis (*MSMO1, CYP51A1, SQLE*) and cluster 1 genes included *PTGDS* and *MCM7*. Finally, cluster 0 was an activated macrophage cluster expressing high levels of LPS responsive genes *CLEC4E, S100A8, S100A9*) (**Figure 1.5C and Supp. Figure 1.3C**).

To identify potential differentiation trajectories of in the AM populations, we performed pseudotime analysis using slingshot where we set the starting point at the infiltrating monocyte cluster. This analysis revealed 5 unique trajectories branching from cluster 7 (**Figure 1.5D**), which all showed increasing expression of tissue resident macrophage markers (*FABP4, MARCO*) and decreasing monocyte markers (*CPVL, TMEM176B*) (**Supp. Figure 1.3D**). We profiled the cellular densities along each trajectory, which revealed a bias in cells from control animals at the start and an increase in cells from EtOH group along the course of the pseudotime (**Figure 1.5E**). This was particularly apparent in lineages 3 and 4, each of which was driven by specific gene subsets (**Supp. Figure 1.4**). Of interest, lineage 3 was driven by increasing expression of oxidative stress- responsive genes (*BTG1, GSTP1, SFPG, PPP1R15B*) along with tissue macrophage genes *CD163* and *MRC1* (**Supp. Figure 1.4**). Lineage 4 was driven by increased expression of *CLEC4E*, associated with inflammatory macrophage responses (**Supp. Figure 1.4**).

We finally examined the redistribution of AM populations with EtOH (**Figure 1.5F**). A modest increase of AM cluster 0 was accompanied by a significant decrease in AM cluster 3 with chronic EtOH drinking (**Figure 1.5F**). Functional enrichment showed that defining genes for cluster 0 were associated with apoptosis and responses to bacterial and fungal pathogens whereas cluster 3 defining genes were associated with membrane raft organization, regulation of fibroblast proliferation and cell adhesion (**Figure 1.5G**). We conclude that EtOH induces shifts in AM cell states, increasing the proportion of activated AM, potentially driven by altered differentiation trajectories of infiltrating monocytes.

EtOH- induced oxidative stress alters AM metabolic-associated processes and functional abilities

To determine potential functional implications of EtOH-induced changes in AMs, we first assessed differential gene expression across aggregated single cell clusters (**Figure 1.6A**). Functional enrichment of the DEG downregulated with EtOH mapped to monocyte chemotaxis (*LGMN, CCL2*), angiogenesis (*ANPEP, ECM1*) and epithelial cell proliferation (*GRN, CCL24*) processes (**Figure 1.6A**). Moreover, as described for the bulk RNA-Seq data (**Figure 1.2D**), downregulated DEG also mapped to wound healing and blood vessel processes along with epithelial cell proliferation. On the other hand, upregulated DEG were associated with oxidative phosphorylation (*COX7A1, ATP8, ND4*), apoptosis (*CD74, RPL11, PPIA*), and antigen processing and presentation (*B2M, FCER1G*) (**Figure 1.6A**). In line with the significant upregulation of genes that enriched to GO term “oxidative phosphorylation”, the module scores for oxidative stress and HIF1A signaling were also elevated with EtOH (**Figure 1.6B, Supp. Figure 1.5A, and Supp. Table 1.4**). To determine whether these

transcriptional shifts towards oxidative phosphorylation were mediated through mitochondrial function, we assessed the impact of chronic EtOH drinking on mitochondrial membrane potential in AM using flow cytometry. Intracellular mitochondria membrane potential in AM was significantly increased with EtOH while that of IM was unchanged (**Figure 1.6C and Supp. Figure 1.5B**). Moreover, levels of intracellular ROS in AM and IM was significantly increased after stimulation with LPS (**Figure 1.6D and Supp. Figure 1.5C**). As EtOH-induced oxidative stress has been shown to affect the phagocytic capacity of AM (57, 58), the module score for phagocytosis determined from scRNA-Seq data was reduced in AM (**Figure 1.6E**). Accordingly, the ability of AM to phagocytose pHrodo-labeled *S. aureus* was significantly reduced with EtOH drinking compared to controls (**Figure 1.6F**). Finally, in line with the exaggerated inflammatory response to LPS and RSV stimulation, the cytokine signaling module score was increased in AM with EtOH (**Supp. Figure 1.5D**). Additionally, as we found increased accessibility of the cathepsin G promoter and corresponding baseline RNA expression, we profiled *CTSG* from the scRNA-Seq data and found that AM clusters 1 and 5 had significantly elevated expression of *CTSG* (**Supp. Figure 1.5E**). In summary, EtOH drinking induces oxidative stress in AM leading to increased ROS production, mitochondrial activation, and oxidative phosphorylation that are coupled with reduced phagocytosis capacity and increased inflammatory gene expression.

DISCUSSION:

Tissue resident macrophages and infiltrating monocytes make up a majority of the immune cells in the alveolar space where they respond to insults to the respiratory tract including toxins, pathogens and allergens (115). They are responsible for both inflammatory responses and tissue remodeling and repair. Under homeostatic conditions, a tight balance between inflammatory and anti-inflammatory responses is maintained. This delicate balance can be dysregulated by environmental factors including pollutants, smoking, and alcohol drinking (55). In fact, chronic heavy alcohol drinking results in increased susceptibility to respiratory diseases, but the mechanisms underlying this increased vulnerability are not completely understood. In this study, we carried out a comprehensive examination of the impact of chronic heavy alcohol drinking on the transcriptome, epigenome, and function of alveolar macrophages (AM) obtained from a rhesus model of voluntary ethanol self-administration. This voluntary drinking model accurately recapitulates human drinking behavior in duration and dose and represents a chronic, not acute, model of alcohol and its metabolites on the body. Specifically, bronchoalveolar lavages (BAL) obtained after 12 months of heavy drinking (>3g ethanol per kg body weight per day or > 12 drinks per day in an average 60kg human). Our findings indicate that chronic EtOH drinking rewires the epigenetic landscape of AM that become poised towards aberrant inflammatory responses and compromised anti-microbial functions.

A prominent and consistent observation of this study is increased expression of cathepsin G (*CTSG*) in AM. This was further confirmed by scRNA-Seq analysis showing specific clusters of AM with increased *CTSG* expression. The increased abundance of *CTSG*

transcripts was accompanied by increased chromatin accessibility at *CTSG* promoter with chronic EtOH drinking. Cathepsins are proteases that are active in low pH lysosomes and have versatile functions in innate immunity, activation, tissue degradation (116). Dysregulated expression of cathepsins has been linked to diseases including arthritis, muscular dystrophy, and tuberculosis (116). The significance of increased cathepsin expression by EtOH in AM needs to be further studied to determine its importance in AM function and lung immunity.

It has been previously reported that AM from patients with alcohol use disorders express elevated levels of inflammatory mediators (117, 118). Similarly, chronic EtOH drinking in macaques resulted in increased surface activation marker CD40 expression on CD163lo AM. As CD163 is associated with an M2 or resolving macrophage phenotype (119), this indicates skewing towards a more inflammatory macrophage population. Additionally, expression of chemokine receptors CCR7, and CX3CR1 correlated with EtOH dose. CCR7 has been associated with an activated phenotype in AM (120), and CX3CR1 has been implicated in TNFα and IL-6 production in tissue resident mononuclear phagocytes in the lungs of smokers (121) as well as in profibrotic macrophage subsets (122). This increased activation was also noted in the scRNA-Seq analysis where the abundance of a pathogen responsive AM cluster and scores of cytokine signaling modules were increased with EtOH. Additionally, transcription factor motif analysis revealed enrichment of binding sites for pro-inflammatory TF AP-1, IRF8, and NFκB with chronic EtOH drinking. These data are in line with our previously reported changes in splenic macrophages and circulating monocytes indicating broad epigenetic rewiring by *in vivo* chronic drinking (24, 123). Collectively, these

alterations at baseline suggest that AM are posed towards heightened inflammatory state, which could lead to increased risk of lung tissue damage and infection.

Previous studies have identified altered production of cytokines and chemokines as well as reduced phagocytic ability in AM with chronic drinking (55, 87). Similarly, here we show that AM from EtOH animals generated a hyper-inflammatory cytokine and chemokine response to LPS. These observations are in line with data from our earlier studies that reported exaggerated inflammatory responses by splenic macrophage and blood monocyte responses to LPS (24, 108, 123), as well as studies on long-term EtOH exposure and increased inflammatory responses in myeloid cells (13). To determine if this hyper-responsiveness extended to a relevant lung pathogen, we stimulated AM with RSV. AM from EtOH animals produced significantly higher levels of IL-6, IL-12, and TGFα than controls. Increased production of IL-6 in response to RSV with EtOH could indicate broad hyper-inflammation. However, as IL-12 and TGFα levels are not increased in control AM after RSV stimulation, we believe the production of increased levels of these factors with EtOH to be indicative of a dysregulated response. Profiling the transcriptional profiles of the AM after infection showed a reduced response. DEG important for response to interferon pathways as well as regulation of immune processes were only detected in control AM, indicating disruptions in antiviral immunity. Indeed, individuals with alcohol use disorders shown increased susceptibility to RSV (46, 47).Coinciding with this finding, repressed promoter regions in AM from EtOH animals mapped to T-helper cell differentiation and regulation of cell migration indicating a suppression of secondary immune activation processes. Therefore, EtOH-induced epigenetic disruptions result in a rewiring of AM that favors development of non-specific inflammation and disruption of anti-microbial functions.

Another critical function of AM is resolution of inflammation and tissue repair where patients with alcohol use disorders have higher risk of developing ARDS (46, 53) and compromised wound healing responses (19). RNA-Seq and scRNA-Seq of AM revealed decreased expression of genes mapping to wound healing and epithelial cell proliferation processes in EtOH AM. We believe these changes are mediated epigenetically, where reduced chromatin accessibility was noted in promoters that regulate genes important for endothelium development and cell junction assembly with EtOH.

scRNA-Seq data revealed significant heterogeneity within tissue resident and monocyte derived macrophage populations. Recent studies on human lung macrophages have also shown significant macrophage diversity with disease states (95). Clusters that were abundant with EtOH drinking exhibited a transcriptional profile consistent with heightened activation and pathogen response. Trajectory analysis further showed altered differentiation of monocytes to macrophages with EtOH. Additional studies are needed to confirm these findings and determine whether these clusters represent independent lineages or different activation states associated with EtOH drinking. Activation and differentiation of macrophages are controlled by complex epigenetic mechanisms (124). It is possible that the heightened activation state as well as differentiation trajectory with EtOH can be attributed to a process akin to innate training where environmental factors lead to epigenetic changes that have long-lasting functional consequences (125).

Functionally, we report reduced phagocytosis of *S. aureus* by AM from the EtOH AM as previously observed in cell culture and rodent models (55, 56), where one suggested mechanism is oxidative stress induced by increased NADPH oxidase (57-59). In fact, scRNA-

Seq data showed increased oxidative stress module scores as well as oxidative phosphorylation in AM from EtOH animals. Prior studies have reported a link between EtOH and its metabolites and changes in global methylation state, histone modifications, and ROS production (63). Our data show increased levels of intracellular ROS in AM with EtOH, which is potentially a direct consequence of EtOH metabolism and downstream oxidative stress (126). As ROS serve as inflammasome activating signals and induce inflammation (127), this could contribute to increased production of cytokines and chemokines in response to stimulation. Because oxidative phosphorylation is linked to mitochondrial activation, we assessed mitochondrial membrane potential to identify increased activation in AM with EtOH. Future studies would be needed to determine the bioenergetics of these mitochondria and whether they are contributing to increased ROS levels and further inflammation in AM (128). As macrophage states are fluid, we argue that EtOH and its metabolites induce several cellular changes in AM, and deconvoluting the complexities of which require more targeted assays.

This study provides a comprehensive examination of AM in the context of chronic alcohol drinking in macaques. We acknowledge several limitations including biological variability within samples due to the outbred macaque model and the use of LPS instead of a bacterial pathogen. Our findings indicate increased baseline activation and inflammation signatures epigenetically and transcriptionally in AM that could contribute to increased non-specific inflammatory response to pathogens and compromised phagocytic ability and transcriptional response to RSV. Potential new targets identified here include increased mitochondrial activation, increased ROS production, epigenetic alterations, and increased

cathepsins in AM with EtOH drinking. These altered AM states could contribute to the increased susceptibility of patients with alcohol use disorders to respiratory infections.

Acknowledgements

We are grateful to the members of the Grant laboratory for expert animal care and sample procurement. We thank Dr. Jennifer Atwood for assistance with sorting in the flow cytometry core at the Institute for Immunology, UCI. We thank Dr. Melanie Oakes from UCI Genomics and High-Throughput Facility for assistance with 10X library preparation and sequencing.

Data availability

The datasets supporting the conclusions of this article are available on NCBI's Sequence Read Archive (SRA#PRJNA767842).

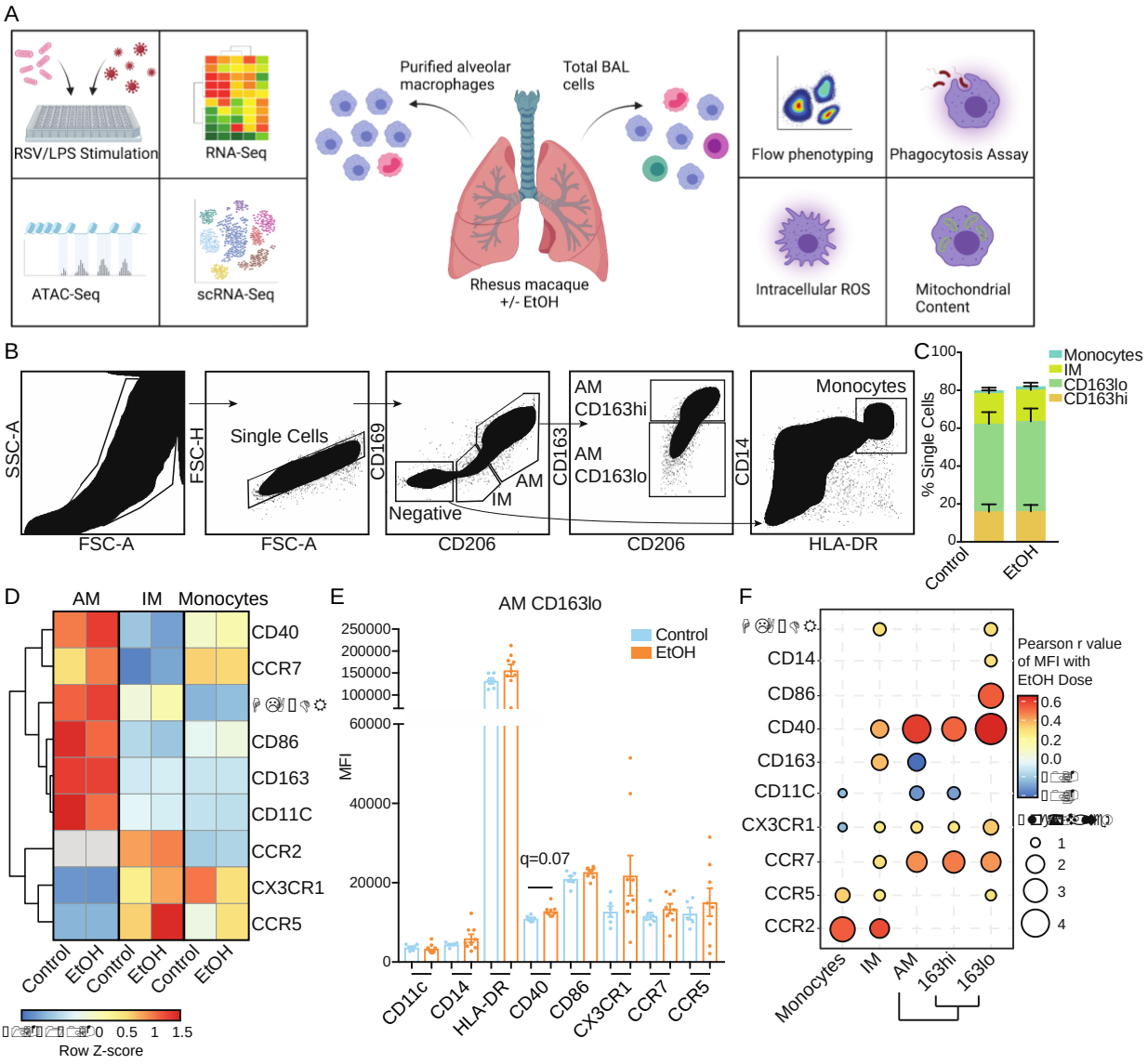

Figure 1.1: EtOH drinking alters alveolar macrophage (AM) phenotype

A) Experimental design of this study created with BioRender.com. B) Gating strategy to identify monocytes, interstitial macrophages (IM), and alveolar macrophages (AM) from bronchoalveolar lavage (BAL) samples. C) Relative distributions of the three myeloid cell subsets in the BAL. D) Heatmap showing averaged median fluorescence intensity (MFI) values for cell surface markers in each indicated subset/group. The scale is row Z-score where blue is lower and red higher expression. E) Median fluorescence intensity (MFI) of activation and chemokine surface markers measured from the CD163lo AM population.

Significance was calculated by t-test with two-stage step-up false discovery rate method of Benjamini, Krieger, and Yekuieli where trending values are shown. F) Bubble plot representing correlations between cell surface markers and EtOH dose in the indicated cell populations. The size of each circle represents the indicates the $-\log_{10}$ transformed p-value significance (All values are <0.1). The color denotes the Pearson r value calculated by correlation.

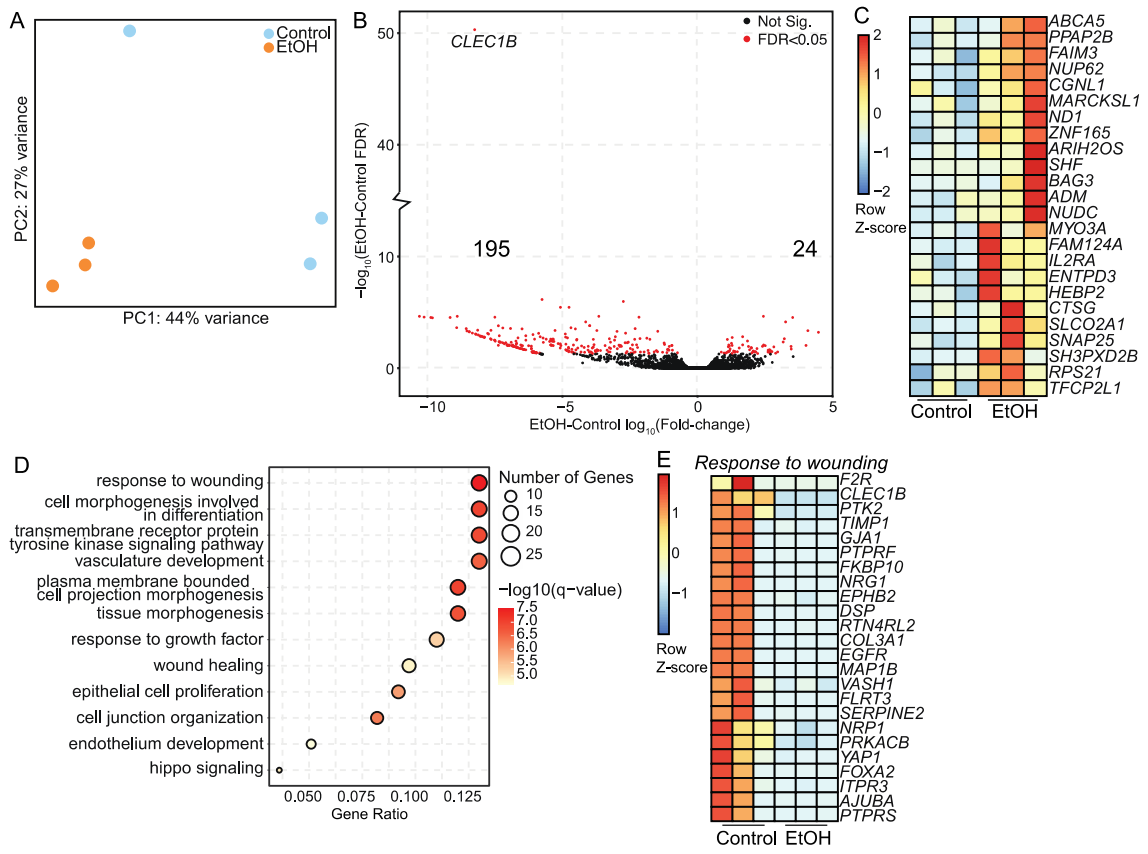

Figure 1.2: Chronic EtOH drinking induces changes in the alveolar macrophage (AM) transcriptome

CD206+ alveolar macrophages (n=3/group) were purified from total BAL using FACS and subjected to bulk RNA-Seq. A) Principal component analysis (PCA) of bulk RNA-Seq libraries from controls and EtOH AM. B) Volcano plot representing the up- and downregulated differentially expressed genes (FDR<0.05) where the X-axis is $\log_{10}$ fold-change and the Y-axis is $-\log_{10}$ FDR. C) Heatmap representing the expression of all DEG upregulated with EtOH where the scale is Row Z-score representing low (blue) and high (red) expression. D) Bubble plot showing GO Biological Process enrichment of downregulated DEG with EtOH compared to controls. The size of the bubble represents the number of genes associated with that term, the color represents $-\log_{10}$ q-value, and the X-axis is the ratio of genes mapping to that term to total genes. E) Heatmap representing the expression of DEG from response to wounding term where the scale is Row Z-score representing low (blue) and high (red) expression.

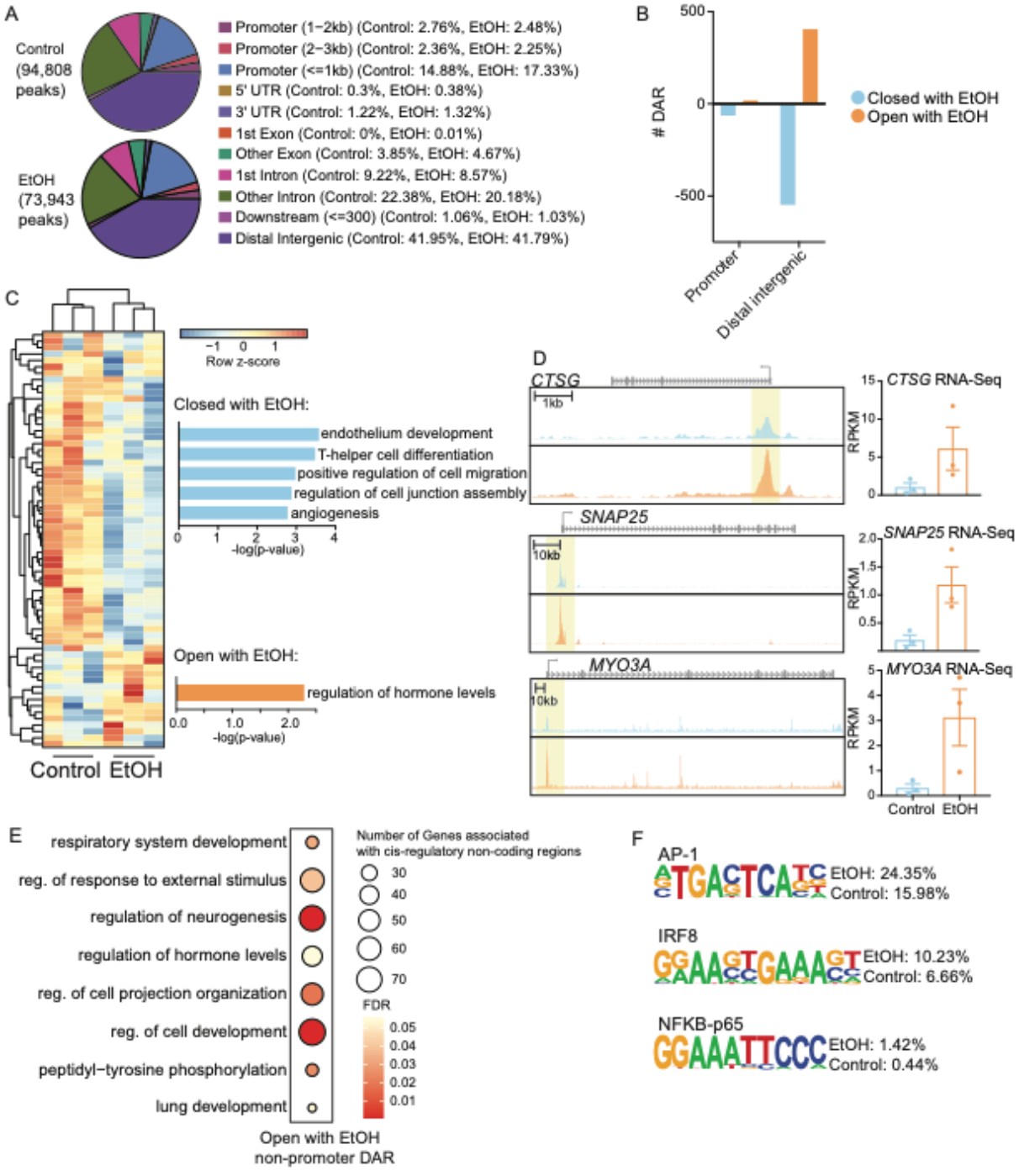

Figure 1.3: Epigenomic analysis of AM with chronic EtOH drinking

Alveolar macrophages (n=3/group) were purified from total BAL by CD206+ sort and nuclei were subjected to ATAC-Seq. A) Pie charts showing genomic feature distribution of

the open chromatin regions (fold-change ≥ 2, FDR ≤ 0.05) in control and EtOH AM. B) Bar chart showing the number of open and closed differentially accessible regions (DAR) (FDR ≤ 0.01) with EtOH in promoter and distal intergenic regions. C) Heatmap representing the open and closed (EtOH-Control) differentially accessible promoter region (FDR ≤ 0.01) counts where the scale is Row Z-score representing low (blue) and high (red) expression. Bar plots to the right represent the functional enrichment of those promoter DAR where the X-axis is $-\log_{10}$ p-value. D) Pile-ups of selected promoter DAR more open with EtOH. Scale is indicated. To the right of each is a bar chart of the RPKM expression value of the gene from bulk RNA-Seq analysis. E) Non-promoter DAR were lifted over to the human genome and enriched for cis-regulatory mechanisms using GREAT. Bubble plot of the open non-promoter DAR with EtOH enrichment where the size of the bubble represents the number of gene regions associated with that term and the color represents the FDR significance where darker red indicates a more significant value. F) Homer motif enrichment of the distal intergenic DAR. All listed motifs have significantly enriched binding sites in the open and closed non-promoter DAR where the percentage value listed is the percentage of target sequences with that motif.

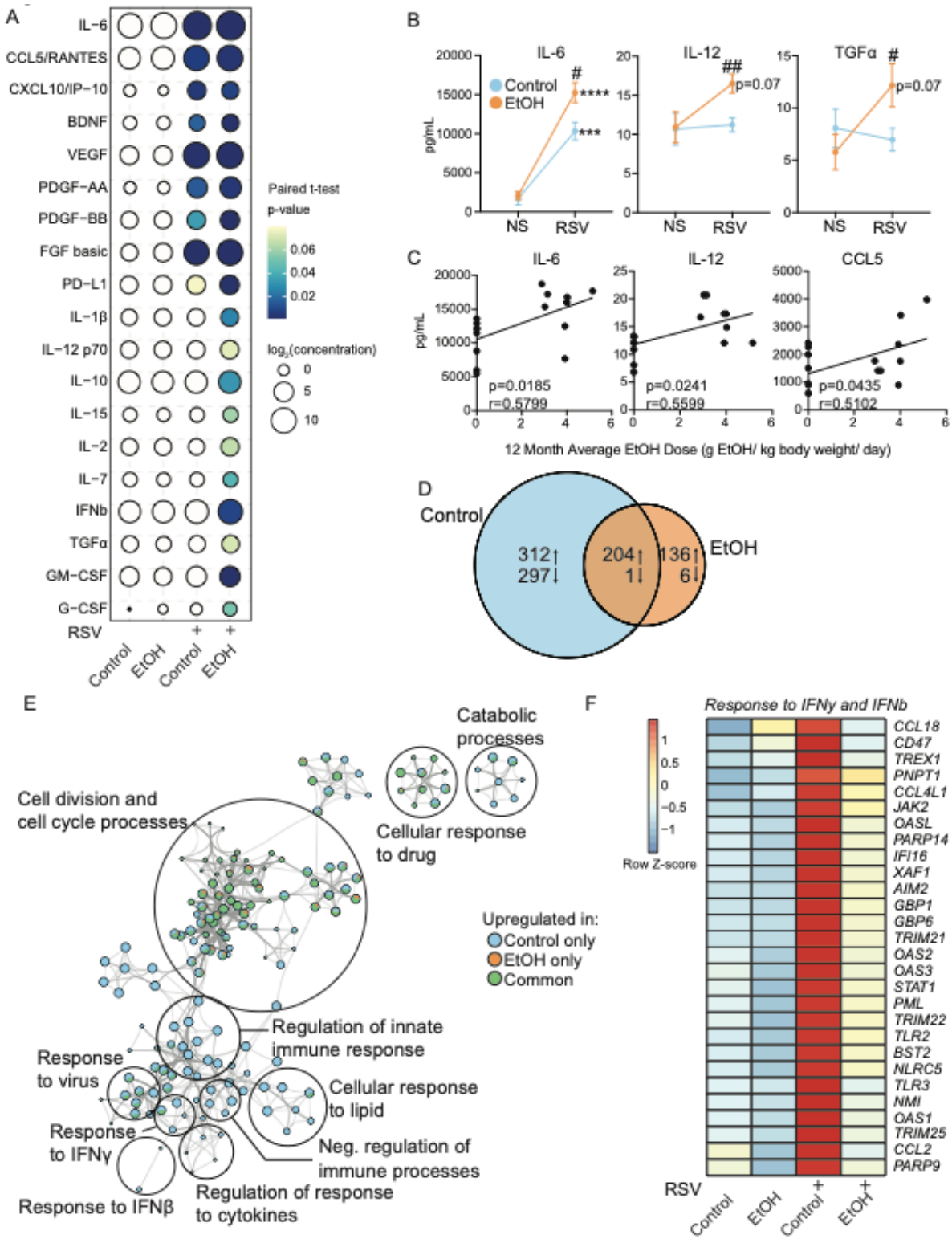
A
IL-6
CCL5/RANTES
CXCL10/IP-10
BDNF
VEGF
PDGF-AA
PDGF-BB
FGF basic
PD-L1
IL-1β
IL-12 p70
IL-10
IL-15
IL-2
IL-7
IFNb
TGFα
GM-CSF
G-CSF
RSV
Control
EtOH
Control
EtOH
Paired t-test
p-value
0.06
0.04
0.02
log2(concentration)
0
5
10
B
IL-6
IL-12
TGFα
Control
EtOH
pg/mL
#
****
***
##
p=0.07
p=0.07
NS
RSV
C
IL-6
IL-12
CCL5
pg/mL
p=0.0185
r=0.5799
p=0.0241
r=0.5599
p=0.0435
r=0.5102
12 Month Average EtOH Dose (g EtOH/ kg body weight/ day)
D
Control
EtOH
312↑
297↓
204↑
1↓
136↑
6↓
E
Catabolic processes
Cell division and cell cycle processes
Cellular response to drug
Upregulated in:
Control only
EtOH only
Common
Regulation of innate immune response
Response to virus
Cellular response to lipid
Response to IFNγ
Neg. regulation of immune processes
Regulation of response to cytokines
Response to IFNβ
F
Response to IFNγ and IFNb
Row Z-score
CCL18
CD47
TREX1
PNPT1
CCL4L1
JAK2
OASL
PARP14
IFI16
XAF1
AIM2
GBP1
GBP6
TRIM21
OAS2
OAS3
STAT1
PML
TRIM22
TLR2
BST2
NLRC5
TLR3
NMI
OAS1
TRIM25
CCL2
PARP9
RSV
Control
EtOH
Control
EtOH

Figure 1.4: EtOH-induced heightened inflammatory with compromised transcriptional response to RSV

AM were purified and stimulated with RSV for 16 hours followed by Luminex analysis of mediator production and RNA-Seq. A) Bubble plot representing immune factor production (pg/ml) in the presence or absence of respiratory syncytial virus (RSV) by AM from control and EtOH animals. The size of each circle represents the indicates the $\log_2$ average concentration of the indicated secreted factor and the color denotes the p-value significance where darker blue represents a more significant value. The p-values were calculated between the unstimulated and stimulated conditions for each group using paired t-test. White circles indicate uncalculated or non-significant p-value. B) Line plots representing the Luminex data for the selected analytes. Significance was tested by paired t-test or unpaired t-test with Welch's correction. C) Scatter plots showing correlation analysis of selected factor concentration with dose of ethanol (g EtOH/ kg body weight/ day). P-value and Pearson r value are indicated. D) Venn diagram comparing up- and downregulated DEG after RSV stimulation in control and EtOH AM. E) Cytoscape plot of functional enrichment to GO Biological Processes of upregulated DEG with RSV from both groups compared to unstimulated conditions. The size of the dot represents the number of genes enriching to that term and the pie chart filling represents the contribution of DEG from each group. Related processes are group into the larger terms circled. F) Heatmap representing the averaged expression of DEG in each group/stimulation condition from the *Response to IFNy* and *Response to IFNb* GO terms where the scale is Row Z-score representing low (blue) and high (red) expression. #=p<0.05, ##=p<0.01, ***=p<0.001, ****=p<0.0001.

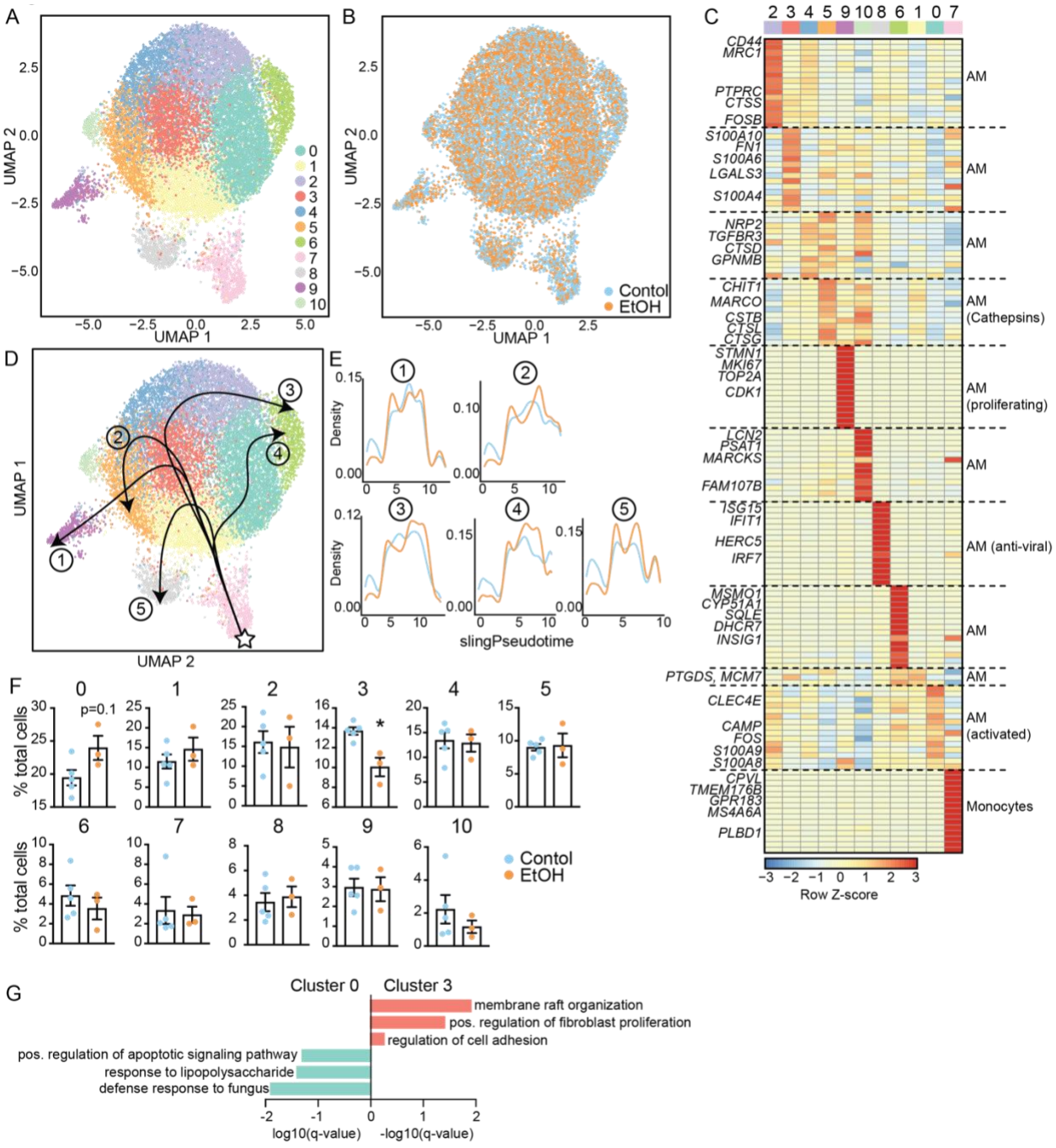

Figure 1.5: scRNA-Seq profiling of AM after chronic EtOH drinking

Macrophages and monocytes (n=3 control female pooled, 4 control male/ 3 EtOH female pooled, 2 EtOH male) were purified from total BAL and subjected to 10X scRNA-Seq analysis. A,B) Visualization of total cells by uniform manifold approximation and projection (UMAP) colored by cluster (A) and by group (B). C) Heatmap representing

averaged expression of cluster marker genes identified using the *FindMarkers* function where the scale is Row Z-score representing low (blue) and high (red) expression. D) UMAP with indicated pseudotime lineages identified by Slingshot trajectory analysis. E) Cell density plots for Control and EtOH groups across each of five trajectory lineages determined by Slingshot. F) Bar graphs showing relative abundance of the cells from control (blue) or EtOH (orange) groups within each identified cluster. Significance was calculated by t-test with Welch's correction. G) Bar plots showing GO functional enrichment terms for Clusters 0 and 3 genes identified using the *FindAllMarkers* function where the x axis is the $\log_{10}$ or $-\log_{10}$(q-value).

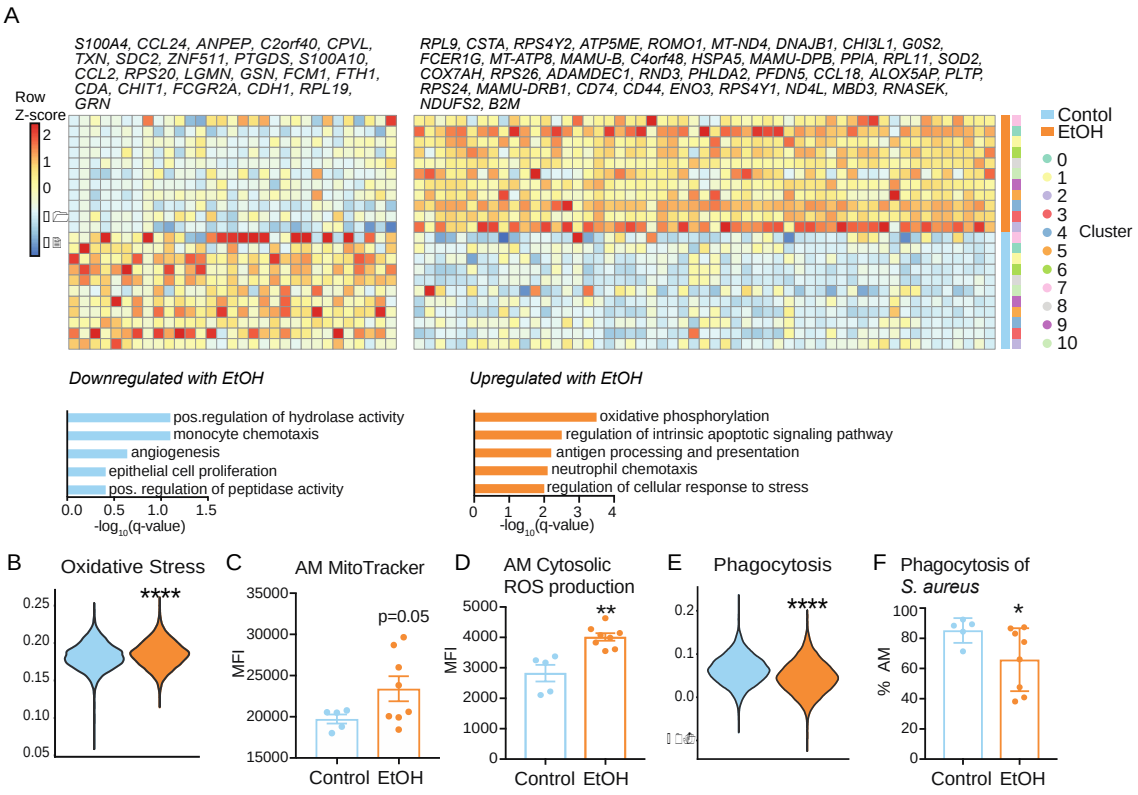

Figure 1.6: Chronic EtOH drinking leads to increased oxidative stress accompanied by functional defects in AM

A) Heatmap (top) representing averaged expression of differentially expressed genes between control and EtOH AM identified using the *FindMarkers* function where the scale is Row Z-score representing low (blue) and high (red) expression. Bar plots (bottom) showing GO Biological processes enriched in down- (left) or up- (right) regulated genes. B) Violin plot representing Oxidative Stress module scoring of total cells from each group. Significance was calculated using Mann-Whitney test. C) Bar plot showing median fluorescence intensity (MFI) of intracellular mitochondrial membrane potential stained with MitoTracker Red in AM. D) Bar plot showing median fluorescence intensity (MFI) of intracellular ROS stained by CellROX Deep Red Reagent in AM. E) Violin plot representing Phagocytosis module scoring of total cells from each group. Significance was calculated using Mann-Whitney test. F) Bar plot representing percentage of AM positive for pHrodo Red *S. aureus* particles. Unless indicated, statistical significance was calculated using t-test with Welch's correction. *=p<0.05, **=p<0.01, ****=p<0.0001.

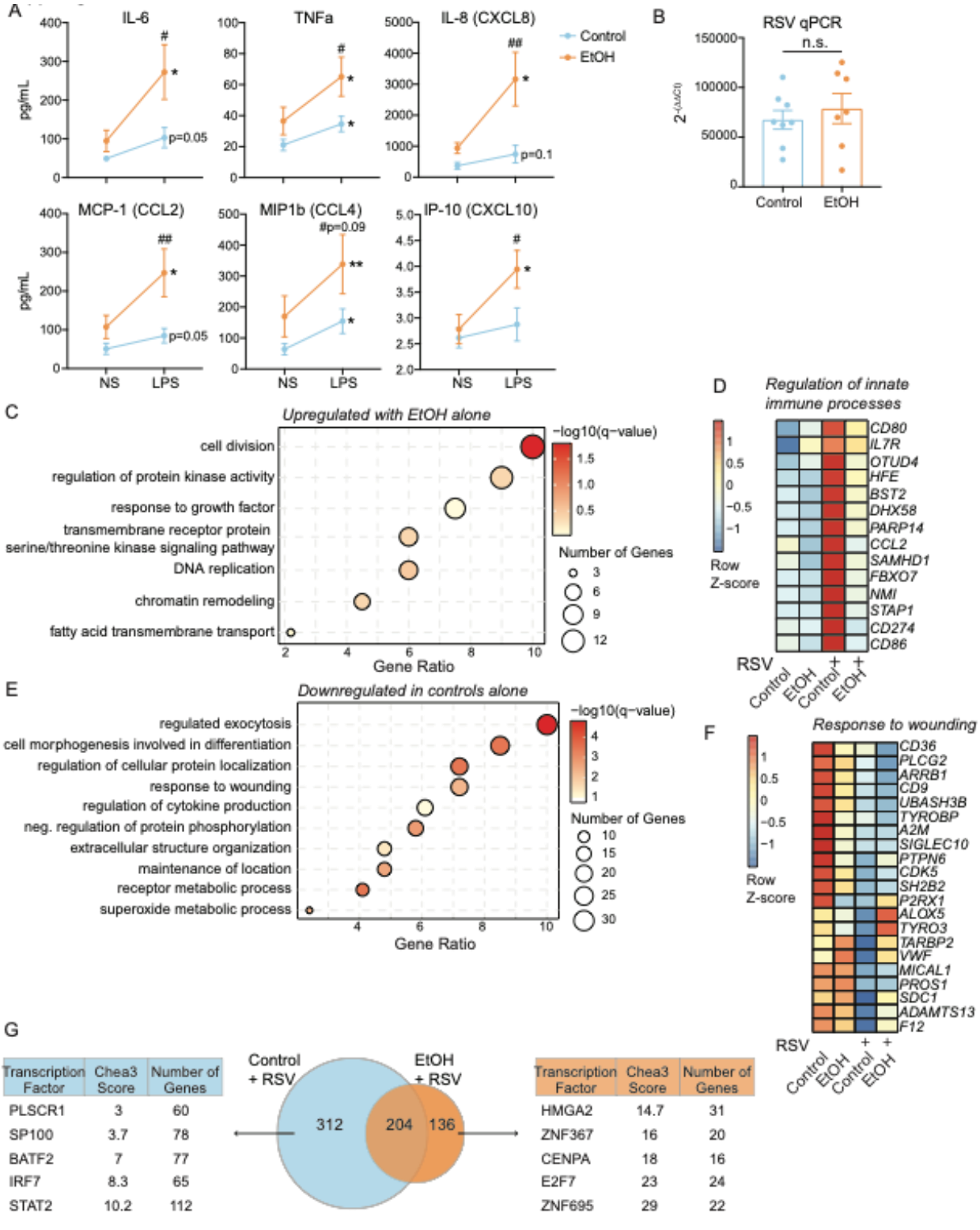

Transcription Factor	Chea3 Score	Number of Genes
PLSCR1	3	60
SP100	3.7	78
BATF2	7	77
IRF7	8.3	65
STAT2	10.2	112

Transcription Factor	Chea3 Score	Number of Genes
HMGA2	14.7	31
ZNF367	16	20
CENPA	18	16
E2F7	23	24
ZNF695	29	22

Supp. Figure 1.1: Chronic EtOH drinking induces defects in pathogen response in AM

AM were purified and stimulated with LPS for 16 hours. A) Supernatants from LPS stimulation were analyzed by Luminex assay. Line plots representing the measure pg/mL values for the selected analytes. Significance between NS and LPS conditions was tested using a paired t-test and between groups was tested by t-test with Welch's correction. B) Bar graph of $2^{\Delta\Delta Ct}$ values from qPCR for RSV transcripts after infection. C) Bubble plot showing GO Biological Process enrichment of upregulated DEG in EtOH group alone with RSV stimulation. The size of the bubble represents the number of genes associated with that term, the color represents $-\log_{10}$ q-value, and the X-axis is the ratio of genes mapping to that term to total genes. D) Heatmap representing the averaged expression of DEG from *Negative regulation of immune response* term where the scale is Row Z-score representing low (blue) and high (red) expression. E) Bubble plot showing GO Biological Process enrichment of downregulated DEG in control group alone with RSV stimulation. The size of the bubble represents the number of genes associated with that term, the color represents $-\log_{10}$ q-value, and the X-axis is the ratio of genes mapping to that term to total genes. F) Heatmap representing the averaged expression of DEG from *Response to wounding* term where the scale is Row Z-score representing low (blue) and high (red) expression. G) Venn diagram comparing upregulated DEG in control and EtOH AM with RSV stimulation. Analysis of the transcription factors regulating the unique DEG was performed using the Chea3 web browser. */#=$p<0.05$, **/##=$p<0.01$. Where indicated # is significance between control and EtOH groups.

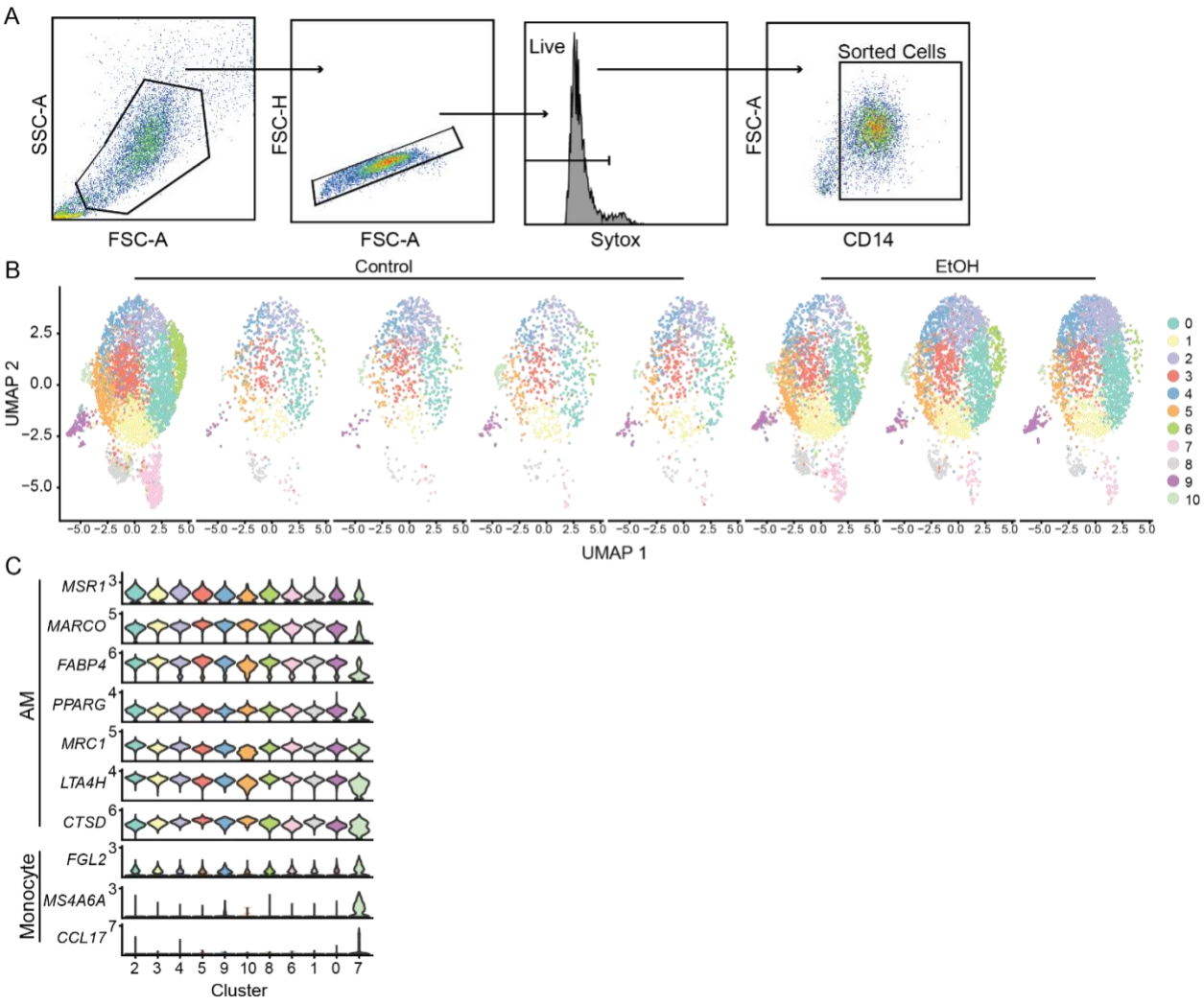

Supp. Figure 1.2: scRNA-Seq of AM after chronic EtOH drinking

A) Gating strategy for cell sorting for the 10X scRNA-Seq experiment. B) UMAPs of each individual sample. C) Violin plots of markers associated with AM (*MSR1, MARCO*, *FABP4, PPARG, MRC1, LTA4H, CTSD*) and monocytes (*FGL2, MS4A6A, CCL17*).

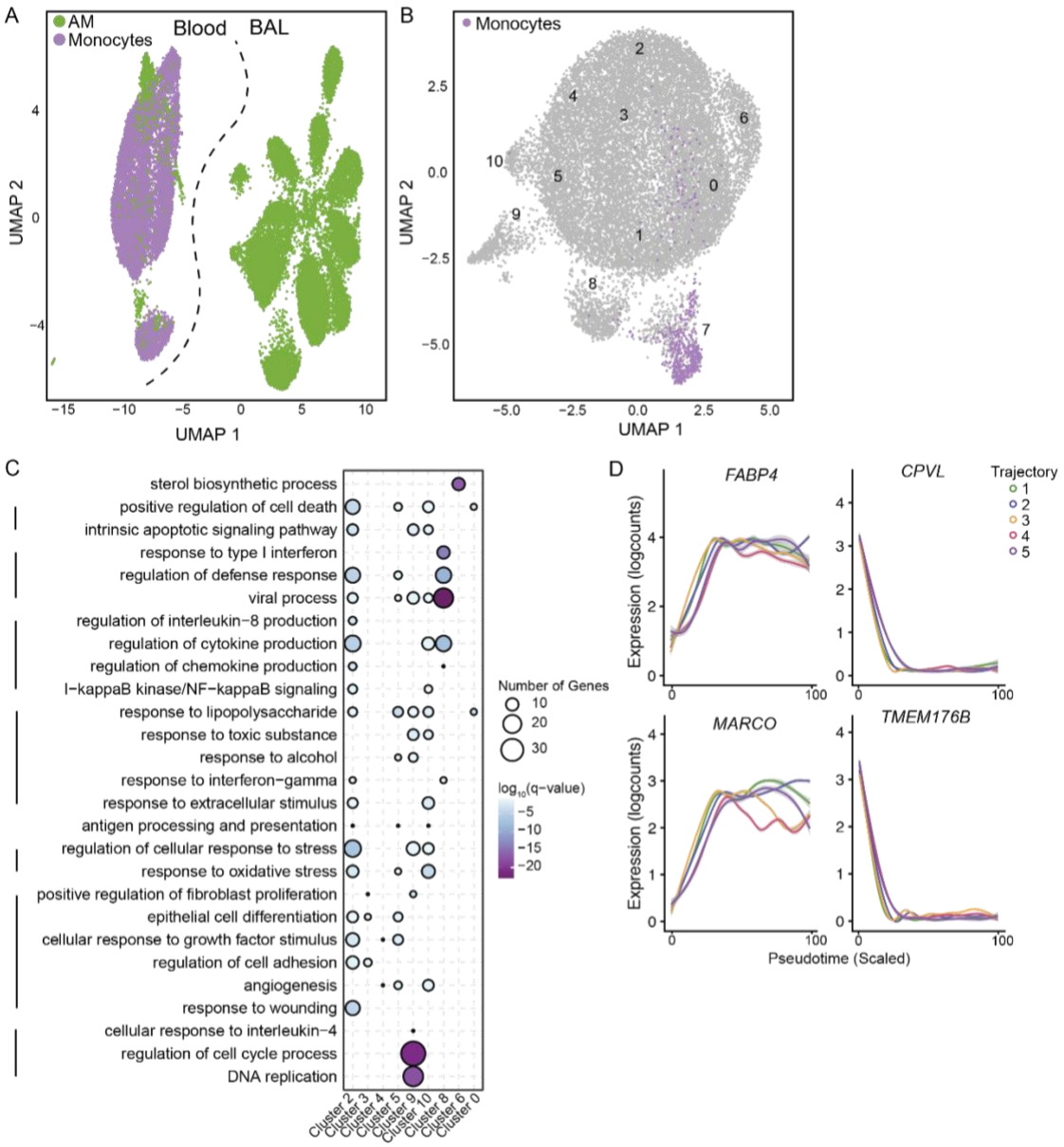

Supp. Figure 1.3: Identification of infiltrating monocytes in the BAL using scRNA-Seq

A) UMAP of integrated blood (123) and BAL analysis for identification of infiltrating monocytes in the BAL. B) Identified monocytes highlighted in the original UMAP from Figure 5A. C) Bubble plot of GO enrichment for highly expressed genes from clusters 2, 3, 4, 5, 9, 10, 8, 6, and 0 identified using the *FindAllMarkers* function where the size of the bubble is the number of genes associated with that term and the color is the $\log_{10}$(q-value). D) Log expression of *FABP4, MARCO, CCL17, TMEM176B* plotted for each cell across the indicated scaled slingshot pseudotime trajectory (trendline shown).

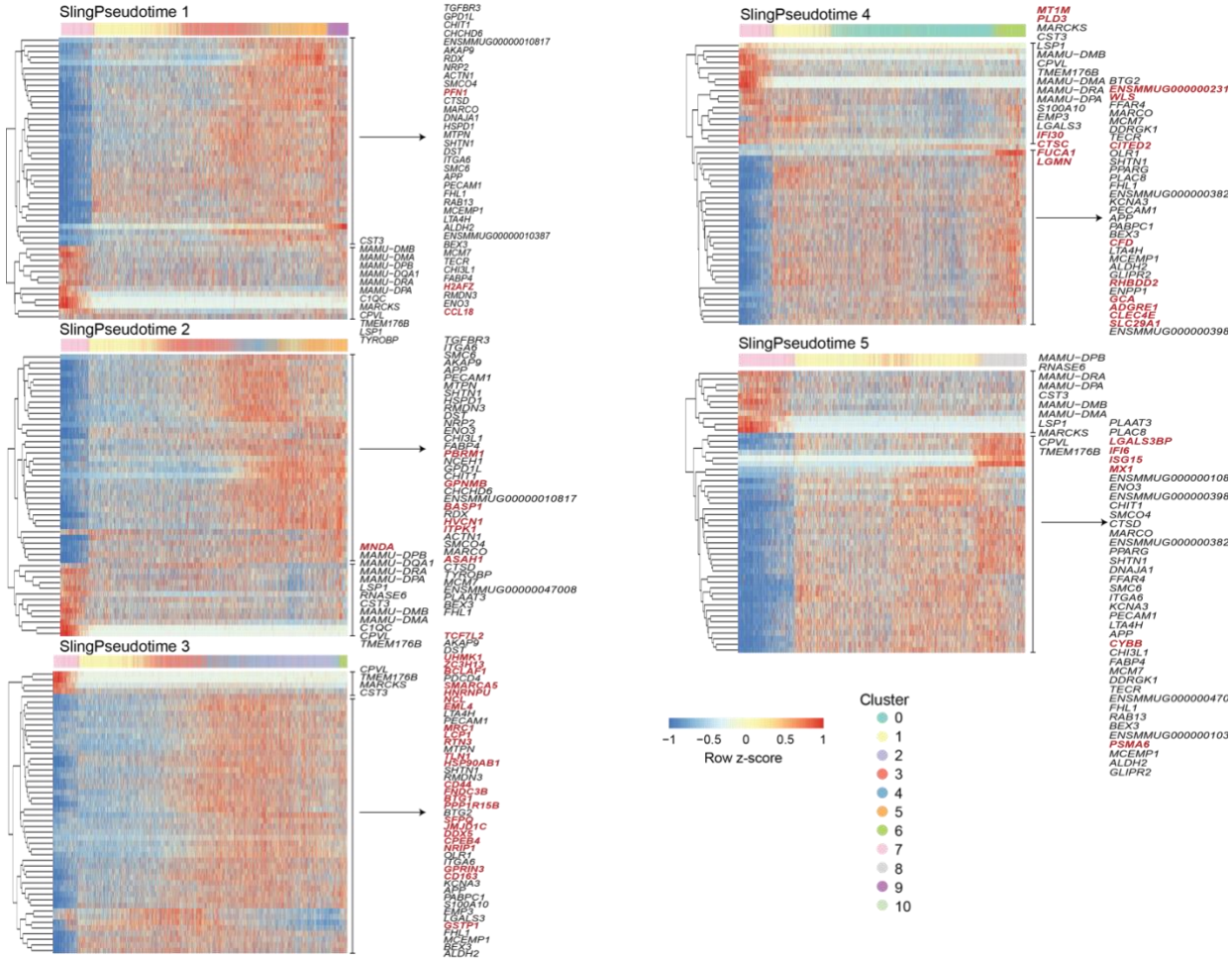

Supp. Figure 1.4: Slingshot trajectory heatmaps

Heatmaps showing the top 50 genes explaining each indicated trajectory. Genes highlighted in red are unique to that lineage.

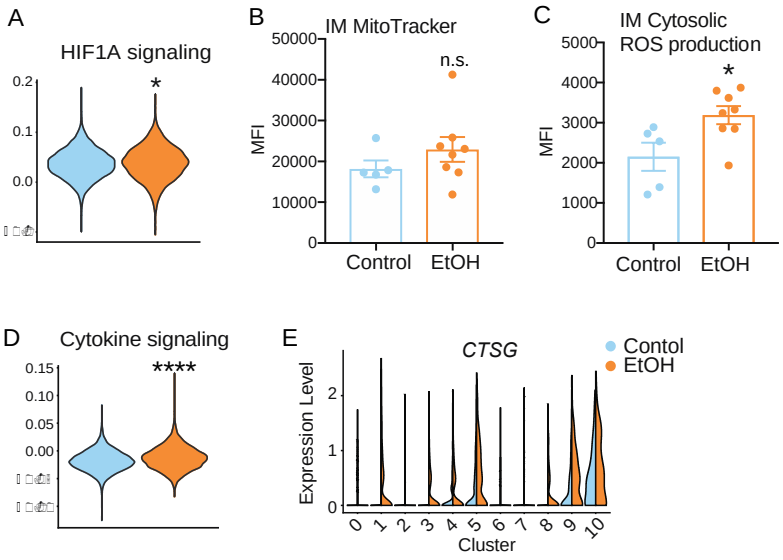

Supp. Figure 1.5: Functional implications of chronic EtOH drinking on AM and IM

A) Violin plot representing HIF1A signaling module score of total cells from each group. B) Bar plot showing median fluorescence intensity (MFI) of intracellular mitochondrial membrane potential stained with MitoTracker Red in IM. C) Bar plot showing median fluorescence intensity (MFI) of intracellular oxidative stress stained by CellROX Deep Red Reagent in IM. D) Violin plot representing Cytokine Signaling module score of total cells from each group. E) Split violin plots representing *CTSG* expression for each cluster. Significance for bar plots was calculated using t-test with Welch's correction. Significant for violin plots was calculated using Mann-Whitney test. *=p<0.05, ****=p<0.0001.

SUPPLEMENTARY TABLES:

Supp. Table 1.1: Characteristics of animal cohort and samples used for each assay

Supp. Table 1.2: Immune mediator production by AM following LPS or RSV stimulation

Supp. Table 1.3: Genes associated with each scRNA-Seq cluster

Supp. Table 1.4: Module Scoring gene lists

Supp. Table 1.5: edgeR and Homer analyses

CHAPTER 2:

Transcriptional, epigenetic, and functional reprogramming of blood monocytes in non-human primates following chronic alcohol drinking

Sloan A. Lewis[1,2], Suhas Sureshchandra[1,2], Brianna Doratt[1,2], Vanessa A. Jimenez[3], Cara Stull[3], Kathleen A. Grant[3], Ilhem Messaoudi[1, 2]

[1] Department of Molecular Biology and Biochemistry, University of California, Irvine CA, USA
[2] Institute for Immunology, University of California, Irvine CA, USA
[3] Oregon National Primate Research Center, Oregon Health and Science University, Beaverton, OR, USA

*All supplemental tables can be accessed online with the published manuscript:
DOI: 10.3389/fimmu.2021.724015

ABSTRACT

Chronic heavy drinking (CHD) of alcohol is a known risk factor for increased susceptibility to bacterial and viral infection as well as impaired wound healing. Evidence suggests that these defects are mediated by a dysregulated inflammatory response originating from myeloid cells, notably monocytes and macrophages, but the mechanisms remain poorly understood. Our ability to study CHD is impacted by the complexities of human drinking patterns and behavior as well as comorbidities and confounding risk factors for patients with alcohol use disorders. To overcome these challenges, we utilized a translational rhesus macaque model of voluntary ethanol self-administration that closely recapitulates human drinking patterns and chronicity. In this study, we examined the effects of CHD on blood monocytes in control and CHD female macaques after 12 months of daily ethanol consumption. While monocytes from CHD female macaques generated a hyper-inflammatory response to ex vivo LPS stimulation, their response to E.Coli was dampened. In depth scRNA-Seq analysis of purified monocytes revealed significant shifts in classical monocyte subsets with accumulation of cells expressing markers of hypoxia (HIF1A) and inflammation (NFkB signaling pathway) in CHD macaques. The increased presence of monocyte subsets skewed towards inflammatory phenotypes was complemented by epigenetic analysis, which revealed higher accessibility of promoter regions that regulate genes involved in cytokine signaling pathways. Collectively, data presented in this manuscript demonstrate that CHD shifts classical monocyte subset composition and primes the monocytes towards a more hyper-inflammatory response to LPS, but compromised pathogen response.

INTRODUCTION

Alcohol consumption is widespread in the United States with 85% of individuals ages 18 and older engaging in this behavior. While most of these individuals are considered moderate drinkers, 7% are classified as heavy alcohol users (National Survey on Drug Use and Health, 2015). Chronic heavy alcohol consumption or chronic heavy drinking (CHD) is associated with multiple adverse health effects including increased incidence of cardiac disease (5, 6), certain types of cancer (7-10), liver cirrhosis (11), and sepsis (12), making it the third leading preventable cause of death in the United States (129). CHD is also associated with higher susceptibility to bacterial and viral infections including pneumonia and tuberculosis (14, 15), hepatitis C virus, and HIV (16, 17). Moreover, CHD compromises tissue repair, resulting in reduced post-operative healing and poor trauma recovery outcomes (18, 19). These observations strongly suggest that CHD dysregulates immunity and host defense.

While CHD can modulate the function of many immune cell populations, data from several laboratories indicate that the most dramatic and consistent changes are evident in the innate immune branch, specifically in myeloid cells (monocytes, macrophages, dendritic cells, and neutrophils) (13, 24, 25). Monocytes are relatively short-lived phagocytic cells that circulate in the blood, are constantly repopulated from bone marrow progenitors, and can quickly respond to infection or inflammation by extravasation into tissue and differentiation into tissue-resident macrophages (60). A tightly regulated inflammatory response by monocytes is required for effective infection clearance and tissue repair (61).

Alcohol consumption has been shown to disrupt monocyte and macrophage responses in a dose and time dependent manner (13). Specifically, acute alcohol treatment of purified primary human monocytes, rodent monocyte-derived macrophages, or human monocytic cell lines results in decreased production of inflammatory mediators including TNFα following stimulation with lipopolysaccharide (LPS), a TLR4 agonist (65-67). In rodents, acute in vivo (68) exposure to ethanol increases production of the anti-inflammatory cytokine IL-10 through activation of STAT3. Similarly, in healthy human subjects, an acute binge of alcohol increased IL-10 and decreased IL-1β production (69). In contrast, prolonged exposure to alcohol results in increased production of pro-inflammatory mediators, notably TNFα in response to LPS or phorbol myristate acetate (PMA)/ionomycin stimulation (66, 70) potentially due to enhanced activation of NFκB and ERK kinases (71). In line with these observations, monocytes as well as tissue resident macrophages, including Kupffer cells (130), microglia (131), alveolar macrophages (118), and splenic macrophages (24, 132) taken from patients with alcoholic liver disease (ALD) produce higher levels of TNF-α at resting state as well as in response to LPS (133). The enhanced inflammatory response by tissue-resident myeloid cells in the context of CHD is linked to organ damage, most notably in the liver (134) but also the intestine (135), brain (136, 137), and lungs (138).

Despite the studies described above, our understanding of the mechanisms by which chronic alcohol consumption reprograms circulating monocytes and tissue-resident macrophages remains incomplete. Some studies have suggested that CHD-induced gut "leakiness" and translocation of bacterial products including LPS across the gut barrier into the circulation could lead to chronic activation and subsequently organ damage (135). Whether monocytes in circulation are activated prior to organ damage by circulating

bacterial products, ethanol, ethanol metabolites, or a combination of these factors remains unanswered.

Data from clinical studies are confounded by self-reported alcohol intake, the use of nicotine, recreational or illicit drugs, nutritional deficiencies, and presence of organ damage (33). Addressing these questions requires access to a reliable animal model that recapitulates critical aspects of human CHD. Therefore, to better model human CHD and relate immune response of peripheral monocytes to quantified alcohol intakes in the absence of confounders listed above, we leveraged a rhesus macaque model of chronic voluntary ethanol self-administration (34, 35). Using this model, we reported that CHD disrupts the resting transcriptome and results in heightened inflammatory responses by peripheral blood mononuclear cells (PBMC) from male and female macaques (25, 113). Additionally, splenic macrophages from CHD monkeys generate a hyper-inflammatory response following LPS stimulation that is accompanied by increased chromatin accessibility at promoters and intergenic regions that regulate genes important for inflammatory responses (139).

In this study, we examine how CHD alters the ability of blood monocytes to respond properly to stimulation. We show that CHD is associated with increased numbers of circulating monocytes that exhibit a heightened transcriptional and immune mediator response to LPS stimulation, but lower response to bacterial pathogens. To determine the molecular mechanisms of this dysregulated response, we profiled the transcriptome of the monocytes by single cell RNA-Seq and their epigenetic landscape by ATAC-Seq. Our results indicate that CHD significantly alters the epigenetic and transcriptional profiles of circulating

monocytes, priming them towards an inflammatory state but altering their effector function to pathogens.

METHODS AND MATERIALS

Animal studies and sample collection:

These studies used samples from a non-human primate model of voluntary ethanol self-administration established through schedule-induced polydipsia (34, 35, 140). Briefly, in this model, rhesus macaques are introduced to a 4% w/v ethanol solution during a 90-day induction period followed by concurrent access to the 4% w/v solution and water for 22 hours/day for one year. During this time, the macaques adopt a stable drinking phenotype defined by the amount of ethanol consumed per day and the pattern of ethanol consumption (g/kg/day) (34). Blood samples were taken from the saphenous vein every 5-7 days at 7 hrs after the onset of the 22 hr/day access to ethanol and assayed by headspace gas chromatography for blood ethanol concentrations (BECs).

For these studies, blood samples were collected from 9 female and 3 male rhesus macaques (average age 5.68 yrs), with 5 animals serving as controls and 8 classified as chronic heavy drinkers (CHD) based on 12 months of ethanol self-administration (tissue and drinking data obtained from the Monkey Alcohol Tissue Research Resource: www.matrr.com). These cohorts of animals (Cohorts 6 and 7a on matrr.com) were described in two previous studies of innate immune system response to alcohol (25, 113). Peripheral Blood Mononuclear Cells (PBMC) were isolated by centrifugation over histopaque (Sigma, St Louis, MO) as per manufacturer's protocol and cryopreserved until they could be analyzed as a batch. The average daily ethanol intake for each animal is outlined in **Supp. Table 2.1**. CHD animals did not show signs of overt liver damage as measured by alanine transaminase (ALT) and aspartate transaminase (AST) enzyme levels (Supp. Figure 2G and (141)).

LAL and IgM assays:

Endotoxin-core antibodies in plasma samples were measured using an enzyme-immunoassay technique (ELISA) after 12 months of alcohol consumption using EndoCab IgM ELISA kit (Hycult Biotech, Catalog# HK504-IgM). Plasma samples were diluted 50x.

Circulating endotoxin was measured from plasma using a Limulus amebocyte lysate (LAL) assay (Hycult Biotech) following the manufacturers protocol.

Flow cytometry analysis:

1-2x10^6 PBMC were stained with the following surface antibodies (2 panels) against: CD3 (BD Biosciences,SP34, FITC), CD20 (Biolegend, 2H7, FITC), HLA-DR (Biolegend, L243, APC-Cy7), CD14 (Biolegend, M5E2, AF700), CD16 (Biolegend, 3G8, PB), TLR4 (Biolegend, HTA125, APC), TLR2 (Biolegend, TLR2.1, A488), CD40 (Biolegend, 5C3, BV510), CD163 (Biolegend, GHI/61, PerCp-Cy5.5), CD86 (Biolegend, IT2.2, BV605), CD80 (Biolegend, 2D10, PE), CX3CR1 (Biolegend, 2A9-1, PE), CCR7 (Biolegend, GO43H7, BV510), and CCR5 (Biolegend, J418F1, PE-Cy7) and live/dead Sytox Aadvanced (Invitrogen). Monocytes were defined as CD3-CD20-HLA-DR+CD14+. All samples were acquired with an Attune NxT Flow Cytometer (ThermoFisher Scientific, Waltham, MA) and analyzed using FlowJo software (Ashland, OR). Median Fluorescence Intensities (MFI) for all markers within the CD14+ monocyte gate were tested for significant differences using an unpaired t-test with Welch's correction on Prism 7 (GraphPad, San Diego, CA).

CD14 MACS bead Isolation and Purity:

CD14+ monocytes were purified from freshly thawed PBMC using CD14 antibodies conjugated to magnetic microbeads per manufacturers recommendations (Milyenyi Biotec, San Diego, CA). Efficiency of the positive selection of monocytes was assessed by flow cytometry where purity (CD14+HLA-DR+) averaged 87% (SEM ± 1.6).

Monocyte Stimulation Assays:

$1x10^6$ freshly thawed PBMC or $1x10^5$ purified CD14+ monocytes were cultured in RPMI supplemented with 10% FBS with or without 100 ng/mL LPS (TLR4 ligand, E.coli 055:B5; Invivogen, San Diego CA) for 16 or 6 hours, respectively, in 96-well tissue culture plates at 37C in a 5% CO_2 environment. $3.5x10^4$ purified CD14+ monocytes were cultured in RPMI supplemented with 10% FBS with or without $6x10^5$ cfu/mL heat-killed E.coli (Escherichia coli (Migula) Castellani and Chalmers ATCC 11775) for 16 hours in 96-well tissue culture plates at 37C in a 5% CO_2 environment. Plates were spun down: supernatants were used to measure production of immune mediators and cell pellets were resuspended in Qiazol (Qiagen, Valencia CA) for RNA extraction. Both cells and supernatants were stored at -80C until they could be processed as a batch.

Luminex Assay:

Immune mediators in the supernatants from PBMC or purified monocytes stimulated with LPS were measured using a 30-plex panel measuring levels of cytokines (IFNγ, IL-1b, IL-2, IL4, IL-6, IL-7, IL-12, IL-15, IL-17, IL-18, IL-23, TNFα, IL-1RA, IFN-b, and IL-10), chemokines (CCL2(MCP-1), CCL3(MIP-1α), CCL4(MIP-1β), CCL11(Eotaxin), CXCL8(IL-8), CXCL9(MIG), CXCL11(I-TAC), CXCL13(BCA-1), CXCL10(IP-10), and CXCL12(SDF-1a)), and other factors (PD-L1, PDGF-BB, S100B, GM-CSF, and VEGF-A) validated for NHP (R&D Systems,

Minneapolis, MN, USA). Standard curves were generated using 5-parameter logistic regression using the xPONENT™ software provided with the MAGPIX instrument (Luminex, Austin TX).

Immune mediators in the supernatants from monocytes stimulated with E.coli were measured using a more sensitive ProcartaPlex 31-plex panel measuring levels of cytokines (IFNα, IFNγ, IL-1β, IL-10, IL-12p70, IL-15, IL-17A, IL-1RA, IL-2, IL-4, IL-5, IL-6, IL-7, MIF, and TNFα), chemokines (CXCL13(BLC), CCL11(Eotaxin), CXCL11(I-TAC), CXCL8(IL-8), CXCL10(IP-10), CCL2(MCP-1), CXCL9(MIG), CCL3(MIP-1α), CCL4(MIP-1β))), growth factors (BDNF, G-CSF, GM-CSF, PDGF-BB, VEGF-A) and other factors (CD40L, Granzyme B) (Invitrogen, Carlsbad, CA). Differences in induction of proteins post stimulation were tested using unpaired t-tests with Welch's correction. Dose-dependent responses were modeled based on g/kg/day ethanol consumed and tested for linear fit using regression analysis in Prism (GraphPad, San Diego CA). Raw data included in **Supp. Table 2.2**.

RNA isolation and library preparation:

Total RNA was isolated from PBMC or purified CD14+ monocytes from female macaques using the mRNeasy kit (Qiagen, Valencia CA) following manufacturer instructions and quality assessed using Agilent 2100 Bioanalyzer. Libraries from PBMC RNA were generated using the TruSeq Stranded RNA LT kit (Illumina, San Diego, CA, USA). Libraries from purified CD14+ monocytes RNA were generated using the NEBnext Ultra II Directional RNA Library Prep Kit for Illumina (NEB, Ipswitch, MA, USA), which allows for lower input concentrations of RNA (10ng). For both library prep kits, rRNA depleted RNA was fragmented, converted to double-stranded cDNA and ligated to adapters. The roughly 300bp-long fragments were

then amplified by PCR and selected by size exclusion. Libraries were multiplexed and following quality control for size, quality, and concentrations, were sequenced to an average depth of 20 million 100bp reads on the HiSeq 4000 platform.

Bulk RNA-Seq data analysis:

RNA-Seq reads were quality checked using FastQC (https://www.bioinformatics.babraham.ac.uk/projects/fastqc/), adapter and quality trimmed using TrimGalore(https://www.bioinformatics.babraham.ac.uk/projects/trim_galore/), retaining reads at least 35bp long. Reads were aligned to Macaca mulatta genome (Mmul_8.0.1) based on annotations available on ENSEMBL (Mmul_8.0.1.92) using TopHat (142) internally running Bowtie2 (143). Aligned reads were counted gene-wise using GenomicRanges (144), counting reads in a strand-specific manner. Genes with low read counts (average <5) and non-protein coding genes were filtered out before differential gene expression analyses. Read counts were normalized using RPKM method for generation of PCA and heatmaps. Raw counts were used to test for differentially expressed genes (DEG) using edgeR (103), defining DEG as ones with at least two-fold up or down regulation and an FDR controlled at 5%. Functional enrichment of gene expression changes in resting and LPS-stimulated cells was performed using Metascape (104) and DAVID (145). Networks of functional enrichment terms were generated using Metascape and visualized in Cytoscape (146). Transcription factors that regulate expression of DEG were predicted using the ChEA3 (114) tool using ENSEML ChIP database.

10X scRNA-Seq data analysis:

PBMC from control (n=3) and CHD (n=3) female macaques were thawed and stained with anti-CD14, HLA-DR antibodies and sorted for live CD14+/HLA-DR+ cells on a BD FACSAria Fusion on the same day. Sorted monocytes were pooled and resuspended at a concentration of 1200 cells/ul and loaded into the 10X Chromium gem aiming for an estimated 10,000 cells per sample. cDNA amplification and library preparation (10X v3 chemistry) were performed according to manufacturer protocol and sequenced on a NovaSeq S4 (Illumina) to a depth of >50,000 reads/cell.

Sequencing reads were aligned to the Mmul_8.0.1 reference genome using cellranger v3.1 (147) (10X Genomics). Quality control steps were performed prior to downstream analysis with Seurat, filtering out cells with fewer than 200 unique features and cells with greater than 20% mitochondrial content. Control and CHD datasets were down sampled to 4680 cells each and integrated in Seurat (148) using the IntegrateData function. Data normalization and variance stabilization were performed, correcting for differential effects of mitochondrial and cell cycle gene expression levels. Clustering was performed using the first 20 principal components. Small clusters with an over-representation of B and T cell gene expression were removed for downstream analysis. Clusters were visualized using uniform manifold approximation and projection (UMAP) and further characterized into distinct monocyte subsets using the FindMarkers function (**Supp. Table 2.3**).

Pseudo-temporal analysis:

Pseudotime trajectory monocytes was reconstructed using Slingshot (107). The UMAP dimensional reduction performed in Seurat was used as the input for Slingshot. For

calculation of the lineages and pseudotime, the most abundant classical monocyte cluster, MS1, was set as the root state.

Differential expression analyses:

Differential expression analysis (CHD to Control) was performed using DESeq under default settings in Seurat. Only statistically significant genes (Fold change cutoff ≥ 1.2; adjusted p-value ≤ 0.05) were included in downstream analysis.

Module Scoring and functional enrichment:

For gene scoring analysis, we compared gene signatures and pathways from KEGG (https://www.genome.jp/kegg/pathway.html) (Supp. Table 4) in the monocytes using Seurat's AddModuleScore function. Over representative gene ontologies were identified using 1-way, 2-way or 4-way enrichment of differential signatures using Metascape (104). All plots were generated using ggplot2 and Seurat.

ATAC-Seq library preparation:

Following the Omni-ATAC protocol, $2x10^4$ purified monocytes from female macaques were lysed in lysis buffer (10mM Tris-HCl (pH 7.4), 10mM NaCl, 3mM $MgCl_2$, 10% Np-40, 10% Tween, and 1% Digitonin) on ice for 3 minutes (149). Immediately after lysis, nuclei were spun at 500 g for 10 minutes at 4C to remove supernatant. Nuclei were then incubated with Tn5 transposase for 30 minutes at 37C. Tagmented DNA was purified using AMPure XP beads (Beckman Coulter, Brea, CA) and PCR was performed to amplify the library under the following conditions: 72C for 5 min; 98 for 30s; 5 cycles of 98C for 10s, 63C for 30s, and 72C for 1min; hold at 4C. Libraries were then purified with warm AMPure XP beads and

quantified on a Bioanalyzer (Agilent Technologies, Santa Clara CA). Libraries were multiplexed and sequenced to a depth of 50 million 100bp paired reads on a NextSeq (Illumina).

ATAC-Seq data analysis:

Paired ended reads from sequencing were quality checked using FastQC and trimmed to a quality threshold of 20 and minimum read length 50. Trimmed reads were aligned to the Macaca Mulatta genome (Mmul_8.0.1) using Bowtie2 (-X 2000 -k 1 --very-sensitive --no-discordant --no-mixed). Reads aligning to mitochondrial genome were removed using Samtools and PCR duplicate artifacts were removed using Picard. Samples from each group were concatenated to achieve greater than $5x10^6$ non-duplicate, non-mitochondrial reads per group.

Accessible chromatin peaks were called using Homer's findPeaks function (105) (FDR<0.05) and differential peak analysis was performed using Homer's getDifferentialPeaks function ($P < 0.05$). Genomic annotation of open chromatin regions in monocytes and differentially accessible regions (DAR) with CHD was assigned using ChIPSeeker (150). Promoters were defined as -1000bp to +100bp around the transcriptional start site (TSS). Functional enrichment of open promoter regions was performed using Metascape (http://metascape.org).

Due to the lack of available macaque annotation databases, distal intergenic regions from the macaque assembly were converted to the human genome (hg19) coordinates using the UCSC liftOver tool. Cis-Regulatory roles of these putative enhancer regions were identified using GREAT (http://great.stanford.edu/public/html/). Transcription factor motif analysis was

performed using Homer's findMotifs function with default parameters. Promoter regions for every annotated macaque gene were defined in ChIPSeeker as -1000bp to +100bp relative to the TSS. A counts matrix was generated for these regions using featureCounts (151), where pooled bam files for each group were normalized to total numbers of mapped reads.

Statistical Analysis:

All statistical analyses were conducted in Prism 7(GraphPad). Data sets were first tested for normality. Two group comparisons were carried out an unpaired t-test with Welch's correction. Differences between 4 groups were tested using one-way ANOVA (α=0.05) followed by Holm Sidak's multiple comparisons tests. Error bars for all graphs are defined as $\pm$ SEM. Linear regression analysis compared significant shifts in curve over horizontal line, with spearman correlation coefficient reported. Statistical significance of functional enrichment was defined using hypergeometric tests. P-values less than or equal to 0.05 were considered statistically significant. Values between 0.05 and 0.1 are reported as trending patterns.

RESULTS:

Chronic heavy drinking results in enhanced responses to LPS by PBMC

Recent bulk RNA seq analysis of resting PBMC obtained from female rhesus macaques after 12 months of chronic heavy drinking (CHD) indicated that most of the differential gene expression originated from innate immune cells (monocytes and dendritic cells (DCs)) (25). Moreover, studies using PBMC from male macaques showed increased responses to ex vivo LPS stimulation after 12 months of chronic heavy ethanol consumption (113). To assess if CHD also led to changes in inflammatory responses by circulating innate immune cells in female macaques, PBMC obtained from CHD (n=6) and control (n=3) females were stimulated ex vivo with LPS for 16 hours followed by measurement of immune mediator production by Luminex assay and transcriptional changes by bulk RNA Seq (Supp. Figure 1A). LPS stimulation resulted in a robust inflammatory response (TNFα, IL-6, IL-18, IL-4, IL-8, GMCSF and S100B) by PBMC from both CHD and control animals (**Figure 2.1A**). However, PBMC from CHD animals produced significantly elevated levels of additional inflammatory mediators notably IL-1β, IL-12, IFNγ, CCL3, and CCL4 compared to their unstimulated condition (**Figure 2.1A**). Moreover, production of inflammatory cytokines IL-6, IL-23 and to lesser extent soluble PD-L1 was higher by CHD PBMC following LPS stimulation compared to controls (**Figure 2.1A**). In addition, levels of TNFα, CCL4, IL-6, IL-15, IL-23, and sPD-L1 were positively correlated with ethanol dose (**Figure 2.1B and Supp. Figure 2.1B**).

We next assessed transcriptional differences in response to LPS between the two groups. Differential analysis indicated a heightened response to LPS by CHD PBMC relative to control PBMC (**Figure 2.1C**). While signatures of immune activation were observed in both groups

following LPS stimulation, DEGs upregulated in PBMC from controls enriched more significantly to pathways involved in antiviral immunity ("response to IFNg" and "response to virus"), whereas DEGs upregulated in PBMC from CHD animals enriched more significantly to leukocyte activation and inflammation pathways (**Figure 2.1D and Supp. Figure 2.1C**). Enrichment of the downregulated genes shows significant enrichment to GO terms associated with chemotaxis, leukocyte differentiation and metabolism in the PBMC from control animals (**Figure 2.1E and Supp. Figure 2.1D**). These findings indicate disruption of innate immune responses with CHD and further highlight that the heightened inflammatory response to LPS by PBMC is not restricted to male macaques.

Chronic heavy drinking impacts monocyte frequencies and functional responses to LPS stimulation

To measure changes in frequencies and phenotypes of monocyte subsets with CHD in female macaques, we profiled PBMC by flow cytometry. Interestingly, while the total white blood cell numbers were unchanged with CHD (25), the proportions of monocytes within PBMC from CHD macaques were significantly elevated (**Figure 2.2A**). However, the relative distribution of the monocyte sub-populations was comparable between the groups (**Supp. Figure 2.2A, B**). We profiled several TLRs, chemokine, and activation receptors on monocytes by flow cytometry, but found no significant differences (**Supp. Figure 2.2C**). To assess whether the heightened inflammatory response detected in PBMC was due to increased numbers of monocytes or cell-intrinsic changes caused by CHD, monocytes were purified from each group and subjected to bulk RNA-Seq at resting state and after LPS stimulation (**Supp. Figure 2.1A**). A modest number of DEG were detected at resting state

(58 upregulated and 112 downregulated) between CHD and control monocytes (**Figure 2.2B**). The DEG upregulated with CHD enriched to pathways associated with inflammatory response such as "pattern recognition receptor activity" (e.g. *NLRP3*) and "cytokine production" (e.g. *FCN1*) (**Figure 2.2C, and Supp. Figure 2.2D**). DEG downregulated with CHD mapped to gene ontology (GO) terms "activation of immune response" (e.g. *IFNG*) "lymphocyte proliferation" (e.g. *HSPD1*) and "chemotaxis" (e.g. *CCR7*) (**Figure 2.2C**). One potential mechanism for this enhanced monocyte transcriptional activation at resting state could be increased microbial products in circulation due to altered barriers (31). Therefore, we measured circulating levels of bacterial endotoxin (LAL) and IgM bound endotoxin. We found slightly increased levels of circulating LAL with CHD, but no changes in IgM-bound endotoxin (**Supp. Figure 2.2E,F**). Additionally, levels of alanine transaminase (ALT) and aspartate transaminase (AST) levels, both of which are indicators of liver damage, were also comparable between the two groups (**Supp. Figure 2.2G**).

Secreted levels of cytokines, chemokines, and growth factors were measured after 6-hour incubation in the presence or absence of LPS by Luminex assay. No significant differences in immune mediators' secretion were noted in the non-stimulated conditions. As observed for PBMC, significantly enhanced production of pro-inflammatory cytokines TNFα, IL-6, and IL-15, chemokines CCL4, and CXCL11, and to a lesser extent IL-4 and IL-7 by CHD monocytes were noted (**Figure 2.2D and Supp. Figure 2.3A**). The LPS response was also assessed at the transcriptional level using RNA-Seq. Principal component analysis (PCA) showed that stimulation accounts for the bulk of the transcriptional changes (PC1, 75% of the differences) (**Supp. Figure 2.3B**) with 357 and 262 DEG between CHD and controls in the NS, and LPS conditions, respectively (**Supp. Figure 2.3C, D**). The DEG from these comparisons showed

that genes associated with myeloid inflammatory pathways were upregulated (*TNFSF21*, *MMP2*, *TLR2*, *MMP1*) while genes associated with adaptive immune activation were downregulated (*IL21R, CD40*, *MAMU-DOA, CCR6*) in CHD compared to control monocytes (**Supp. Figure 2.3C, D**).

We then identified DEG in the LPS relative to NS condition for each group. A greater number of DEG was detected in the CHD group, with a large overlap between the two groups, and few DEG detected solely in the control group (**Figure 2.2E**). As expected, DEG common between the two groups enriched to GO terms associated with monocyte activation including "regulation cytokine production", "leukocyte migration", and "JAK-STAT cascade" (**Figure 2.2F**). The DEG detected only in control animals mapped to "Carbohydrate catabolic process". The DEG unique to monocytes from CHD animals mapped to cytokine production and signaling pathways (**Figure 2.2F**). The expression of inflammatory genes was broadly upregulated in the CHD monocytes following LPS stimulation including *CEBPB, CCL20, CCL4, STAT3, FOS, S100A8, HIF1A*, and *TLR4* (**Figure 2.2G**). Additional predictive analysis revealed that LPS-responsive DEGs detected in the CHD monocytes are regulated by canonical transcription factors NFKB2, RELB, and JUNB with over 250 genes mapping to each (**Supp. Figure 2.3E**).

Chronic heavy drinking alters the monocyte transcriptome and cell subset distribution at the single cell level

To gain a deeper understanding of the heightened activation state of monocytes with CHD, we performed single cell RNA sequencing (scRNA-Seq) on sorted CD14+HLA-DR+ monocytes from CHD and control female macaques (n=3 pooled samples/group). UMAP

clustering of all 9,360 monocytes revealed 9 distinct monocyte subsets (MS) (**Figure 2.3A**). These clusters could be categorized into the three major monocyte subtypes typically identified by flow cytometry: non-classical, intermediate, and classical based on expression of *CD14, MAMU-DRA*, and *FCGR3*(CD16) (**Supp. Figure 2.4A**). As shown by flow cytometry, the frequency of these three major subsets was comparable between controls and CHD animals by scRNA-Seq analysis (**Supp. Figure 2.4B**). The non-classical monocytes formed one cluster (MS6) exhibiting high expression of *CX3CR1, MS4A7*, and *FCGR3* and lower expression of *CD14* and MHC II molecule *MAMU-DRA* (**Figure 2.3A, B, and Supp. Figure 2.4C**). The intermediate monocytes also fell into one cluster (MS4), expressing lower levels of non-classical (*MS4A7, FCGR3*) and classical (*CD14, S100A8*) markers with higher expression of MAMU-DRA (**Figure 2.3A, B, and Supp. Figure 2.4C**). Finally, 7 clusters of classical monocytes were identified (MS1, MS2, MS3, MS5, MS7, MS8, and MS9), based on expression of *CST3, GOS2, S100A8, S100A9, HIF1A, SOD2, EGR1*, and *HERC5* (**Figure 2.3A, B, and Supp. Figure 2.4C).** These data reveal considerable, previously unappreciated transcriptional heterogeneity within the classical monocytes. Subsets MS5, MS7 were primarily detected in monocytes from CHD animals while MS8 was primarily detected in monocytes from control animals (**Figure 2.3 and Supp. Figure 2.4D**). Module scoring revealed that MS5 had the lowest expression of genes that play a role in antigen presentation as well as hypoxia, while MS5 and MS7 had higher expression of genes within the TLR- and IL-6- signaling pathways (**Supp. Figure 2.4E**).

To identify the biological implications of these subsets, we extracted the genes that define each cluster and performed functional enrichment (**Figure 2.3C**). Although genes that define MS5 (classical – CHD) and MS8 (classical – control) subsets enriched to similar GO terms

("Regulated exocytosis", "granulocyte activation/migration"), only genes highly expressed in MS5 (CHD animals) enriched to "Response to alcohol" and "Wound healing", notably FOSB, HIF1A, and FN1. Interestingly, genes that define MS7 subset (classical – CHD) enriched to "Cytokine-mediated signaling pathway" including *CSF3R, IRF1, IRF7, NFKBIA, STAT1, STAT3,* and *VEGFA*. Classical subsets MS1 and MS2 were slightly more abundant in monocytes from control animals and expressed high levels of *CST3* and *GOS2* as well as *S100A8* and *S100A9*, respectively.

To better understand the relationships between the classical monocyte clusters and their differentiation/activation states, we performed a trajectory analysis. The monocyte clusters were ordered by pseudotime, starting with the most abundant MS1 cluster which resulted in four unique trajectory lineages (**Figure 2.3D**). Lineages 1, 2 and 4 indicate transitions culminating in MS8, MS3, and MS5, respectively. Lineage 3 is the classical to non-classical differentiation trajectory. Density plots revealed enrichment of control monocytes at the start of each lineage (less differentiated) and enrichment of the CHD monocytes at the end of the lineages (more differentiated), most notably in Lineage 4 (**Figure 2.3E**).

We next assessed differential gene expression with CHD in the 3 major subsets (**Supp. Figure 2.4F**). This analysis showed that IFN-inducible genes *WARS* and *IDO* were upregulated in the classical CHD monocytes, whereas MHC-II gene *MAMU-DRB1* was downregulated (**Supp. Figure 2.4F**). In the intermediate monocytes, CHD induced upregulation of inflammatory signaling genes *MAP3K* and *S100P* but led to decreased expression of FC-receptor gene *FCGR3* (**Supp. Figure 2.4F**). The 33 DEG downregulated in the non-classical monocytes from the CHD group relative to controls enriched to antigen

processing and IFNγ signaling pathways (**Supp. Figure 2.4G**). Finally, we detected a significant reduction in lysosome and Fcg-receptor mediated phagocytosis modules in the CHD monocytes (**Figure 2.3F**) while gene modules for NFkB signaling and HIF1A signaling were increased (**Figure 2.3G**).

Chronic heavy drinking impacts the epigenome of circulating monocytes

To uncover epigenetic basis for the altered transcriptional profile in resting monocytes and altered functional responses with CHD, we profiled the chromatin accessibility in purified resting monocytes from female macaques (n=3/group) using the assay for transposase-accessible chromatin sequencing (ATAC-Seq) (149). We identified 11,717 differentially accessible regions (DAR) that were open in the CHD monocytes compared to 9,173 DAR that were accessible in the controls (**Figure 2.4A**). More than 25% of the accessible regions in the CHD monocytes mapped to promoter regions and were closer to the transcription start site compared to accessible regions in monocytes from control animals (**Figure 2.4A and Supp Figure 2.5A**). Genes regulated by promoter regions open in the CHD monocytes enriched to GO terms associated with cytokine production and myeloid cell activation (**Figure 2.4B**). Additional analysis using GREAT showed that cis-regulatory elements in the distal intergenic regions open in CHD monocytes enriched to processes involved with apoptotic signaling, MAPK signaling cascade, and myeloid cell differentiation (**Supp Figure 2.5B**). Motif enrichment analysis of open chromatin regions in the CHD and control monocytes demonstrated increased putative binding sites for transcription factors important for monocyte differentiation and activation SP1, FRA1, FOS, JUNB, BATF, and PU.1 with CHD (152-156)(**Figure 2.4C**). To link the resting epigenome of the CHD monocytes to

the enhanced transcriptional response after LPS stimulation, we compared the genes associated with the open promoter regions (<1kb) and the DEG identified after LPS stimulation and identified 281 common genes (**Figure 2.4D**). Functional enrichment of these genes showed significant mapping to Biological Process "Cytokine-mediated signaling" including transcription factors *FOS, HIF1A, STAT3* and *JUNB* (**Figure 2.4E**). These genes as well as inflammatory *CCL20, TLR2, CD81* and *TNFSF14* had both open promoters in the resting CHD monocytes as well as upregulated gene expression in the LPS-stimulated CHD monocytes, linking open chromatin under resting conditions with CHD to transcriptional LPS responses (**Figure 2.4F**).

CHD impairs monocyte response to E. coli

We next asked whether CHD would affect the monocyte response to pathogens. Monocytes from male and female macaques (n=3 controls; n=6 CHD) were co-cultured with heat-killed E. coli for 16 hours and immune mediator production was measured using Luminex (**Supp. Figure 2.1A**). In contrast to the response to purified LPS, monocytes from CHD animals generated a dampened response to E. coli characterized by reduced levels of IL-1b, IL-6, CCL4 (MIP-1β), and IL-15 and to a lesser extent I-TAC and IL-5 compared to their control counterparts (**Figure 2.5 A, B**). No sex differences were noted in these assays, indicating that defects in monocyte responses to bacterial pathogens are comparable in male and female macaques. Moreover, these data suggests that CHD differentially impacts pathogen recognition and activation pathways within monocyte.

DISCUSSION:

It is well-appreciated that chronic alcohol drinking exerts a profound impact on peripheral innate immune cells. However, the limitations provided by the complexity of studying alcohol consumption in humans has left major gaps in understanding mechanisms that underlie the immune response under conditions of heavy alcohol drinking. In this study, we utilized a macaque model of voluntary ethanol self-administration to profile peripheral monocytes in animals after 12 months of daily alcohol drinking. We first demonstrated that circulating monocytes from CHD animals generate a hyper-inflammatory response to ex vivo LPS stimulation at the transcript and protein level. A comprehensive profiling of the monocytes by scRNA-Seq and ATAC-Seq revealed alterations in differentiation state as well as epigenetic landscape with CHD. In contrast to what we observed following ex vivo stimulation with LPS, monocytes from CHD animals generated a dampened production of immune mediators following *ex vivo* E. *coli* stimulation. This highlights critical aspects of the complexity of immune cell responses and the necessity of utilizing both purified stimulants as well as real pathogens to uncover the underlying mechanisms of response.

The enhanced inflammatory responses in response to *ex vivo* stimulation with LPS by PBMC from CHD female macaques are in line with our previous data for PBMC from CHD male macaques (113), indicating that this consequence of CHD is sex independent. Our follow up phenotyping revealed that there were in fact more CD14+ monocytes in the PBMC of CHD animals, but no changes were observed in the distribution of classical, non-classical, and intermediate monocyte populations. Further analysis of purified monocytes indicated that this hyper-inflammatory response is mediated largely by intrinsic changes within monocytes and not just increased cell numbers. Indeed, CHD induced significant

transcriptional differences consistent with activation of inflammatory pathways in monocytes at resting state. Moreover, LPS stimulation resulted in a drastic increase in numbers of DEG from the CHD monocytes with increased expression of genes associated with inflammatory response. In contrast, genes involved in carbohydrate catabolic processes were not upregulated in monocytes from CHD animals suggesting metabolic rewiring associated with a heightened inflammatory state (157). The increased non-specific inflammatory mediator production in response to *ex vivo* LPS stimulation are in line with previous in vitro studies that have reported hyper-activation of myeloid cells with prolonged alcohol exposure. This also fits with hyper-inflammatory phenotypes associated with patients with alcohol use disorders, especially those with alcoholic liver disease (4, 13, 71).

To elucidate the molecular basis for this dysregulated inflammatory response, we profiled monocytes from CHD and control animals by scRNA-Seq. This analysis revealed tremendous diversity amongst classical monocytes that has not been previously appreciated. We identified two unique classical clusters within monocytes from CHD animals expressing high levels of hypoxia factor *HIF1A* (MS5), and antioxidant defense molecule *SOD2* (MS7). Alcohol and the products of its metabolism can induce oxidative stress which can alter cellular transcriptional profiles, potentially explaining the profile of the MS5 cluster (63). CHD animals also had a higher number of cells within the anti-viral cluster MS9 that expressed high levels of interferon stimulated (ISG) genes such as *HERC5*. This observation is in line with our earlier study that reported higher levels of ISG within PBMC from these same animals (25). Functional module scoring of all the monocytes revealed downregulation of genes involved in lysosome function and Fcg receptor mediated phagocytosis, but upregulation of NFkB signaling and HIF1A signaling. Moreover, trajectory within the

monocyte subsets revealed that CHD accelerates differentiation/activation of classical monocyte subsets making them potentially poised towards a hyper-inflammatory response.

Although the non-classical and intermediate monocytes fell into single clusters with equal numbers of cells from controls and CHD animals, differential gene expression analysis revealed significant downregulation of genes associated with MHC class II, antigen processing and presentation, and IFNg signaling pathways in the CHD monocytes. This observation provides a potential explanation for the reduced response to vaccination observed in CHD animals (158). Further, monocytes from CHD male and female macaques generated a dampened cytokine and chemokine response to heat killed E. coli. This was an unexpected outcome since stimulation with LPS resulted in a heightened inflammatory response and suggests a rewiring of monocytes with CHD towards non-specific inflammatory responses and away from anti-microbial functions. This discrepancy could be explained by the fact that LPS signals exclusively through TLR4, whereas heat killed E. coli could trigger a number of TLRs including TLR2/6 (159). Additionally, CHD interferes with phagocytosis and ROS production in macrophages (55), which could interfere with pathogen sensing. While the mechanisms underlying the differences between the heightened response to LPS and dampened response to whole organisms is complex and require further study, our observations provide potential explanation for the reported increased susceptibility of patients with alcohol use disorders to bacterial infections (14, 15).

Ethanol metabolites notably acetaldehyde and acetate in addition to minor byproducts such as reactive oxygen species (ROS) and lipid metabolism products can modulate gene expression by binding transcription factors and/or modifying chromatin

accessibility (63). Therefore, we profiled chromatin accessibility of monocytes from control and CHD animals by ATAC-Seq. We discovered that promoter regions that regulate genes important for cytokine production and myeloid cell activation were more accessible in monocytes from CHD animals. These open regions contained putative binding sites for transcription factors important for monocyte activation and differentiation. Integrative analyses showed correlation between chromatin accessibility and expression levels of key inflammatory genes in CHD monocytes, including *FOS, HIF1A*, and *JUNB*. This suggests that the monocytes are poised epigenetically towards heightened inflammatory responses.

One proposed mechanism of this hyper-inflammatory state in monocytes (134, 136-138) and macrophages with CHD is the translocation of bacterial products into circulation through impaired gut barrier caused by ethanol consumption (135). We detected modestly elevated levels of LAL in circulation but no changes in IgM bound endotoxin. A small increase in these circulating bacterial products could significantly impact the activation state of monocytes; however, it is difficult to tease these effects out from circulating ethanol and its metabolic products (acetaldehyde, acetate). Additionally, liver enzyme levels remained within normal ranges for the duration of the study. Long term exposure to activating agents, like LPS, is believed to lead to tolerance and a decreased response to secondary stimulation in monocytes and macrophages defined by specific changes in chromatin structure (22, 160-162). Interestingly, we see enhanced inflammatory responses of monocytes and macrophages from CHD animals with LPS, akin to innate immune training (125, 163). Indeed, ethanol and its metabolites have been found to directly act on histone modifications, creating changes in accessible chromatin (63, 164, 165). This could be occurring in circulating monocytes, tissue macrophages, or the progenitors of these cells in the bone marrow;

perhaps on all three levels, altering the epigenetic structure and therefore functional capacities of these cells (75). In fact, observations in patients with alcohol use disorders suggest an effect of alcohol on hematopoiesis (166). Because blood monocytes are under constant repopulation from bone marrow progenitors, it is conceivable that the progenitors themselves or the process of myelopoiesis are disrupted with CHD.

In summary, this study provides a novel, in-depth, and integrative analysis of the effects of long-term in vivo alcohol drinking on monocytes in non-human primates. Our findings indicate that alcohol drinking alters the baseline epigenetic and transcriptional states of monocytes, which is associated with heightened inflammatory responses but reduced anti-microbial activity. Future studies will focus on linking epigenetic modifications to functional outcomes and investigating the impact of alcohol drinking on bone marrow progenitors.

Acknowledgements

We are grateful to the members of the Grant laboratory for expert animal care and sample procurement. We thank Dr. Jennifer Atwood for assistance with sorting in the flow cytometry core at the Institute for Immunology, UCI. We thank Dr. Melanie Oakes from UCI Genomics and High-Throughput Facility for assistance with 10X library preparation and sequencing.

Data availability

The datasets supporting the conclusions of this article will be available on NCBI's Sequence Read Archive upon publication (SRA# PRJNA723053).

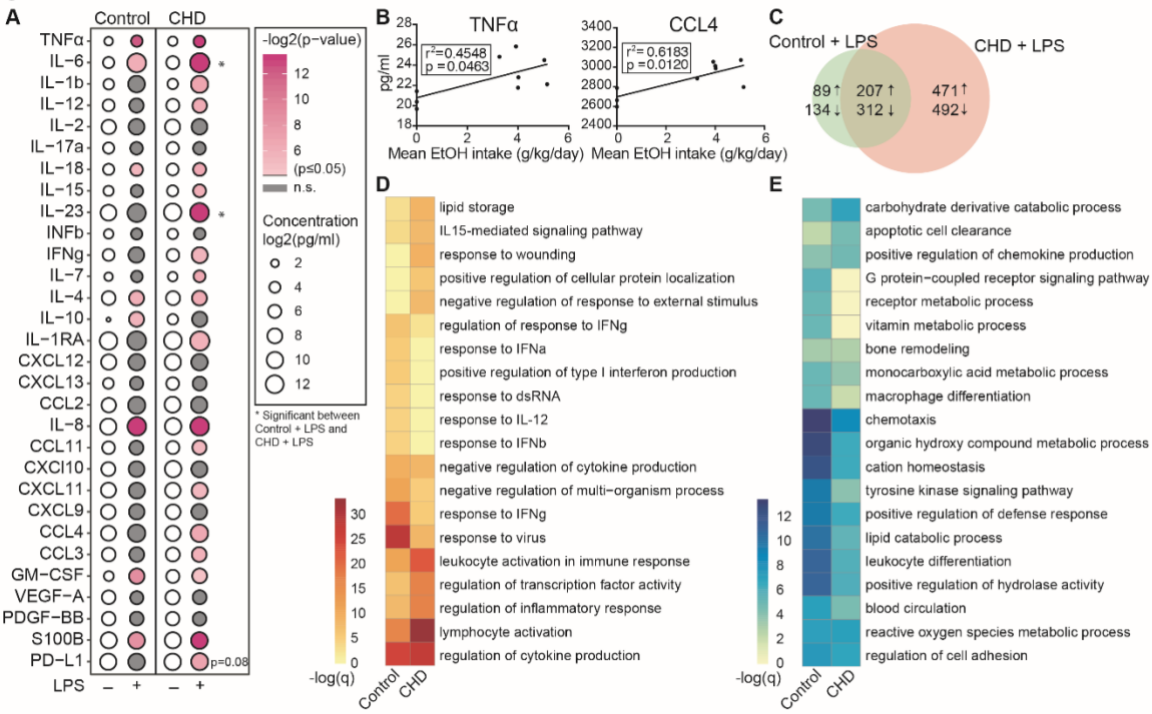

Figure 2.1: CHD induced enhanced innate immune response in the periphery

PBMC from control (n=3) and chronic heavy drinking (CHD) (n=6) female macaques were stimulated with LPS for 16 hours. A) Bubble plot representing immune factor production (pg/ml) in the presence or absence of LPS stimulation of PBMC from control and CHD animals. The size of each circle represents the $\log_2$ mean concentration of the indicated secreted factor and the color denotes the $-\log_2$ transformed p value with the darkest pink representing the most significant value. The p-values were calculated between the unstimulated and stimulated conditions for each group by One-way ANOVA and a p-value cut-off of 0.05 was set. White circles indicate non-significant p-value. * Indicates significance between control and CHD for each stimulation condition. B) Scatter plots showing Spearman correlation between average EtOH dose (grams EtOH/kg body weight/day) and concentration (pg/ml) of the secreted factors TNFα and CCL4. C) Venn diagram comparing LPS-induced DEG in controls and CHD PBMC. D, E) Heatmaps of significant GO terms to which upregulated (D) and downregulated (E) DEG identified following LPS stimulation of PBMC from controls and CHD animals enriched using Metascape. The scales of the heatmaps are -log(q-values) associated with the enrichment to selected pathways.

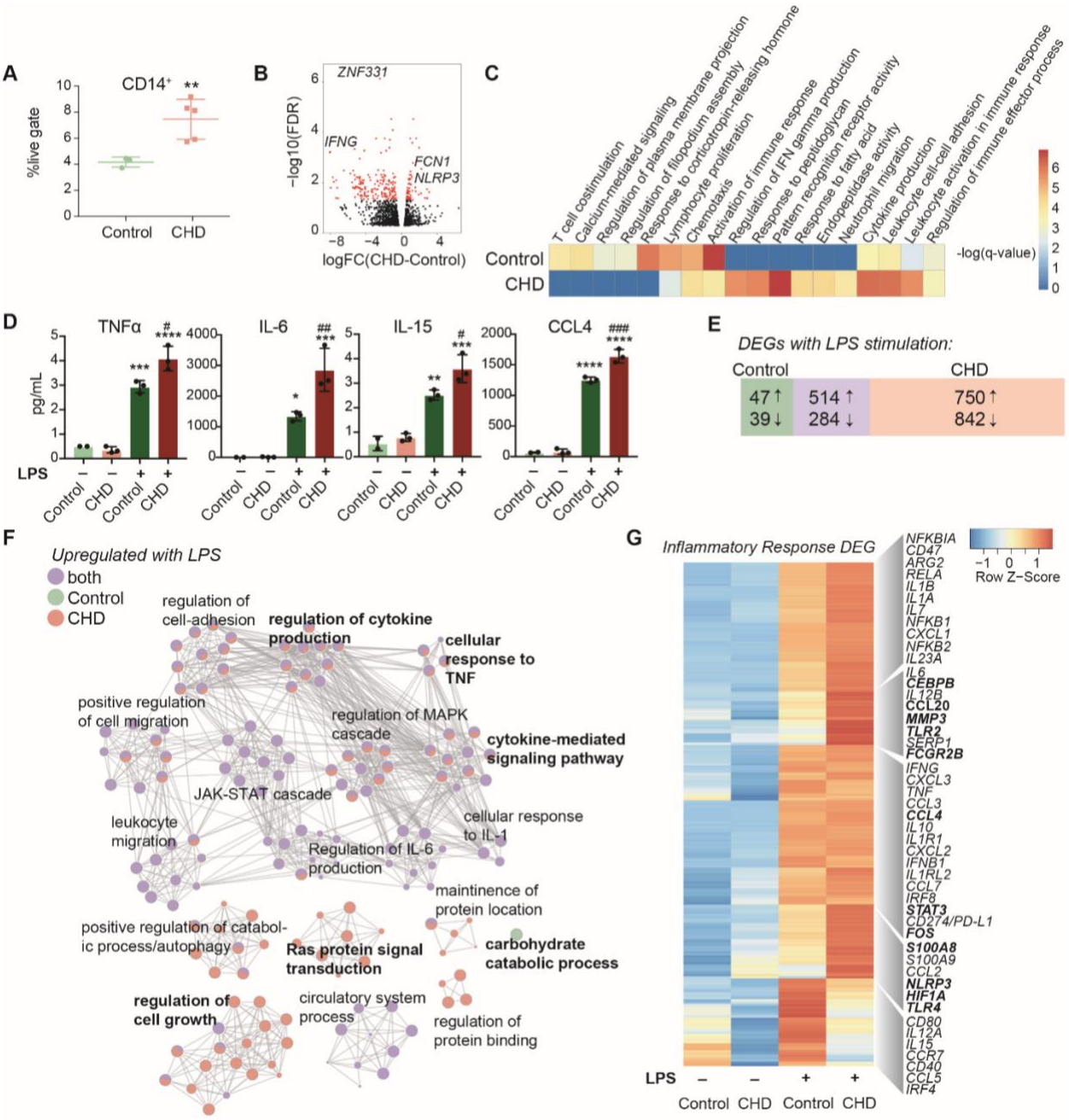

Figure 2.2: Impact of CHD on the monocyte functional and transcriptomic response to LPS

A) Abundance of live CD14+ cells in PBMC from control (n=3) and CHD (n=5) female macaques measured by flow cytometry. Significance calculated by t-test with Welch's correction. B) Volcano plot representing up- and downregulated differentially expressed genes (DEG) with CHD in resting monocytes. Red = significant with an FDR ≤ 0.05 and fold

change ≥ 2. C) Heatmap of significant GO terms (identified using Metascape) to which DEGs downregulated and upregulated with CHD in monocytes enriched. The scales of the heatmaps are -log(q-values) associated with the enrichment to selected pathways. D) Purified monocytes were stimulated with LPS for 6 hours and supernatants were analyzed by Luminex assay. Bar plots showing concentration (pg/ml) of selected immune mediators (TNFα, IL-6, IL-15, CCL4) (*=p<0.05, **=p<0.01, ***=p<0.001, ****=p<0.0001 between LPS and unstimulated condition, # is significance between CHD and control for each stimulation condition calculated by One-way ANOVA). E) Venn diagram showing overlap between DEG identified in control and CHD monocytes after LPS stimulation. F) Network visualization of functional enrichment analysis of DEG upregulated with LPS in monocytes from controls only, CHD only, and both using Metascape. The size of each node represents the number of DEGs associated with a given gene ontology (GO) term and the pie chart filling represents relative proportion of DEGs from each group that enriched to that GO term. Similar GO terms are clustered together and are titled with the name of the most statistically significant GO term within that cluster. The gray lines denote shared interactions between GO terms. Density and number of gray lines indicates the strength of connections between closely related GO terms. G) Heatmap of average normalized expression of genes associated with inflammatory response pathways.

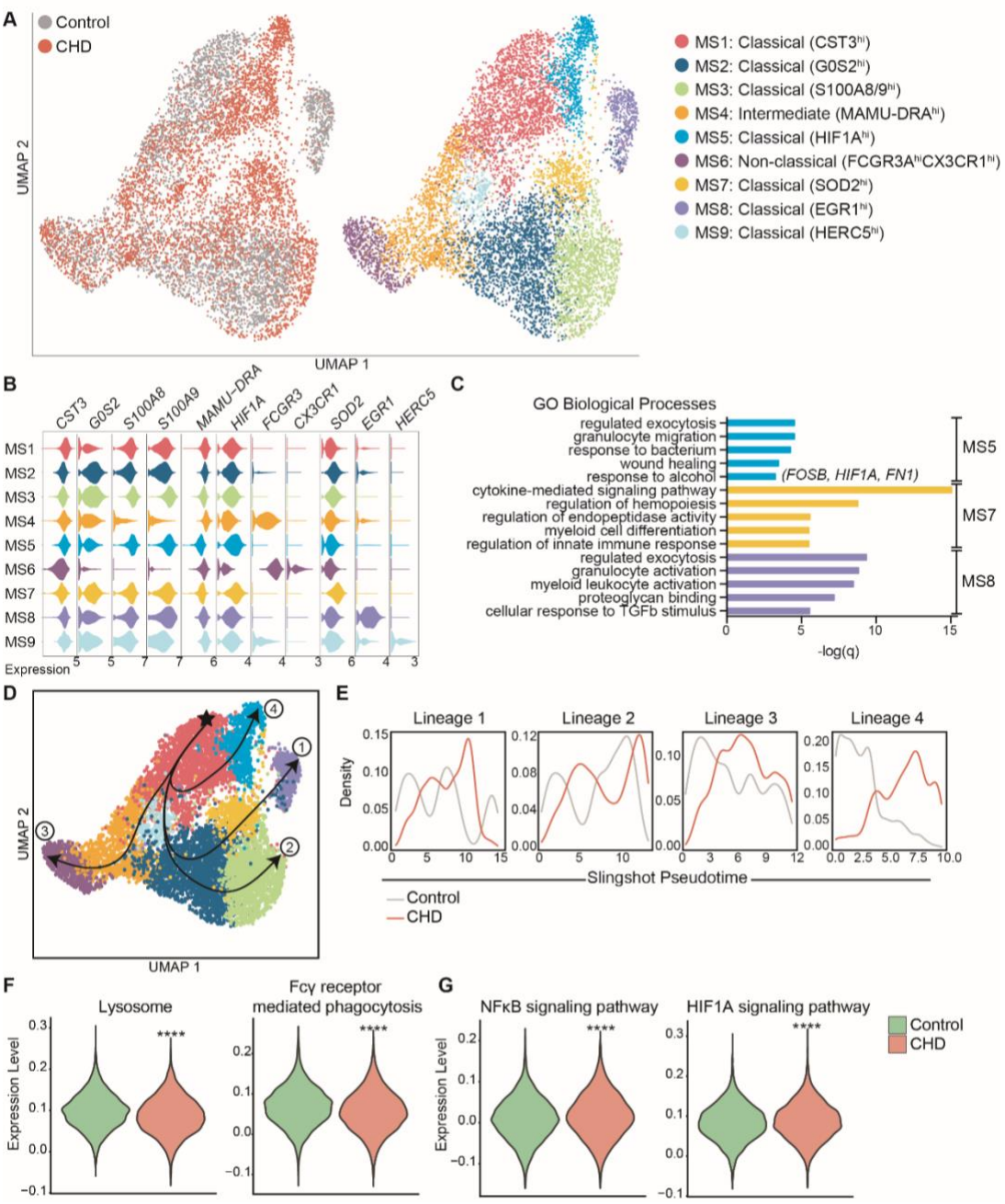

Figure 2.3: Single cell RNA-Seq analysis of monocytes with CHD

Monocytes (n=3 control/ 3 CHD) were purified from total PBMC from female macaques and subjected to 10X scRNA-Seq analysis. A) Visualization of 9,360 monocytes by uniform manifold approximation and projection (UMAP) colored by group (control and CHD) as well as by identified clusters. B) Stacked violin plots representing expression of key genes used for cluster identification, grouped by monocyte subset cluster. C) GO Biological

Process enrichment from Metascape of genes highly expressed in MS5, MS7, and MS8, defined by q-value. D) Trajectory analysis of monocytes determined using Slingshot. E) Cell density plots for Control and CHD groups across each of four trajectory lineages determined by Slingshot. F,G) Violin plots comparing (F) Lysosome and Fcg receptor-mediated phagocytosis and (G) NFkB signaling and HIF1A signaling pathway module scores in all monocytes of both groups. Statistical analysis of module scores was performed using a t-test with Welch's correction where *=$p<0.05$, **=$p<0.01$, ***=$p<0.001$, ****=$p<0.0001$.

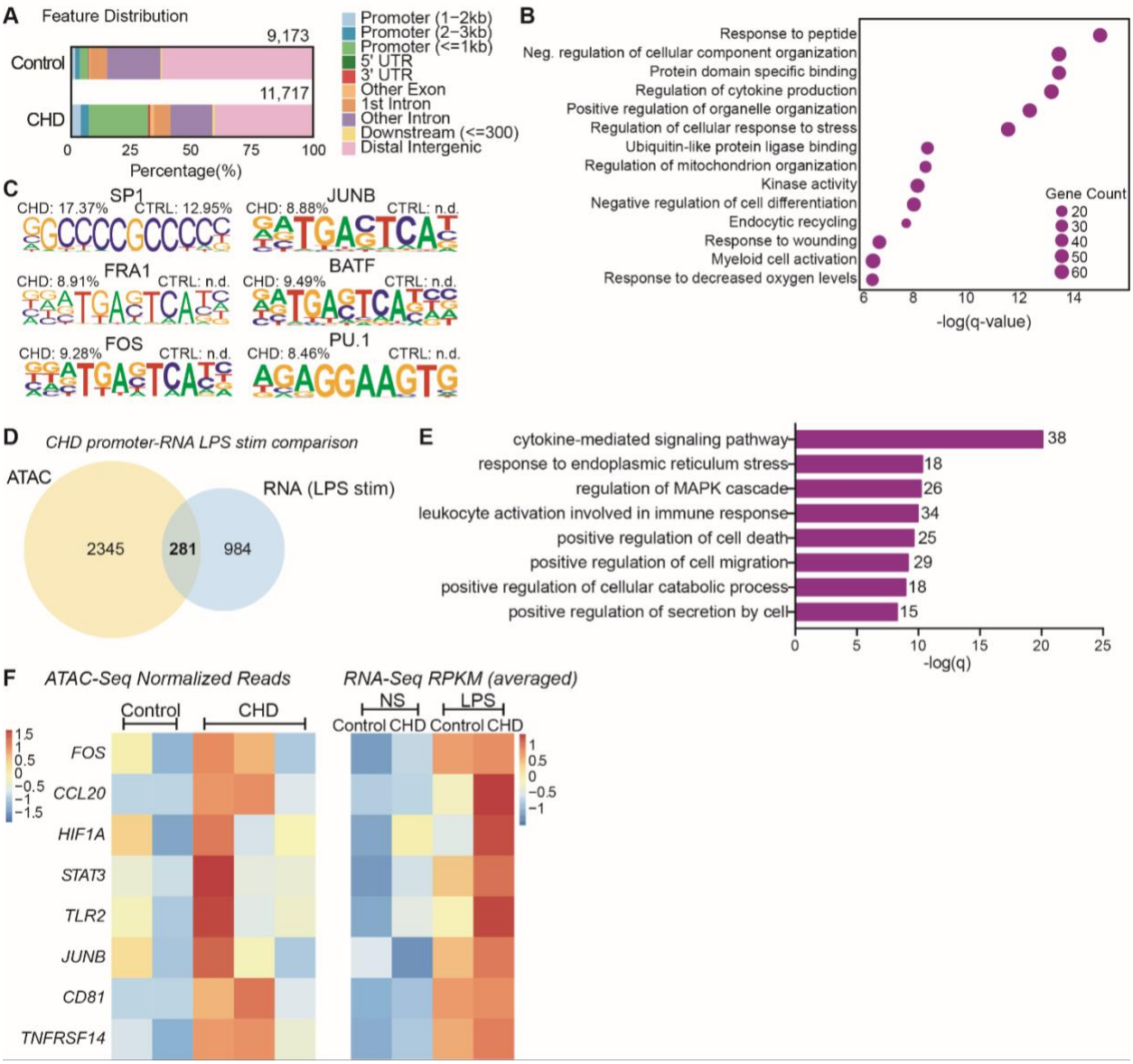

Figure 2.4: CHD primes the monocyte epigenome for inflammatory response

Monocytes (n= 2 Control/ 3 CHD) were purified from PBMC from female macaques and subjected to ATAC-Seq analysis. A) Bar plot showing genomic feature distribution of the open chromatin regions (fold-change ≥ 2) in control and CHD monocytes at resting state. B) GO Biological process enrichment from Metascape of genes regulated by the open promoter regions (≤ 1kb, fold-change ≥ 3) in CHD monocytes. The X-axis represents -log(q-value) and the size of the dot represents the number of genes within that term. C) Homer motif enrichment of the open chromatin regions. All listed motifs have significantly

enriched binding sites in the CHD monocytes where the percentage value listed is the percentage of target sequences with that motif. D) Venn diagram of genes regulated by the open promoter regions (≤ 1kb, fold-change ≥ 3) and DEG detected following LPS stimulation in the CHD monocytes. E) GO Biological process enrichment terms from Metascape of the 281 overlapping genes from (D). F) Heatmaps of the normalized expression of open promoter region counts and RPKM from bulk RNA-Seq analysis for selected common genes.

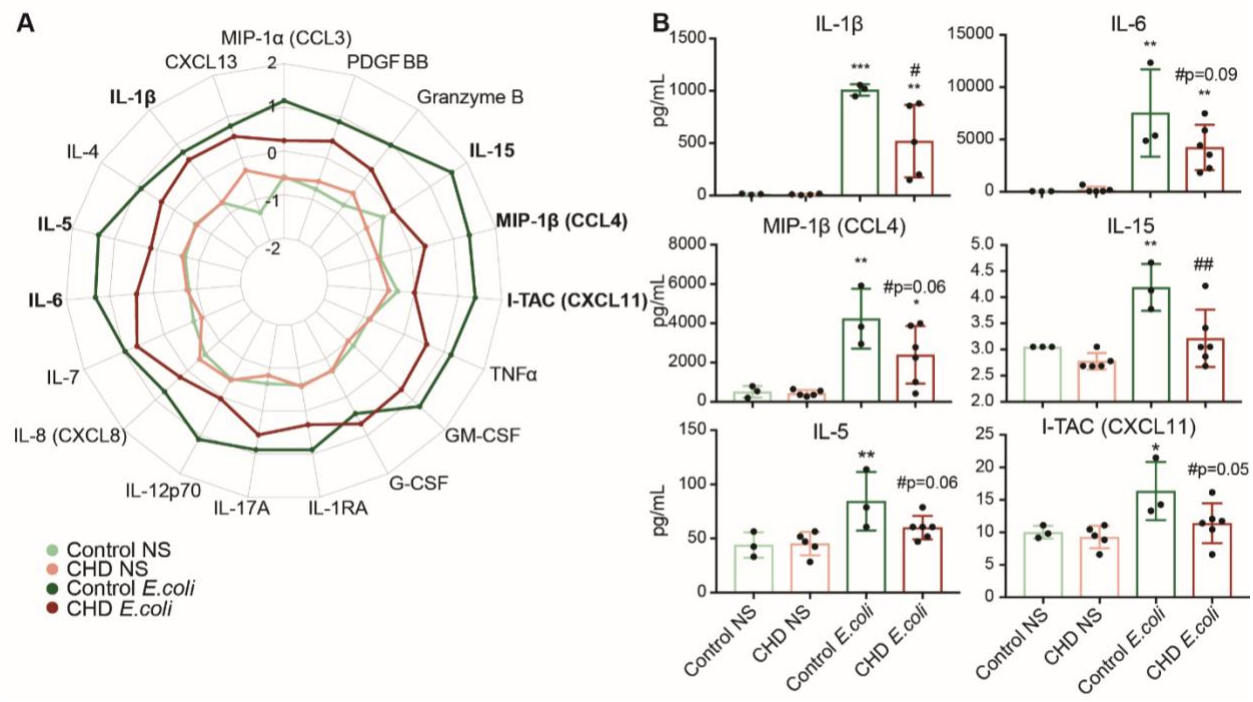

Figure 2.5: Monocyte response to E.*coli* is dampened with CHD.

Purified monocytes (n=2 Control Male, 1 Control Female/ 2 CHD Male, 4 CHD Female) were stimulated with heat-killed E.*coli* bacteria for 16 hours. A) Spider plot representing average Z-scores for each group across the indicated analytes measured by Luminex. B) Bar plots showing concentration (pg/ml) of selected immune mediators (TNFα, IL-6, CCL4(MIP-1β), IL-15, IL-5, I-TAC). *=p<0.05, **=p<0.01, ***=p<0.001, ****=p<0.0001 between LPS and unstimulated condition. If indicated, # is significance between CHD and control for each stimulation condition.

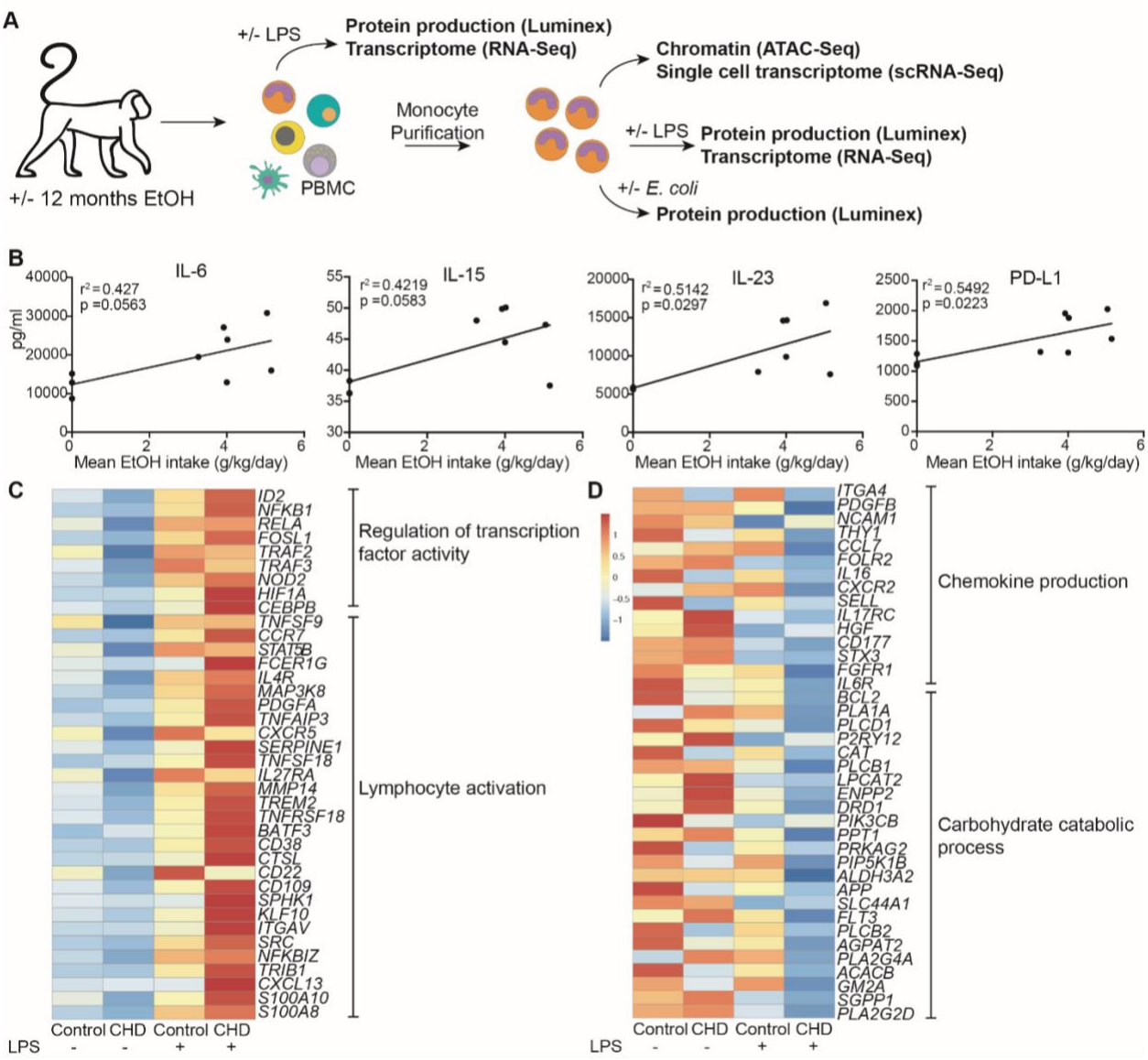

Supp. Figure 2.1: A) Experimental Design figure for this study. B) Scatter plots showing Spearman correlation between average EtOH dose (grams EtOH/kg body weight/day) and concentration (pg/ml) of the secreted factors IL-6, IL15, IL-23, PD-L1. C) Heatmap of genes related to Regulation of transcription factor activity and Lymphocyte activation upregulated in CHD PBMC with LPS. D) Heatmap of genes involved in Chemokine production and Carbohydrate catabolic process pathways downregulated in CHD PBMC with LPS.

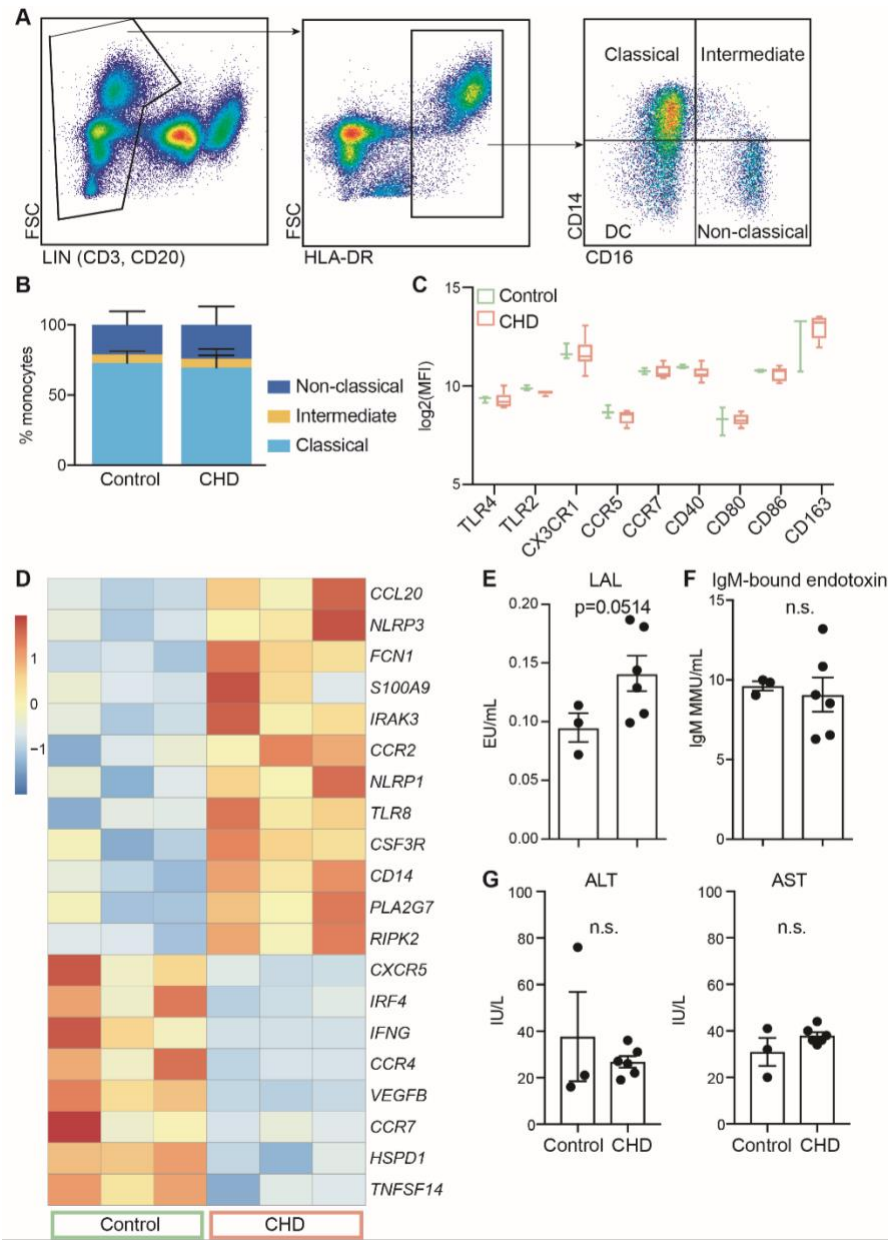

Supp. Figure 2.2: A) Gating strategy used to identify the three populations of monocytes in the blood. B) Relative percentages of the three monocyte populations in the controls and CHD macaques. C) Log_2 median fluorescence intensities (MFI) of monocyte cell surface markers across the controls and CHD macaques. D) Heatmap of normalized expression of differentially expressed genes between resting control and CHD monocytes. E,F) LAL (E) and IgM-bound endotoxin (F) levels measured from plasma by ELISA. G) Alanine transaminase (ALT) and aspartate transaminase (AST) were measured to test for overt liver damage. T-test with Welch's correction was used to measure significance.

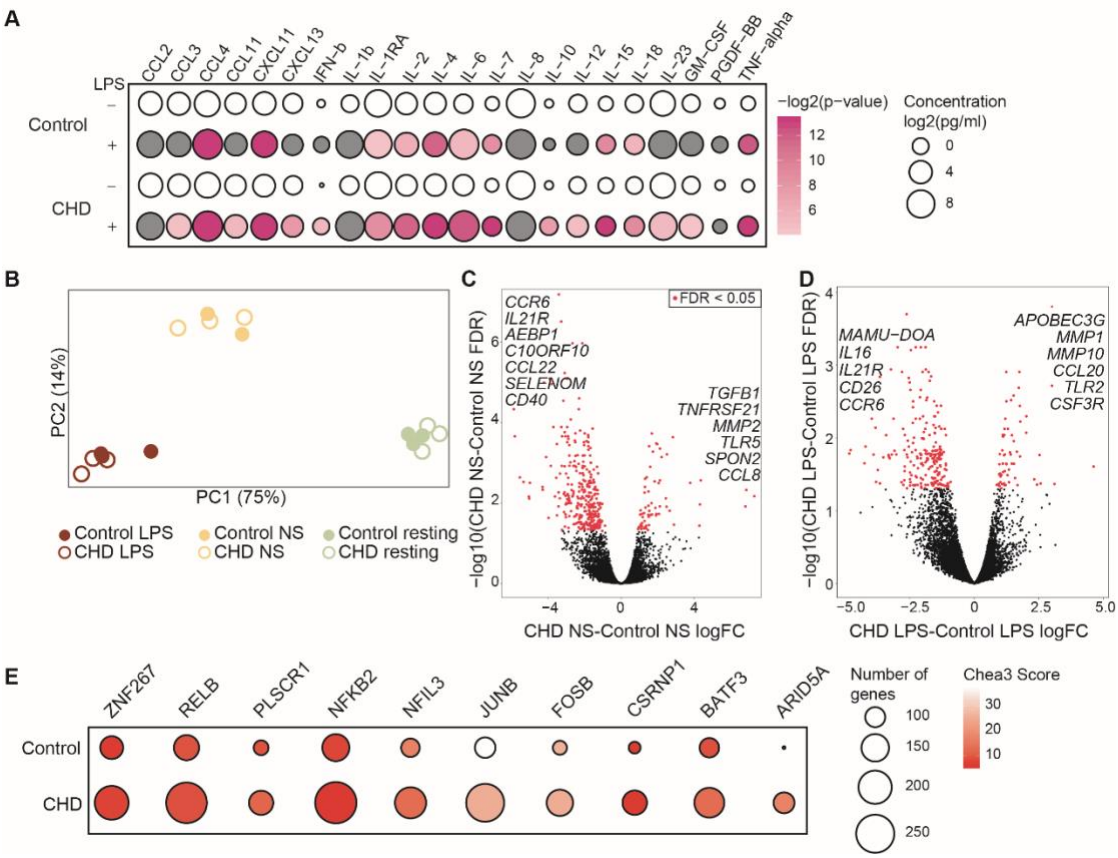

Supp. Figure 2.3: A) Bubble plot representing immune factor production (pg/ml) in the presence or absence of LPS stimulation of monocytes from control and CHD animals. The size of each circle represents the indicates the $\log_2$ mean concentration of the indicated secreted factor and the color denotes the $-\log_2$ transformed p value with the darkest pink representing the most significant value. The p-values were calculated between the unstimulated and stimulated conditions for each group using One-way ANOVA and a p-value cut-off of 0.05 was set. White circles indicate non-significant p-value. B) Principal component analysis (PCA) of CHD and control monocytes under resting, unstimulated (6 hours of media) and LPS stimulation (6 hours) conditions. C,D) Volcano plot representing up- and downregulated DEG with CHD in non-stimulated (C) and LPS stimulated (D) monocytes. Red = significant with an FDR ≤ 0.05 and fold change ≥ 2. E) Bubble plot representing transcription factors predicted to regulate LPS-responsive DEGs. The size of the dot represents the number of genes and the color represents Chea3 score where lower number is more significant. Analysis was performed using the Chea3 web browser.

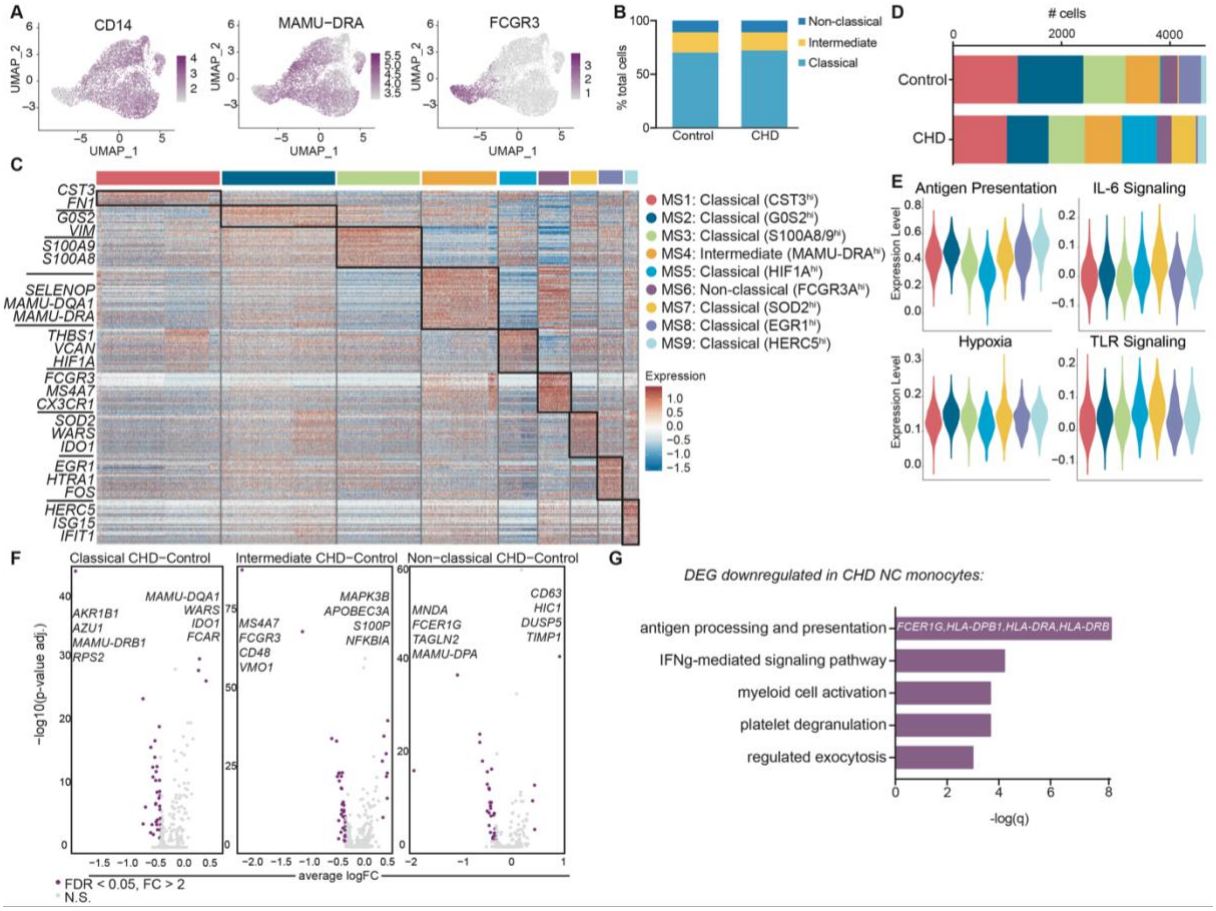

Supp. Figure 2.4: A) Feature plots showing relative gene expression of canonical monocyte markers CD14, MAMU-DRA, and FCGR3 in all monocytes. B) Stacked bar graph depicting relative abundance of non-classical, intermediate, and classical monocytes in control and CHD monocytes. C) Heatmap showing relative gene expression of the representative genes used for clustering and subset identification. D) Stacked bar graph depicting abundance of cells clustered in each monocyte subset in control and CHD groups. E) Violin plots comparing antigen presentation, IL-6 signaling, hypoxia, and TLR signaling module scores with the classical monocyte subsets. F) Volcano plots of the up-and downregulated genes comparing CHD to control non-classical, intermediate, and classical monocytes. The purple color indicates significant DEG where FDR ≤ 0.05 and fold-change ≥ 2. G) Bar graph showing functional enrichment pathways of DEG downregulated with CHD in the non-classical monocyte cluster (MS6), defined by q-value.

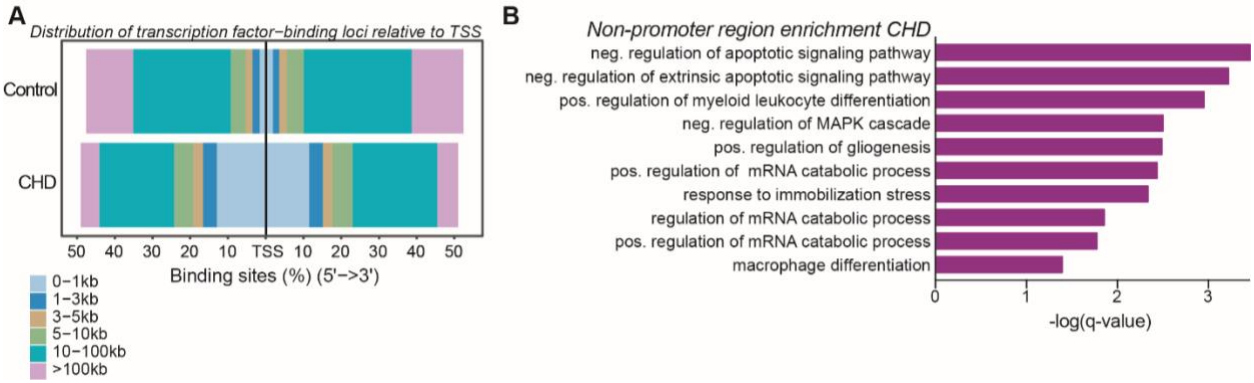

Supp. Figure 2.5: A) Distribution of the open chromatin regions in the CHD and control monocytes relative to the transcription start site (TSS). B) Top GO Biological process enrichment of the genes predicted to be cis-regulated by non-promoter regions more open with CHD. Genomic regions were lifted over from rhesus macaque to homo sapien genome (UCSC) and further enriched using the GREAT.

SUPPLEMENTARY TABLES:

Supp. Table 2.1: Animals and EtOH g/kg values

Supp. Table 2.2: Immune mediator production by PBMC or purified monocytes following LPS or E.*coli* stimulation.

Supp. Table 2.3: Genes associated with each MS cluster

Supp. Table 2.4: Module Scoring genes

CHAPTER 3:

Chronic alcohol drinking disrupts monocyte production and function from progenitors in the bone marrow niche in non-human primates

Sloan A. Lewis[1,2], Brianna Doratt[1,2], Kathleen A. Grant[3], Ilhem Messaoudi[1, 2, 4]

[1] Department of Molecular Biology and Biochemistry, University of California, Irvine CA 92697, USA
[2] Institute for Immunology, University of California, Irvine CA 92697, USA
[3] Oregon National Primate Research Center, Oregon Health and Science University, Beaverton, OR, USA
[4] Center for Virology Research, University of California, Irvine CA 92697, USA

This manuscript is in preparation for submission.

ABSTRACT

Chronic alcohol drinking affects frequency and function of circulating monocytes and tissue-resident macrophages, resulting in a rewiring of the cells towards heightened inflammatory but compromised anti-microbial responses. Molecular underpinnings of these perturbations remain poorly understood. In this study, we leverage a nonhuman primate (NHP) model of chronic ethanol self-administration and show that these perturbations persist in the face of a month-long abstinence period. These observations, strongly suggest that chronic ethanol consumption may impact monocyte progenitors in the bone marrow. To test this hypothesis, we conducted a comprehensive study where single cell genomics were integrated with functional assays to profile bone marrow CD14+ and CD34+ cells collected after 12 months of daily alcohol drinking. Analysis of bone marrow CD14+ cells revealed heightened inflammatory responses to bacterial agonists that was accompanied by increased expression of activation markers and transcriptional signatures of cellular activation with alcohol drinking. In vitro differentiation of CD34+ cells into monocytes revealed skewing towards monocytes with neutrophil-like markers with heightened inflammatory responses to bacterial agonist stimulation with alcohol drinking. Single cell transcriptional analysis of CD34+ cells showed increased expression of inflammation-associated markers in more differentiated clusters from the myeloid lineage. Transcriptional signatures of oxidative stress and oxidative phosphorylation were apparent in both the CD14+ and CD34+ cells with alcohol drinking. Finally, CD169+ bone marrow macrophages from alcohol drinking animals exhibited transcriptional markers of cellular stress suggesting defects in stem cell maintenance with chronic alcohol drinking.

INTRODUCTION

Alcohol drinking is widespread in the United States and globally, with more than 2 billion current drinkers worldwide (167). Alcohol and its metabolic products induce organ damage and increase incidence of cardiovascular disease (5, 6), certain types of cancer (7-10), liver cirrhosis (11), and sepsis (12). Moreover, heavy alcohol drinking has been linked to increased susceptibility to a number of bacterial and viral infections (14-17). Increased vulnerability to infectious diseases is believed to be mediated by functional, transcriptomic, and epigenomic changes in blood monocytes and tissue-resident macrophages leading to increased inflammation but compromised antimicrobial responses (13, 25, 108, 113). Whether chronic alcohol consumption impacts mature monocytes/macrophages, their progenitors in the bone marrow, or both remains to be determined.

Monocytes continuously arise from hematopoietic stem and progenitor cells (HPSC) in the bone marrow through a number of progressively restricted lineage committed progenitors (72, 73). It has been shown in mice that two independent pathways of monocyte production exist starting from common myeloid progenitors (CMP) and proceeding through either granulocyte-monocyte progenitors (GMP) to monocyte progenitors (MP) or monocyte-DC progenitors (MDP) to common monocyte progenitors (cMoP) (72, 168). Myelopoiesis in humans is not as well characterized, but CMP, GMP, MDP, and cMoP populations have been identified from their mouse counterparts (73, 169, 170). Mature monocytes are classified into three subsets, classical, intermediate, and non-classical, which can be found stored in the bone marrow as well as circulating through the blood (60). Infection, inflammation, or stress can alter monocyte production and even induce "emergency monopoiesis" from the bone marrow compartment (72, 171, 172).

Chronic alcohol drinking is known to affect bone marrow stem cells and hematopoiesis. Specifically, lymphopenia, anemia, and thrombocytopenia are observed in patients with alcohol use disorders (76, 173-177). Studies in rodent models of alcohol exposure have reported impairment of hematopoietic precursor cell activation as well as perturbation of granulocyte precursor responses and differentiation resulting in reduced bacterial clearance (79, 80). Lastly, studies in NHP have reported impaired mitochondrial function of HPSC, alteration in the bone marrow niche with chronic ethanol consumption (178), and increased numbers of mature macrophage and osteoclasts in the bone marrow with alcohol and simian immune deficiency virus (SIV) co-infection (179).

In this study, we utilize an NHP model of voluntary ethanol (EtOH) self-administration to assess the impacts of chronic heavy alcohol drinking on monocytes and their progenitors in the bone marrow compartment. We collected bone marrow cells from the femurs of male and female animals that consumed >3g EtOH per kilogram body weight per day for 12 months. We performed phenotypic, functional, and single cell transcriptomic assays on both CD14+ monocytes within the bone marrow and CD34+ progenitor cells. Our analysis revealed broad increases in inflammatory and oxidative stress-associated signatures in bone marrow CD34+ and CD14+ cells with EtOH. This was accompanied by skewing of the CD34+ cells to produce more neutrophil-like monocytes with heightened inflammatory properties as well as increased inflammation in intermediate monocytes in the bone marrow.

METHODS AND MATERIALS

Animal studies and sample collection:

These studies used samples from an NHP model of voluntary ethanol self-administration established through schedule-induced polydipsia (34, 35, 140). Briefly, in this model, rhesus macaques are introduced to a 4% w/v ethanol solution during a 90-day induction period followed by concurrent access to the 4% w/v solution and water for 22 hours/day for one year. During this time, the macaques adopt a stable drinking phenotype defined by the amount of ethanol consumed per day and the pattern of ethanol consumption (g/kg/day) (34). Blood samples were taken from the saphenous vein every 5-7 days at 7 hrs after the onset of the 22 hr/day access to ethanol and assayed by headspace gas chromatography for blood ethanol concentrations (BECs).

For these studies, blood and bone marrow samples were collected through the Monkey Alcohol Tissue Research Resource (www.matrr.com) where more information about the animals can be obtained. Blood samples (2 timepoints) were collected from 7 male rhesus macaques with 3 animals serving as controls and 4 classified as heavy drinkers based on 12-month daily averages of ethanol self-administration (Cohort 14 on www.matrr.com). Bone marrow samples were collected from one male cohort of 8 animals and one female cohort of 9 animals for a total of 7 controls and 10 heavy drinkers (Cohorts 6a and 7a on www.matrr.com). Data from Cohorts 6 and 7a have been reported in three previous studies of innate immune system response to alcohol (25, 108, 113). Peripheral Blood Mononuclear Cells (PBMC) bone marrow cells were cryopreserved until they could be analyzed as a batch.

The average daily ethanol intake and other cohort information for each animal is outlined in **Supp. Table 3.1**.

Flow cytometry analysis:

0.5-1x10^6 PBMC were stained with the following surface antibodies against: CD14 (Biolegend, M5E2, AF700), HLA-DR (Biolegend, L243, APC-Cy7) to identify monocytes. 0.5-1x10^6 bone marrow cells were stained with the following surface antibodies (2 panels) against: CD14 (Biolegend, M5E2, AF700), HLA-DR (Biolegend, L243, APC-Cy7), CD16 (Biolegend, 3G8, PB), CD80 (Biolegend, 2D10, PE), CD86 (Biolegend, IT2.2, BV605), CD169 (Biolegend, 7-239, PE-Cy7), and Sytox Green to identify monocyte and macrophage populations; CD20 (Biolegend, 2H7, BV510), CD3 (BD Biosciences, SP34-2, V500), CD14 (Biolegend, M5E2, AF700), CD38 (StemCell, AT-1, FITC), CD123 (Biolegend, 6H6, PerCP-Cy5.5), CD34 (Biolegend, 561, PE-Cy7), CD45RA (Miltenyi, T6D11, PE), CD64 (Biolegend, 10.1, BV711), CD90 (Biolegend, 5E10, APC), CD127 (Miltenyi, , PE-Vio615), and Sytox Blue to identify bone marrow progenitor populations. Progenitor populations were defined as: HSC (Lin.-CD34+CD38-CD45RA-CD90+), MPP(Lin.-CD34+CD38-CD45RA-CD90-), CLP(Lin.-CD34+CD38+CD127+), CMP(Lin.-CD34+CD38+CD45RA-CD123+), MEP (Lin.-CD34+CD38+CD45RA-CD123-), GMP(Lin.-CD34+CD38+CD45RA+CD123+CD64-), cMoP(Lin.-CD34+CD38+CD45RA+CD123+CD64+). All samples were acquired with an Attune NxT Flow Cytometer (ThermoFisher Scientific, Waltham, MA) and analyzed using FlowJo software (Ashland, OR). Percentage of live cells or Median Fluorescence Intensities (MFI) were assessed for each marker.

PBMC and bone marrow Stimulation Assays:

$1x10^6$ freshly thawed PBMC were cultured in RPMI supplemented with 10% FBS with or without 1 ug/mL LPS (TLR4 ligand, *E.coli* 055:B5; Invivogen, San Diego CA) and Brefeldin A for 6 hours in 96-well tissue culture plates at 37C in a 5% CO_2 environment. They were next stained with an antibody cocktail of CD20 (Biolegend, 2H7, BV510), CD3 (BD Biosciences, SP34-2, V500), CD14 (Biolegend, M5E2, AF700), and HLA-DR (Biolegend, L243, APC-Cy7) and Fixable Yellow Live/Dead stain. Stained cells were then fixed and permeabilized using Fixation buffer (BioLegend) and incubated overnight with intracellular antibody TNFα (BD Biosciences, MAb11, APC).

$1x10^6$ freshly thawed bone marrow cells were cultured in RPMI supplemented with 10% FBS with or without a bacterial agonist cocktail (2ug/mL Pam3CSK4 (TLR1/2 agonist, InvivoGen), 1 ug/mL FSL-1 (TLR2/6 agonist, Sigma Aldrich), and 1 ug/mL LPS (TLR4 agonist from E. coli O111:B4, InvivoGen)) and Brefeldin A for 6 hours in 96-well tissue culture plates at 37C in a 5% CO_2 environment. They were next stained with an antibody cocktail of CD14 (Biolegend, M5E2, AF700), HLA-DR (Biolegend, L243, APC-Cy7), CD34 (Biolegend, 561, PE-Cy7), CD16 (Biolegend, 3G8, PB), and CD169 (Biolegend, 7-239. Stained cells were then fixed and permeabilized using Fixation buffer (BioLegend) and incubated overnight with a cocktail of intracellular antibodies - IL-6 (BD Biosciences, MQ2-6A3, FITC), TNFα (BD Biosciences, MAb11, APC), CCL4 (MIP-1β) (BD Biosciences, D21-1351, PE).

All samples were acquired with an Attune NxT Flow Cytometer (ThermoFisher Scientific, Waltham, MA) and analyzed using FlowJo software (Ashland, OR).

Monocyte Differentiation Assay:

$1x10^3$ sorted CD34+ cells/well were plated in a 96-well plate in 100uL StemSpan SFEM Media supplemented with StemSpan Myeloid Expansion Supplement II containing TPO, SCF, Flt3, GM-CSF, M-CSF and incubated at 37C in a 5% CO_2 environment. On culture day 4, the volume of the cultures was brought up to 200uL with the same media. On culture day 7, the cultures were incubated with or without a bacterial agonist cocktail (2ug/mL Pam3CSK4 (TLR1/2 agonist, InvivoGen), 1 ug/mL FSL-1 (TLR2/6 agonist, Sigma Aldrich), and 1 ug/mL LPS (TLR4 agonist from E. coli O111:B4, InvivoGen)) for 6 hours. Supernatants were collected and stored short-term at -80C. The cells were further stained with an antibody cocktail of: CD34 (Biolegend, 561, PE-Cy7), CD14 (Biolegend, M5E2, AF700), HLA-DR (Biolegend, L243, APC-Cy7), CD11C (Invitrogen, 3.9, PE-eFluor610), CD115 (Biolegend, 9-4D2-1E4, PE), and CCR2 (R&D, 48607, PerCP-Cy5.5). All samples were acquired with an Attune NxT Flow Cytometer (ThermoFisher Scientific, Waltham, MA) and analyzed using FlowJo software (Ashland, OR).

Luminex Assay:

Immune mediators in the supernatants from monocyte cultures were measured using a Milliplex Multiplex assay panel measuring levels of TNFα, IL-6, IL-1β, G-CSF, CCL3(MIP-1α), and IL-2 (Millipore, Burlington, MA). Differences in induction of proteins post stimulation were calculated using $\log_{10}$(pg/mL fold-change +1). Undiluted samples run in duplicates on the Magpix Instrument (Luminex, Austin, TX). Data were fit using a 5P-logistic regression on xPONENT software (version 7.0c).

Colony Forming Unit Assay:

MethoCult colony-forming unit (CFU) assay was performed with MethoCult H4435-enriched medium (STEMCELL Technologies, Vancouver, Canada) following manufacturer's protocol. Briefly, CD34+ cells were FACS sorted from freshly thawed bone marrow cells and resuspended in IMDM+2% FBS to achieve a final plating concentration of 1000 cells per culture dish. Cells were gently mixed with 3mL MethoCult and plated into 35mm culture dishes in triplicate. Cultures were incubated at 37C in a 5% CO_2 environment. Total colonies were counted on days 7 and 10, and additional colony identification was performed on day 10.

Single cell RNA library preparation- CD14+:

Bone marrow cells from control females (n=3 pooled), control males (n=4), EtOH females (n=3 pooled), and EtOH males (n=4), were thawed and subjected to the following downstream protocols. CD14+ cells (mature monocytes) were sorted using a BD FACSAria Fusion. Sorted CD14+ cells from the control and EtOH groups of female animals were pooled and resuspended at a concentration of 1,200 cells/ul and loaded into the 10X Chromium Controller aiming for an estimated 10,000 cells per sample. cDNA amplification and library preparation (10X v3 chemistry) were performed for samples according to manufacturer protocol and sequenced on a NovaSeq S4 (Illumina) to a depth of >30,000 reads/cell.

Freshly thawed bone marrow cells from male animals were first incubated with TruStain FcX for 10 minutes followed by surface staining with anti-CD14 antibody. Cells were washed in PBS + 0.04% BSA and then incubated with 10X CellPlex oligos (10X Genomics) for 5 minutes. CD14+ cells were sorted into respective control or EtOH pools for live, CD14+ cells using a BD FACSAria Fusion. After sorting, pools were resuspended at a concentration of 1,600

cells/uL and loaded into the 10X Chromium Controller aiming for an estimated 18,000 cells per sample. cDNA amplification and library preparation (10X v3.1 dual index chemistry) were performed for samples according to manufacturer protocol and sequenced on a NovaSeq S4 (Illumina) to a depth of >30,000 reads/cell. Cell multiplexing libraries were constructed according to manufacturer protocol and sequenced on a NovaSeq S4 (Illumina) to a depth of >5,000 reads/cell.

Single cell RNA library preparation- monocyte differentiation cultures:

Monocyte differentiation culture cells from control (n=2 male + 2 female pooled) and EtOH (n=2 male + 2 female pooled) cultures were counted for viability (>70%) and pooled according to group. Pools were resuspended at a concentration of 1,200 cells/ul and loaded into the 10X Chromium Controller aiming for an estimated 10,000 cells per sample. cDNA amplification and library preparation (10X v3 chemistry) were performed for samples according to manufacturer protocol and sequenced on a NovaSeq S4 (Illumina) to a depth of >30,000 reads/cell.

Single cell RNA library preparation- CD34+:

Bone marrow cells from control females (n=3), control males (n=4), EtOH females (n=3), and EtOH males (n=4), were thawed and stained with anti-CD34 antibodies and sorted for live CD34+ cells on a BD FACSAria Fusion. Sorted CD34+ samples from female animals were resuspended at a concentration of 1,200 cells/ul and loaded into the 10X Chromium Controller aiming for an estimated 10,000 cells per sample. cDNA amplification and library preparation (10X v3 chemistry) were performed for samples according to manufacturer protocol and sequenced on a NovaSeq S4 (Illumina) to a depth of >30,000 reads/cell.

Freshly thawed bone marrow cells from male animals were first incubated with TruStain FcX for 10 minutes followed by surface staining with anti-CD34 antibody. Cells were washed in PBS + 0.04% BSA and then incubated with 10X CellPlex oligos (10X Genomics) for 5 minutes. CD34+ cells were sorted into respective control or EtOH pools for live, CD34+ cells on a BD FACSAria Fusion. After sorting, pools were resuspended at a concentration of 1,600 cells/uL and loaded into the 10X Chromium Controller aiming for an estimated 18,000 cells per sample. cDNA amplification and library preparation (10X v3.1 dual index chemistry) were performed for samples according to manufacturer protocol and sequenced on a NovaSeq S4 (Illumina) to a depth of >30,000 reads/cell. Cell multiplexing libraries were constructed according to manufacturer protocol and sequenced on a NovaSeq S4 (Illumina) to a depth of >5,000 reads/cell.

Single cell RNA-Seq sequencing and data analysis:

Sequencing reads were aligned to the Mmul_8.0.1 reference genome using cellranger v6.0.1 (147) (10X Genomics) using the *count* function for single sample libraries and the *multi* function for multiplexed samples. Quality control steps were performed prior to downstream analysis with *Seurat* (148), filtering out cells with fewer than 200 unique features (ambient RNA) and cells with greater than 20% mitochondrial content (dying cells). Data normalization was performed using *SCTransform* (180), correcting for differential effects of mitochondrial and cell cycle gene (only CD14+ dataset) expression levels. Sample integration was performed using the *SelectIntegrationFeatures* (using 3000 features), *PrepSCTIntegration*, *FindIntegrationAnchors*, and *IntegrateData* functions. Clustering was performed using the first 20, 10, and 30 principal components for the CD14+, monocyte

differentiation, and CD34+ datasets, respectively. Contaminating clusters with an over-representation of B or T cell gene expression were removed for downstream analysis. Clusters were characterized into distinct subsets using the *FindAllMarkers* function (**Supp. Table 3.2**). Figures were generated using *Seurat, ggplot2*, and *pheatmap*.

Differential expression analyses:

Differential expression analysis (EtOH relative to Control) was performed using MAST under default settings in *Seurat*. Only statistically significant genes (Log_{10}(Fold change) cutoff ≥ 0.25; adjusted p-value≤ 0.05) were included in downstream analysis.

Pseudo-temporal analysis:

Pseudotime trajectory of the monocyte differentiation and CD34+ datasets were reconstructed using *Slingshot* (107). The UMAP dimensional reduction performed in *Seurat* was used as the input for *Slingshot*. For calculation of the lineages and pseudotime, the progenitor/HSC population was selected as the start. Temporally expressed genes were identified by ranking all genes by their variance across pseudotime and then further fit using the generalized additive model (GAM) with pseudotime as an independent variable.

Module Scoring and functional enrichment:

For gene scoring analysis, we compared gene signatures and pathways from KEGG (https://www.genome.jp/kegg/pathway.html) and the Human Cell Atlas bone marrow single cell analysis (181) (**Supp. Table 3.3**) in the clusters/groups using *Seurat's AddModuleScore* function. Values for module scores were further exported from *Seurat* and tested for significance in Prism 7. Over representative gene ontologies were identified by

enrichment of differential signatures using Metascape. All plots were generated using *ggplot2* and *Seurat*.

RNA isolation and library preparation for bulk RNA-Seq:

Total RNA was isolated from sorted CMP/GMP using the mRNeasy kit (Qiagen, Valencia CA) following manufacturer instructions and quality assessed using Agilent 2100 Bioanalyzer. Libraries from purified progenitor RNA were generated using the NEBnext Ultra II Directional RNA Library Prep Kit for Illumina (NEB, Ipswitch, MA, USA). rRNA depleted RNA was fragmented, converted to double-stranded cDNA and ligated to adapters. The roughly 300bp-long fragments were then amplified by PCR and selected by size exclusion. Libraries were multiplexed and following quality control for size, quality, and concentrations, were sequenced to an average depth of 20 million 100bp reads on the NovaSeq S4 platform.

Bulk RNA-Seq data analysis:

RNA-Seq reads were quality checked using FastQC (https://www.bioinformatics.babraham.ac.uk/projects/fastqc/), adapter and quality trimmed using TrimGalore(https://www.bioinformatics.babraham.ac.uk/projects/trim_galore/), retaining reads at least 35bp long. Reads were aligned to *Macaca mulatta* genome (Mmul_8.0.1) based on annotations available on ENSEMBL (Mmul_8.0.1.92) using TopHat (142) internally running Bowtie2 (143). Aligned reads were counted gene-wise using GenomicRanges (144), counting reads in a strand-specific manner. Genes with low read counts (average <5) and non-protein coding genes were filtered out before differential gene expression analyses. Raw counts were used to test for differentially expressed genes

(DEG) using edgeR (103), defining DEG as ones with at least two-fold up or down regulation and an FDR controlled at 5%. edgeR analysis is provided in **Supp. Table 3.4**.

Statistical Analysis:

All statistical analyses were conducted in Prism 7(GraphPad). Data sets were first tested for normality and outliers. Two group comparisons were carried out an unpaired t-test with Welch's correction or Mann-Whitney test. Differences between 3 groups were tested using one-way ANOVA (α=0.05) followed by Holm Sidak's multiple comparisons tests. Error bars for all graphs are defined as ± SEM. Statistical significance of functional enrichment was defined using hypergeometric tests. P-values less than or equal to 0.05 were considered statistically significant. Values between 0.05 and 0.1 are reported as trending patterns.

RESULTS:

EtOH-induced heightened inflammatory state of circulating and bone marrow monocytes is sustained through abstinence

We have previously shown that long term EtOH drinking in NHPs leads to heightened inflammation in circulating monocytes and tissue resident macrophages at the epigenetic, transcriptional and functional levels (24, 108). As monocytes are relatively short-lived cells in circulation (5-7 days), we set to determine whether circulating monocytes would revert to a control state following a 1-month abstinence period (60). We collected peripheral blood mononuclear cells (PBMC) from one cohort of male macaques after 12 months of open access to EtOH and then again after a one-month abstinence period (**Figure 3.1A and Supp. Table 3.1**). As we have previously reported, percentages of monocytes in circulation as well as TNFα production in response to lipopolysaccharide (LPS) stimulation were increased after 12 months of chronic EtOH drinking relative to control cells treated with the same treatment (**Figure 3.1B**). Both the frequency of monocyte and TNFα production in response to LPS remained increased through a one-month abstinence period (**Figure 3.1C**).

This observation suggests that EtOH may impact the progenitor population in the bone marrow compartment and monocyte production. To test this hypothesis, we comprehensively profiled monocytes that reside within the bone marrow compartment from one female and one male cohort of NHPs that drank chronically for 12 months (**Figure 3.1D**). We first phenotypically profiled the monocytes from bone marrow (**Figure 3.1E**). Although no differences in the relative abundance of classical, intermediate, and non-classical monocyte populations, we noted an increase of CD80 MFI on classical monocytes

suggesting increased baseline activation (**Figure 3.1F,G**). Next, bone marrow cells were stimulated with a bacterial TLR cocktail (Pam3CSK4, LPS, and FSL-1) and percentages of TNFα, IL-6, and CCL4 (MIP-1β) positive cells were determined using flow cytometry (**Figure 3.1H**). Interestingly, no differences were noted in responses of the classical or non-classical monocyte populations, however, a greater percentage of intermediate monocytes from EtOH animals generated a TNFα response with a modest increase in IL-6 and CCL4 (MIP-1β) producing cells (**Figure 3.1H**). In summary, increased activation and heightened inflammatory responses to bacterial stimulation with EtOH persist for at least a month following abstinence. Additionally, our initial examination of bone marrow monocytes revealed increased baseline activation of classical monocytes and increased inflammatory responses to bacterial stimulation in intermediate monocytes with EtOH.

scRNA-Seq of bone marrow CD14+ cells reveals increased oxidative stress and inflammatory transcriptional signatures with EtOH

To capture transcriptional changes occurring in these bone marrow monocytes with EtOH at high resolution, we performed scRNA-Seq on purified bone marrow CD14+ cells following 12 months of chronic ethanol consumption (n=3 female controls pooled, 4 male controls, 3 female EtOH pooled, 4 male EtOH; **Supp. Figure 3.1A**). After integration of all datasets, 11 clusters were broadly identified as classical (*CD14, LYZ*), intermediate (Int.; *MAMU-DRA, S100A10*), and non-classical (N.C.; *FCGR3*) monocytes based on the indicated canonical markers (**Figure 3.2A,B and Supp. Figure 3.1B**). We were also able to identify a cluster of bone marrow macrophages (Mac.; *FABP4, SIGLEC1*). The classical monocyte clusters were further subdivided into 8 clusters, each with a unique gene expression profile (C1-8; **Figure**

3.2C and Supp. Table 3.2) as identified by the *FindAllMarkers* function in *Seurat*. Chronic EtOH consumption was associated with a significant increase in classical cluster C8, which was defined by high expression of *CREBRF, HERPUD1*, *FOSB* (**Figure 3.2D**) and *CXCR4*, the receptor for SCF-1 and also expressed on a population of promonocytes (182) (**Figure 3.2E**). Module scoring on the intermediate cluster revealed increased expression of genes involved in NFκB and cytokine signaling pathways (**Figure 3.2F and Supp. Table 3.3**).

To identify any transcriptional changes occurring in the other clusters with EtOH, we performed differential analysis. In cells within the non-classical subset, expression of genes important for defense response (*MRC1, STAT1*) and stem cell differentiation (*MEF2C, CITED2*) was reduced, while that of genes that play a role in wound healing (*SERPINA1, THBS1*) and migration (*MIF, FN1*) was increased with EtOH (**Supp. Figure 3.1C**). Differential analysis of the classical clusters revealed significant upregulation of genes mapping to chemotaxis (*CSF3R, VEGFA*), response to wounding (*CD44, FN1*), and chronic inflammatory response (*S100A8, S100A9*) with EtOH (**Figure 3.2G,H**). Broadly, we noted decreased expression of *HSPA8, CCL4L1, EGR1, MAMU-DQA1*, and *SELENOP* and increased expression of *IL1B, S100A9, THBS1, HIF1A*, and *IFI27* across classical, intermediate, and non-classical clusters with EtOH (**Figure 3.2I**). This was accompanied by increased module score expression associated with oxidative stress, HIF1A Signaling, and chronic inflammation in all monocyte clusters with EtOH (**Figure 3.2J**). CCR2 is associated with monocyte egress from the bone marrow compartment and into circulation (183). Interestingly, we identified that *CCR2* expression, while expressed on only a small percentage of cells, was higher on classical bone marrow monocytes with EtOH (**Figure 3.2K**).

It has been suggested that there are two distinct lineages of monocyte production in the bone marrow (72, 73, 168); therefore, we assessed the impact of chronic EtOH consumption on the expression of genes associated with MDP-derived versus GMP-derived classical monocytes. C2 and C4 expressed high levels of *S100A8/9* while C1, C3, C5, C6, C7, C8 had higher expression of *CD74* and *MAMU-DRA* (**Supp. Figure 3.1D**). While we did not note significant changes in the distributions of MDP- versus GMP-derived clusters with EtOH (**Figure 3.2D**), we did identify that the GMP-derived clusters had higher expression of *S100A8/9* and the MDP-derived clusters had lower expression of *CD74/MAMU-DRA* with EtOH (**Supp. Figure 3.1D**). In summary, scRNA seq analysis revealed heightened inflammatory and oxidative stress transcriptional signatures in bone marrow monocyte populations with EtOH. Additionally, higher frequency of *CXCR4*hi cells, increased *CCR2* expression, and increased expression of GMP-derived monocyte markers on classical monocytes pointing to disruptions in the bone marrow monocyte compartment and potentially monocyte production and export with EtOH.

EtOH drinking skews the production of functional monocytes and colony formation of CD34+ progenitors

Next, we investigated the impact of chronic ethanol consumption on the functional properties of CD34+ progenitor cells. First, we purified CD34+ cells and cultured them for 7 days with a monocyte skewing supplement (**Figure 3.3A**). We then profiled the cultures by flow cytometry to measure proportions of CD14+ cells. Cultures from EtOH group showed reduced capacity to differentiate into CD14+ cells (lacking CD34) as indicated by the higher frequency of CD34+CD14+ and CD34+ cells compared to control animals (**Figure 3.3B,C and**

Supp. Figure 3.2A). Although CD34+CD14+ cells are likely an artifact of the in vitro culture system, the increase in this population with EtOH suggest disrupted maturation. Expression of monocyte maturation markers CD11C and CD115 increased similarly in the cultured CD14+ populations regardless of EtOH exposure (**Supp. Figure 3.2B**). Additionally, no differences were detected in CCR2 expression, but the percentage of HLA-DR+ CD34+CD14+ cells and HLA-DR MFI in CD34+ cells were increased with EtOH consumption (**Supp. Figure 3.2C**). Although we found no differences in CCR2 surface expression with EtOH, we do note significant and trending increases in CCR2 percentage and MFI on CD34+CD14+ cells compared CD34+ or CD14+ populations, respectively (**Figure 3.3D**).

To better assess the monocyte production in these cultures at the transcriptional level, we pooled control and EtOH cultures and performed scRNA-Seq. Using highly expressed gene markers, we were able to identify remaining progenitor cells (*CD34, STMN1, CD38*), GMP-(*S100A8/9*) and MDP-derived (*IRF8, CX3CR1*) lineages of monocytes, a cluster of monocyte-derived macrophages (*SIGLEC1, S100A11*), and two clusters of contaminating megakaryocyte/erythroid progenitors (*PLEK, HBA, GPX4*) (**Figures 3.3E,F and Supp. Table 3.2**). Pseudotime analysis further confirmed this annotation, defining a trajectory for each of the monocyte lineages (**Figure 3.3E**). The GMP lineage was defined by increasing expression of *AZU1* and *MPO*, whereas increasing *MAMU-DRA* and *CD74* defined the MDP lineage (**Figure 3.3G**). Further analysis shows that while control CD34+ cells were more likely to differentiate along the MDP lineage into DC-monocytes, CD34+ cells from a EtOH group were likely to differentiate along the GM lineage towards Neutrophil-monocytes (**Figure 3.3H**, **I**). To test whether the monocytes derived from the EtOH CD34+ progenitor cells are poised towards a heightened inflammatory response, we stimulated them with a bacterial TLR

cocktail and measured cytokine, chemokine, and growth factor production by Luminex (**Figure 3.3A**). Production of inflammatory TNFα, IL-6, and IL1β, growth factor G-CSF, chemokine CCL3 (MIP-1α) and cytokine IL-2 was significantly increased in EtOH after the stimulation (**Figure 3.3J**).

Finally, to assess the impact of chronic EtOH consumption on the ability of CD34+ progenitor cells to differentiate into cells of the myeloid lineage, we performed a colony forming unit (CFU) assay. No differences were noted in total number of colonies after 7 or 10 days of culture, but a skewing of the progenitors towards granulocyte/monocyte-containing colonies (CFU-GM and CFU-GEMM) and away from erythroid only colonies (CFU-E and BFU-E) was evident at day 10 in EtOH cultures (**Figure 3.3K-M and Supp. Figures 3.2D,E**). These observations indicate that EtOH alters the differentiation potential of CD34+ progenitors, skewing monocyte differentiation towards a more inflammatory GMP-derived lineage and increasing the production of granulocyte/monocyte progenitor colonies.

scRNA-Seq of CD34+ progenitors reveals increased oxidative stress and inflammatory pathways in myeloid progenitors with EtOH

Next, we assessed the impact of chronic ethanol consumption on the distribution of major progenitor populations by flow cytometry (**Supp. Figure 3.3A**). Frequency of CD34+CD38-CD45RA-CD90- multipotent progenitors (MPP) (**Figure 3.4A**), CD34+CD38-CD45RA-CD90+ hematopoietic stem cells (HSC), and CD34+CD38+CD45RA-CD123+CD64- common myeloid progenitors (CMP) were slightly increased in the EtOH group (**Figure 3.4A**). To uncover transcriptional changes in these progenitor populations with EtOH, we profiled purified CD34+ bone marrow cells by scRNA-Seq (n=3 female controls, 4 male controls, 3 female

EtOH, 4 male EtOH). UMAP clustering revealed 17 cell populations which were defined using highly expressed gene markers (**Figure 3.4B,C, Supp. Figure 3.3B, and Supp. Table 3.2**). These clusters could be broadly defined by differentiation state and lineage markers with HSC clusters expressing high levels of *HOPX, CD164, MKI67*, and *STMN1* (**Figure 3.4C**). Cells from the erythroid lineage including megakaryocyte/erythroid progenitors expressed *CPA3* and *KLF1* while those from the lymphoid lineage expressed *RAG1, IL7R*, and *CD79B* (**Figure 3.4C**). Within the myeloid lineage, monocyte-DC progenitors (MDP) could be identified based on the expression of *IRF8, MAMU-DRA,* and *BATF3,* while granulocyte-monocyte progenitors (GMP) were identified based on the expression of *LYZ, ELANE*, and *MPO* (**Figure 3.4C**). Pro-neutrophils expressed lower levels of *LYZ* and the highest levels of *ELANE* and *MPO* (**Figure 3.4C**). On the other hand, more differentiated monocyte clusters (cMoP, MP, and pro-monocytes) were defined by increased expression of *FCER1A* and *CD14* (**Figure 3.4C**). Cluster assignments were confirmed using module scoring based on gene lists from the Human Cell Atlas bone marrow single cell dataset (181) as well as our differential analysis of sorted macaque GMP and CMP bulk RNA-Seq to define less mature CMP, granulocyte progenitors and two MDP modules (**Supp. Figure 3.3C, Figure 3.4D and Supp. Tables 3.3,4**). Chronic EtOH consumption was associated with a reductions in the CMP/GMP and GMP-2 clusters that was accompanied by a slight increase in the CLP/pre T cell clusters (**Supp. Figure 3.4A,B**).

We next utilized pseudotime analysis to assess the differentiation trajectories in the progenitors from HSC through the myeloid lineage. We identified four unique lineages, three of which (1, 3, 4) proceeded through GMP or MDP progenitors to cMoP/MP or pro-monocyte populations (**Supp. Figure 3.4C**). Lineage 2 leads through GMP-1 and into the pro-

neutrophil population (**Supp. Figure 3.4C**). A higher density of cells from the EtOH group was detected at the end of lineages 1 and 3 (more mature monocytes), while a higher frequency of control cells was detected at the end of lineages 2 and 4 (pro-neutrophils and cMoP/MP (**Supp. Figure 3.4D**). These differences, however, were rather modest suggesting early differentiation towards monocyte progenitors may not significantly contribute to later changes in monocyte production with EtOH.

To assess transcriptional changes in progenitor populations that could contribute to altered monocyte output and function, we performed differential analysis on HSC, MDP, GMP, and more mature monocyte progenitors (cMoP, MP, pro-monocytes) comparing EtOH to control cells. Functional enrichment was carried out to elucidate the biological processes impacted (**Figure 3.4E,F**). Upregulated DEG from all four comparisons enriched significantly to oxidative phosphorylation (*ATP6, ATP8, COX1, NDL4*) highlighting potential metabolic shifts in the bone marrow compartment with EtOH (**Figure 3.4E,G**). Additionally, upregulated DEG detected in HSC, GMP, and monocyte progenitors, but not MDP mapped to "response to oxidative stress" (*ND5, TRA2B, TXNIP*), "immune response" (*CAMP, LYZ, S100A9*), and "cell activation" (*GRN, PLEK, NR4A3*) processes (**Figure 3.4E,G**). Downregulated DEG in HSC, GMP, and monocyte progenitors enriched to gene ontology (GO) terms associated with cytokine and chemokine production (*AIF1, ANXA4, AZU1, ELANE*) pathways, as well as cell-cell adhesion (*HSPD1, SELL, HSPH1*) in monocyte progenitors (**Figure 3.4F,G**). As described for bone marrow CD14+ cells (**Figure 3.2**), genes associated with inflammation/activation including *S100A8, S100A9, IFI27* were increased in monocyte progenitors whereas genes that play a role in antigen presentation (*MAMU-DQA1, MAMU-DRA*, and *HSPA8*) were down regulated with EtOH drinking (**Figure 3.4G**). To conclude, transcriptional changes observed

in monocyte progenitors in the bone marrow point to increased oxidative stress and inflammatory pathways associates with EtOH drinking.

EtOH drinking disrupts bone marrow niche macrophage responses and transcriptional profiles

Bone marrow macrophages have critical functions in homeostatic maintenance of stem cells and bone marrow niche (184, 185). We previously showed that EtOH drinking dysregulated function and transcriptome of tissue macrophages (24). No difference in percentage of CD169+ cells was observed with EtOH, but CD14 and CD86 expression (percentage and MFI) were decreased with EtOH (**Figure 3.5A-C**). Moreover, CD169+ macrophages from EtOH drinking macaques upregulated HLA-DR MFI significantly less than their control counterparts following stimulation with a bacterial TLR cocktail (**Figure 3.5D**).

The CD14+ bone marrow scRNA-Seq revealed the presence of a *FABP4*hi, *SIGLEC1*hi macrophage population (**Figure 3.2B and Figure 3.5E**). Although the frequency of this cluster did not differ between the two groups (**Figure 3.5F**), considerable transcriptional changes were detected with EtOH. Downregulated DEG mapped to response to stimulus (*CCL8, CCL13, CCL24, CCL4L1*) and developmental processes (*DDX5, EGR1, FOS, BTG2*), whereas upregulated DEG mapped to metabolic (*MT-ATP8, MT-CO2, MT-ND2, NDUFA1*) and cellular migration and adhesion (*IFI27, TREM1, VEGFA, VCAN*) processes (**Figure 3.5G-I**). This analysis suggests that EtOH-induced changes in bone marrow macrophages could alter their ability to properly regulate bone marrow niche homeostasis.

DISCUSSION:

Chronic alcohol drinking has been shown to disrupt anti-microbial defenses and exacerbate inflammatory responses of monocytes and macrophages (13, 24, 108, 113), Some studies have suggested that ethanol and its metabolites modulate monocyte function through epigenetic modification and oxidative stress of both mature cells and hematopoietic progenitors, but the exact mechanisms remain poorly defined (24, 108, 178). In this study, we utilize bone marrow cells collected from NHP after 12 months of voluntary EtOH dinking to assess the phenotypic, functional, and single cell transcriptomic profiles of CD14+ and CD34+ cells.

Using this NHP model, we have previously reported increased percentages of blood monocytes and splenic macrophages relative to total cells with chronic EtOH drinking compared to control animals (24, 108). As monocytes are short-lived cells in the periphery, we first determined that this phenotype was not reversed with a one-month abstinence period from EtOH. We then hypothesized that changes in monocytes and even tissue macrophages could be explained by altered bone marrow monocytes or their progenitor cells. While we noted no differences in percentages of the major mature monocyte populations by flow cytometry in the bone marrow with EtOH, we did identify a population of *CXCR4*hi classical monocytes by scRNA-Seq increased with EtOH. Expression of CXCR4 delineates a population of transitional pre-monocytes that help to maintain the mature monocyte pool in the bone marrow (182). How an increase in this pre-monocyte population with EtOH could affect the bone marrow niche or monocytes in circulation requires further investigation. Additionally, *CCR2* expression was increased on classical monocytes with

EtOH. As CCR2 is critical for monocyte egress from the bone marrow, this points to EtOH-induced alterations in bone marrow monocyte recruitment and escape from the bone marrow (183). We next performed two functional assays on CD34+ cells to assess the production and function of culture-derived monocytes as well as monocyte colony formation. In the first, we noted a reduction in the production of mature CD14+ cells and an increase in less mature populations with EtOH. Coinciding with increased *CCR2* expression in bone marrow monocytes, these less mature cells had increased basal expression of CCR2. This suggests CCR2 expression may play a role in alcohol-induced alterations to monopoiesis and warrants more targeted investigation in the future. The second functional assay also points to altered myelopoiesis where we noted increased production of colonies containing granulocyte/monocyte progenitor cells. Both outcomes could be due to altered composition of progenitors in the starting CD34+ pools, however upon progenitor phenotyping by flow cytometry and scRNA-Seq analysis of CD34+ cells, we noted only small increases in less mature progenitors (HSC, MPP, CMP) with EtOH. These data suggest EtOH-induced shifts in myelopoiesis and monopoiesis, giving rise to functionally altered monocytes and tissue resident macrophages.

In addition to increased monocyte percentages in the periphery, we and others have noted an increase in inflammatory monocyte responses to stimulation with chronic EtOH drinking (13, 24, 108, 113). This phenotype also persists through a one-month abstinence period from EtOH. We next determined that this hyper-inflammatory response profile extended to intermediate bone marrow resident monocytes. These cells responded with increased TNFα, IL-6 and CCL4 (MIP-1β) to bacterial agonists and had increased NFκB and cytokine signaling transcriptional signatures at baseline state. Intermediate monocytes

differentiate from classical monocytes and the role these cells play in the bone marrow compartment are yet to be determined (60). Additionally, the CD14+ scRNA-Seq data pointed to increased transcriptional markers of inflammation broadly across the dataset with EtOH. This corresponds to increased inflammation seen transcriptionally in peripheral monocytes (108). To test whether this phenotype was initiated in the CD34+ progenitor compartment, we further performed scRNA-Seq and a stimulation assay on the monocyte differentiation cultures. This analysis revealed that EtOH not only induced a skewing towards more neutrophil-like monocyte lineage, but also led to a significant increase in inflammatory mediator production from these culture-derived monocytes. Differential expression analysis from scRNA-Seq data of the CD34+ cells also revealed that inflammation-associated *S1008/9* genes were upregulated in more mature progenitor cells (MP, cMoP) with EtOH. Collectively, these data suggest that the hyper-inflammatory profiles of circulating monocytes with EtOH are at least partially derived from their CD34+ progenitors in the bone marrow.

EtOH metabolism produces acetaldehyde and increases NADH levels, which in turn promotes reactive oxygen species (ROS) production (166). These products induce DNA damage as well as oxidative stress on cells and can have direct effects on cellular function including HPSC (166, 186). In both the CD14+ and CD34+ compartments of the bone marrow, we noted increases in transcriptional signatures of oxidative stress and oxidative phosphorylation, suggesting EtOH-induced shifts to cellular metabolism in the bone marrow. In fact, a study in NHP bone marrow notes altered mitochondrial function with daily EtOH drinking (178).

One of the mechanisms by which EtOH could lead to HPSC and bone marrow niche dysfunction is through altering the bone marrow CD169+ macrophage population, which are critically important for maintenance of the niche (184, 185). Expression of activation markers was decreased in the EtOH group at resting state and upregulation of HLA-DR after bacterial agonist stimulation was impaired. This was accompanied by heightened transcriptional signatures of oxidative phosphorylation. Together with previous reports of reduced macrophage functional capacities with alcohol exposure including phagocytosis (55), these data suggest that the ability of these macrophages to maintain the bone marrow niche are compromised with EtOH.

In summary, data from this study strongly suggest that chronic EtOH drinking alters monopoiesis from the bone marrow compartment in NHPs. Specifically, EtOH disrupts the differentiation of CD34+ cells and leads to the production of monocytes with a hyper-inflammatory phenotype. These disruptions could be mediated by EtOH-induced oxidative stress and altered profiles of niche-maintaining macrophages. Future research efforts will focus on determining a timeline for alcohol-induced bone marrow remodeling, identifying the epigenetic underpinnings of changes in progenitor cells, and determining how alcohol alters monocyte release from the bone marrow compartment. Additionally, this body of work provides a scRNA-Seq resource to study NHP bone marrow monocytes and progenitors.

Acknowledgements

We are grateful to the members of the Grant laboratory for expert animal care and sample procurement. We thank Dr. Jennifer Atwood for assistance with sorting in the flow cytometry core at the Institute for Immunology, UCI. We thank Dr. Melanie Oakes from UCI Genomics and High-Throughput Facility for assistance with sequencing. We thank Dr. Helen Goodridge for assistance with CFU assay protocols and analysis.

Data availability

The datasets supporting the conclusions of this article are available on NCBI's Sequence Read Archive (SRA# Pending).

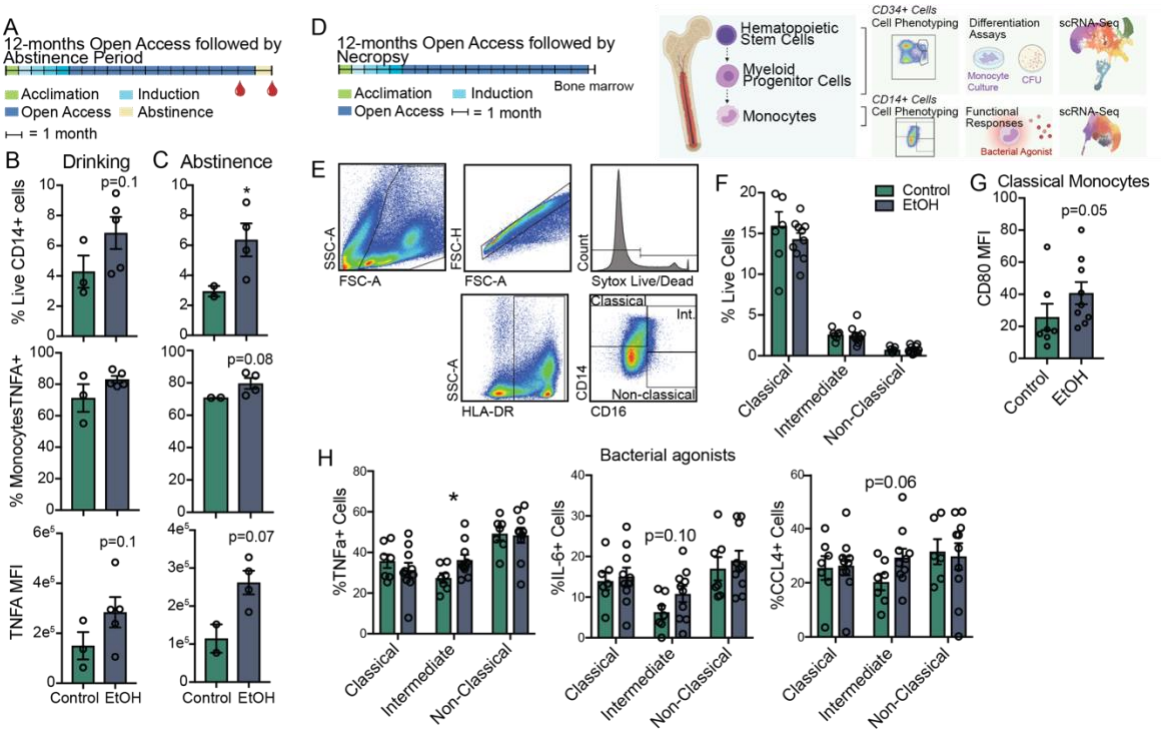

Figure 3.1: Inflammatory blood monocyte phenotype with EtOH drinking extends through abstinence

A) EtOH drinking timeline and blood collection for macaque cohort with abstinence period. Flow cytometry phenotyping and Intracellular cytokine staining (ICS) after 16-hour LPS stimulation were performed on total PBMC at two timepoints indicated in (A). B,C) Bar plots showing % of live CD14+ PBMCs (top), % TNFα + CD14+ monocytes (middle), and TNFα MFI from CD14+ monocytes (bottom) after one year of EtOH drinking (B) and one month abstinence (C) and ICS measurements corrected for the unstimulated condition (Control, green; EtOH, blue bars). D) EtOH drinking timeline and bone marrow collection for two cohorts of macaques. Experimental design for study partially created on Biorender.com. E) Example gating strategy for monocyte populations from the bone marrow. F) Bar plot showing percentages of classical, intermediate, and non-classical monocytes from flow cytometry. G) Bar plot of CD80 MFI on classical monocytes. H) Total bone marrow cells were stimulated with a bacterial TLR cocktail (Pam3CSK4, LPS, and FSL-1) and the percentage of TNFα+ (left), IL-6+ (middle), and CCL4 (MIP-1β) (right) were measured in each monocyte population and corrected for the unstimulated condition. Statistical significance was tested by t-test with Welch's correction where *=p<0.05.

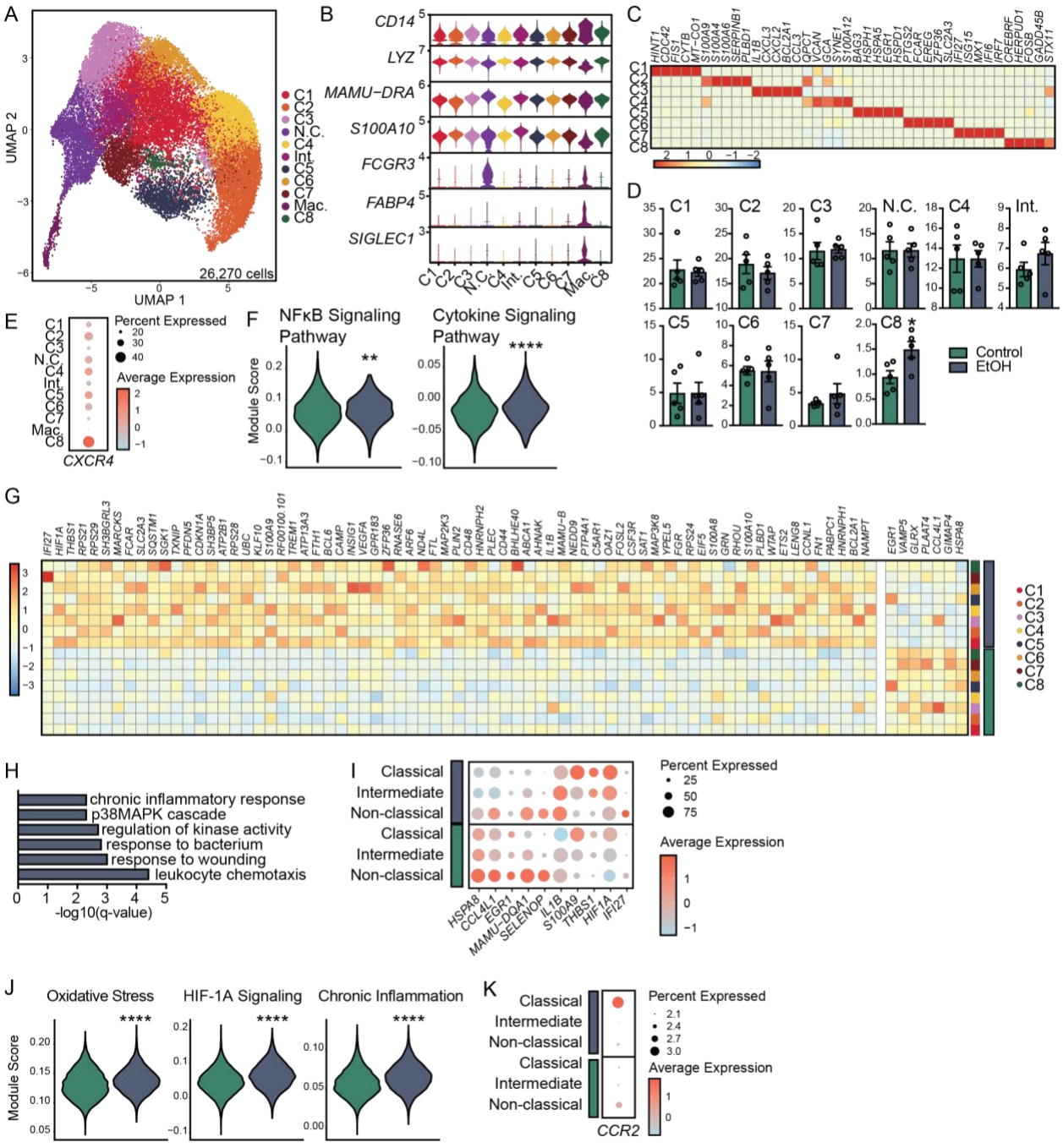

Figure 3.2: Shift in the single cell transcriptional profiles of CD14+ cells from the bone marrow of macaques with EtOH drinking

CD14+ cells were purified from the bone marrow of macaques with (blue bars) and without (green bars) EtOH drinking and subjected to 10X scRNA-Seq. A) UMAP clustering of 26,270 cells. B) Stacked violin plot showing expression of genes identified using Seurat's

FindAllMarkers function. C) Heatmap showing averaged gene expression of highly expressed genes from each classical monocyte cluster. D) Bar plots showing percentage of total cells contributing to each monocyte cluster. E) Dot plot showing expression of *CXCR4* across each cluster where the size of the dot represents percent of cells expressing the gene and the color represents an averaged expression value. F) Violin plots representing module score expression for NFκB and cytokine signaling pathways in intermediate monocytes. Statistical significance was tested using Mann-Whitney test. G) Heatmap showing averaged gene expression of differentially expressed genes from each classical monocyte cluster split by EtOH (top) and control (bottom) groups. H) Bar plot representing $-\log_{10}$(q-value) functional enrichment scores for genes upregulated in classical monocyte clusters with EtOH. I) Dot plot showing expression of up- and down-regulated DEG with EtOH common to all three monocyte subsets where the size of the dot represents percent of cells expressing the gene and the color represents an averaged expression value. J) Violin plots representing module score expression for oxidative stress, HIF-1α signaling, and chronic inflammation pathways in total monocytes. K) Dot plot showing expression of *CCR2* across each monocyte subset split by EtOH and control where the size of the dot represents percent of cells expressing the gene and the color represents an averaged expression value. Unless indicated, statistical significance was tested by t-test with Welch's correction. *=p<0.05, **=p<0.01, ****=p<0.0001.

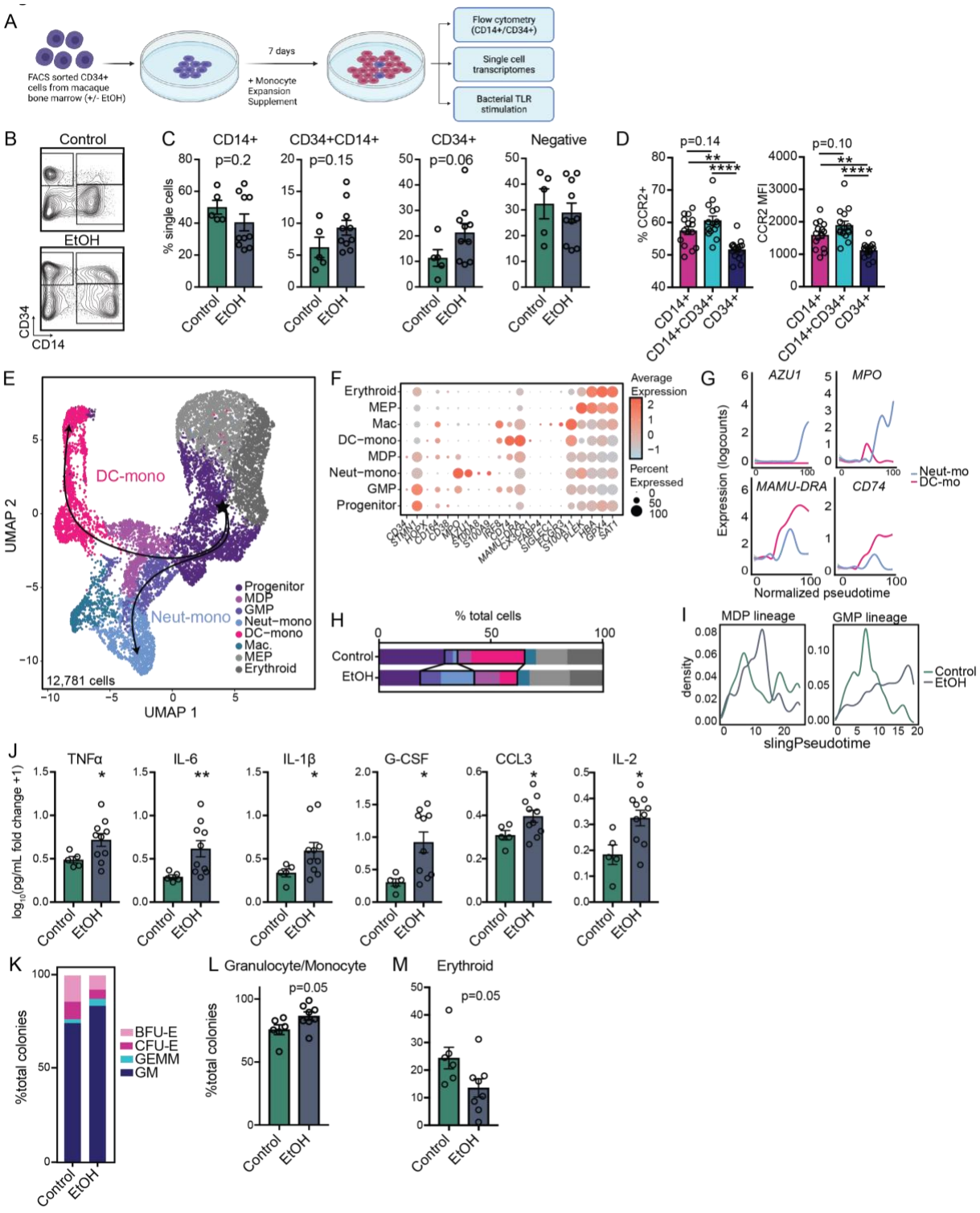

Figure 3.3: EtOH drinking alters CD34+ progenitor cell differentiation to monocytes

A) Experimental design generated on Biorender.com. Sorted CD34+ cells from control and EtOH drinking macaque bone marrow were cultured in monocyte differentiation media

supplement for 7 days. B) Example flow gating showing CD34+ versus CD14+ cells. C) Bar plots showing quantification of the culture output by flow cytometry (Control, green; EtOH, blue bars). D) Bar plots showing %CCR2+ (left) and CCR2 MFI (right) quantification from flow cytometry. Statistical significance was tested using One-way ANOVA with multiple comparisons. E) The same cultures were pooled from each group and subjected to 10X scRNA-Seq. UMAP projection of 12,781 cells overlayed with Slingshot pseudotime lineage lines. F) Dot plot showing expression of genes identified using Seurat's *FindAllMarkers* function across each cluster where the size of the dot represents percent of cells expressing the gene and the color represents an averaged expression value. G) Log expression of *AZU1, MPO, MAMU-DRA, CD74* plotted for each cell across the indicated scaled Slingshot pseudotime trajectory (trendline shown). H) Bar plots showing representative percentages of each cluster across control and EtOH groups. I) Cell density plots for Control and EtOH groups across each trajectory lineage determined by Slingshot. J) Cultures were stimulated for 6 hours with a bacterial TLR cocktail (Pam3CSK4, LPS, and FSL-1). Bar plots showing the $\log_{10}$(fold change +1) concentration of each of the indicated analytes measured by Luminex. K) CFU assays were performed on sorted CD34+ cells and colonies counted and scored after 10 days. Bar plots showing distribution of median values of counted colonies from each group. L,M) Bar plots showing percentages of CFU-GM, CFU-GEMM colonies (L) and CFU-E, BFU-E (M). Unless indicated, statistical significance was tested by t-test with Welch's correction. *=p<0.05, **=p<0.01, ****=p<0.0001.

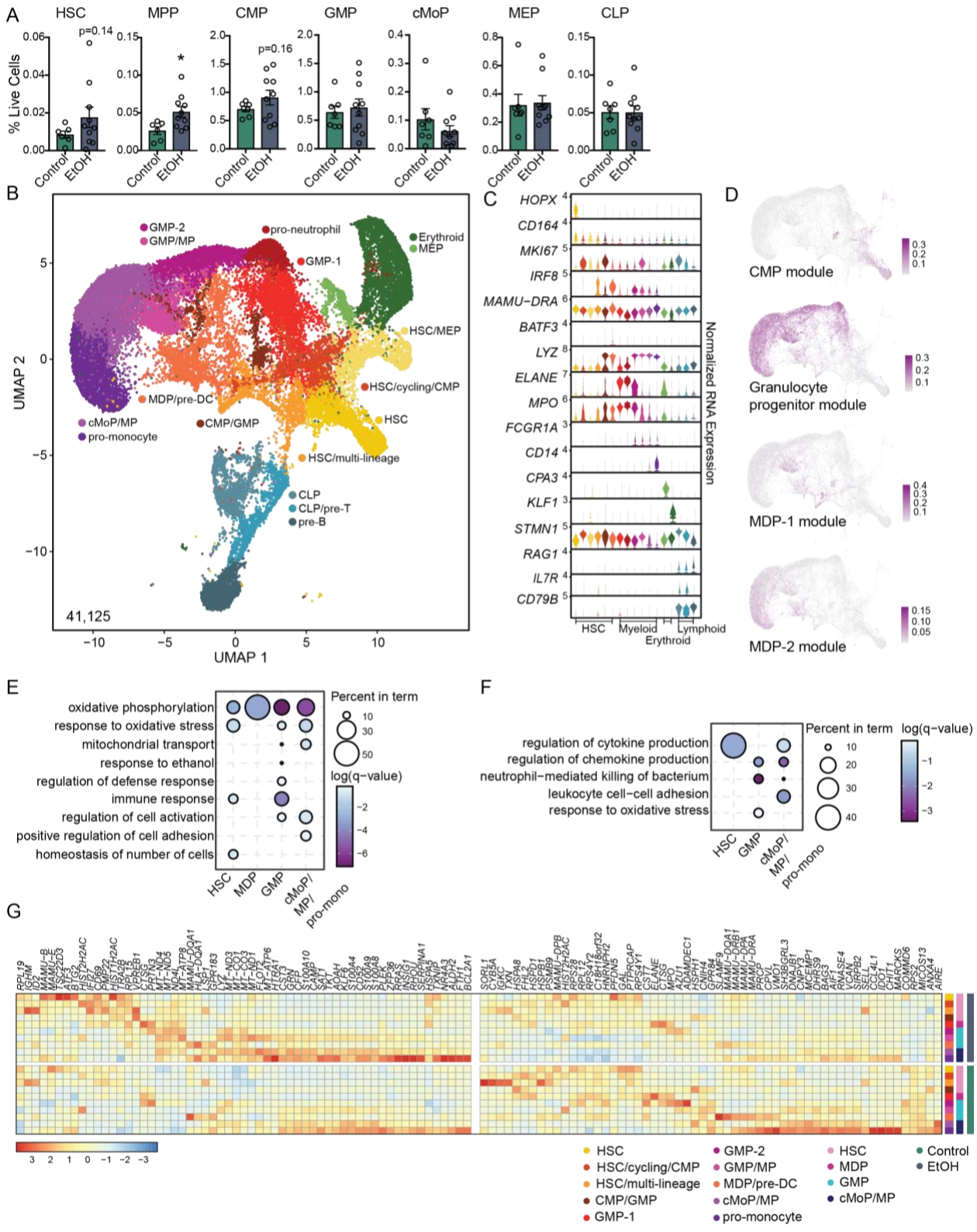
A
HSC
MPP
CMP
GMP
cMoP
MEP
CLP
% Live Cells
p=0.14
p=0.16
*
Control
EtOH
B
GMP-2
GMP/MP
pro-neutrophil
GMP-1
Erythroid
MEP
HSC/MEP
HSC/cycling/CMP
MDP/pre-DC
cMoP/MP
pro-monocyte
CMP/GMP
HSC
HSC/multi-lineage
CLP
CLP/pre-T
pre-B
41,125
UMAP 1
UMAP 2
C
HOPX
CD164
MKI67
IRF8
MAMU-DRA
BATF3
LYZ
ELANE
MPO
FCGR1A
CD14
CPA3
KLF1
STMN1
RAG1
IL7R
CD79B
Normalized RNA Expression
HSC
Myeloid
Lymphoid
Erythroid
D
CMP module
Granulocyte progenitor module
MDP-1 module
MDP-2 module
E
oxidative phosphorylation
response to oxidative stress
mitochondrial transport
response to ethanol
regulation of defense response
immune response
regulation of cell activation
positive regulation of cell adhesion
homeostasis of number of cells
Percent in term
log(q-value)
HSC
MDP
GMP
cMoP/ MP/ pro-mono
F
regulation of cytokine production
regulation of chemokine production
neutrophil-mediated killing of bacterium
leukocyte cell-cell adhesion
response to oxidative stress
Percent in term
log(q-value)
HSC
GMP
cMoP/ MP/ pro-mono
G
HSC
HSC/cycling/CMP
HSC/multi-lineage
CMP/GMP
GMP-1
GMP-2
GMP/MP
MDP/pre-DC
cMoP/MP
pro-monocyte
HSC
MDP
GMP
cMoP/MP
Control
EtOH

Figure 3.4: CD34+ bone marrow progenitor single cell transcriptional profiles with EtOH drinking

A) Bar plots showing percentages of progenitor populations in the bone marrow compartment determined by flow cytometry (Control, green; EtOH, blue bars). B) CD34+ cells were sorted from the bone marrow of control and EtOH drinking macaques and subjected to 10X scRNA-Seq. UMAP clustering of 41,125 cells and indicated cluster identification. C) Stacked violin plot showing expression of genes identified using Seurat's *FindAllMarkers* function. D) Feature plots showing relative expression of module scores for CMP, Granulocyte progenitors, MDP-1, and MDP-2 in the myeloid lineage. E,F) Dot plots showing functional enrichment terms for upregulated (E) and downregulated (F) DEG calculated from HSC, MDP, GMP, and monocyte progenitor clusters. The size of the dot represents the percentage of genes in the list that map to that term and the color represents the $\log_{10}$(q-value). G) Heatmap showing averaged gene expression of differentially expressed genes from each indicated cluster split by EtOH and control groups. Statistical significance was tested by t-test with Welch's correction. *=$p<0.05$.

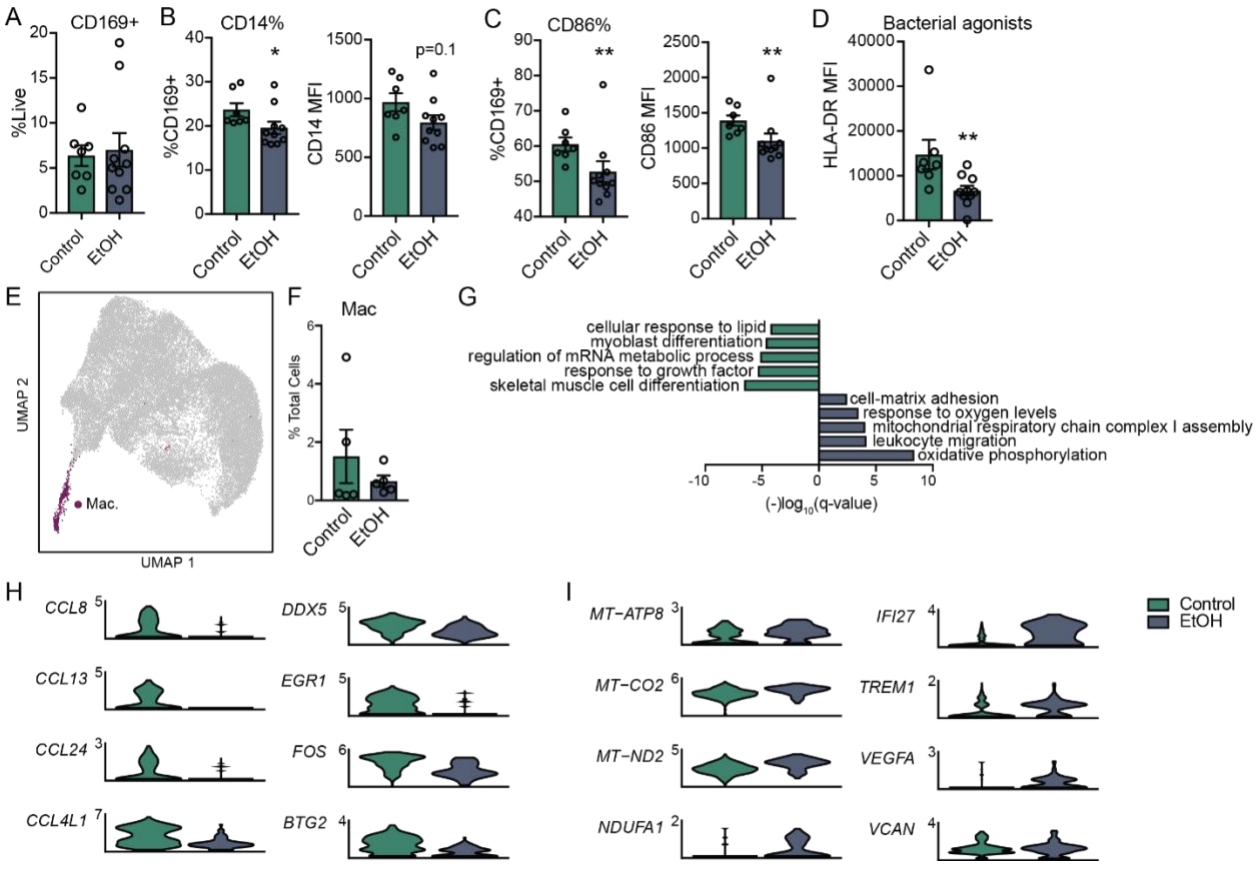

Figure 3.5: Functional and transcriptomic alterations of bone marrow niche macrophages with EtOH

A) Bar plots showing percentage of CD169+ macrophages from the bone marrow compartment determined by flow cytometry (Control, green; EtOH, blue bars). B) Bar plots of %CD14+ (left) and CD14 MFI (right) on CD169+ cells. C) Bar plots of %CD86+ (left) and CD86 MFI (right) on CD169+ cells. D) Total bone marrow cells were stimulated with a bacterial TLR cocktail (Pam3CSK4, LPS, and FSL-1) and HLA-DR MFI was measured by flow cytometry and corrected for the unstimulated condition. E) UMAP showing a macrophage cluster from CD14+ scRNA-Seq (Figure 2) defined by *FABP4* and *SIGLEC1*. F) Bar plot showing macrophage percentages in each group from scRNA-Seq data. G) Bar plot representing -$\log_{10}$(q-value) functional enrichment scores for genes up- and downregulated in the macrophage cluster with EtOH. H,I) Violin plots of down- (H) and up- (I) regulated DEG with EtOH in the macrophage cluster. Statistical significance was tested by t-test with Welch's correction. *=p<0.05, **=<0.01.

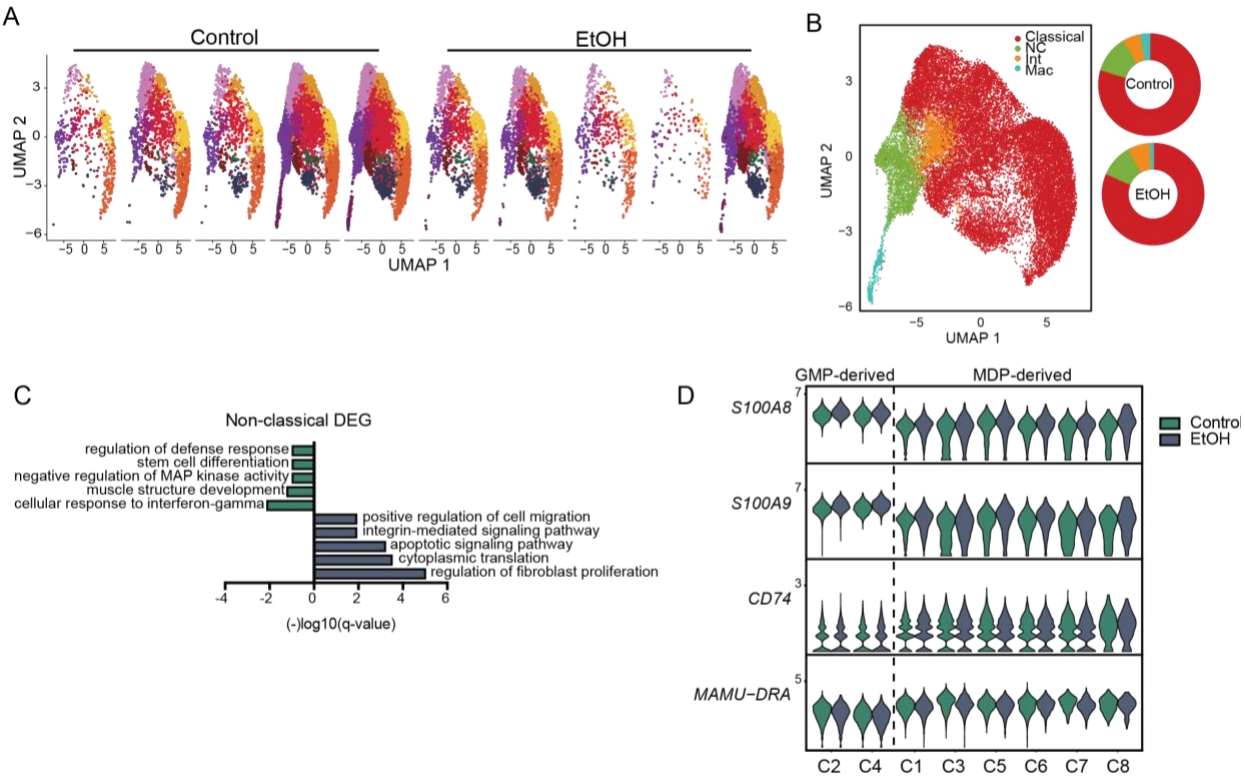

Supp. Figure 3.1: scRNA-Seq of CD14+ cells from the bone marrow

A) UMAPs of each individual macaque sample. B) UMAP annotated by broad classification of cell type and corresponding pie charts of abundance of cells from each group. C) Bar plot representing -$\log_{10}$(q-value) functional enrichment scores for genes up- and downregulated in non-classical monocytes with EtOH. D) Stacked violin plots of genes related to GMP or MDP lineages across each classical cluster and split by EtOH and control groups.

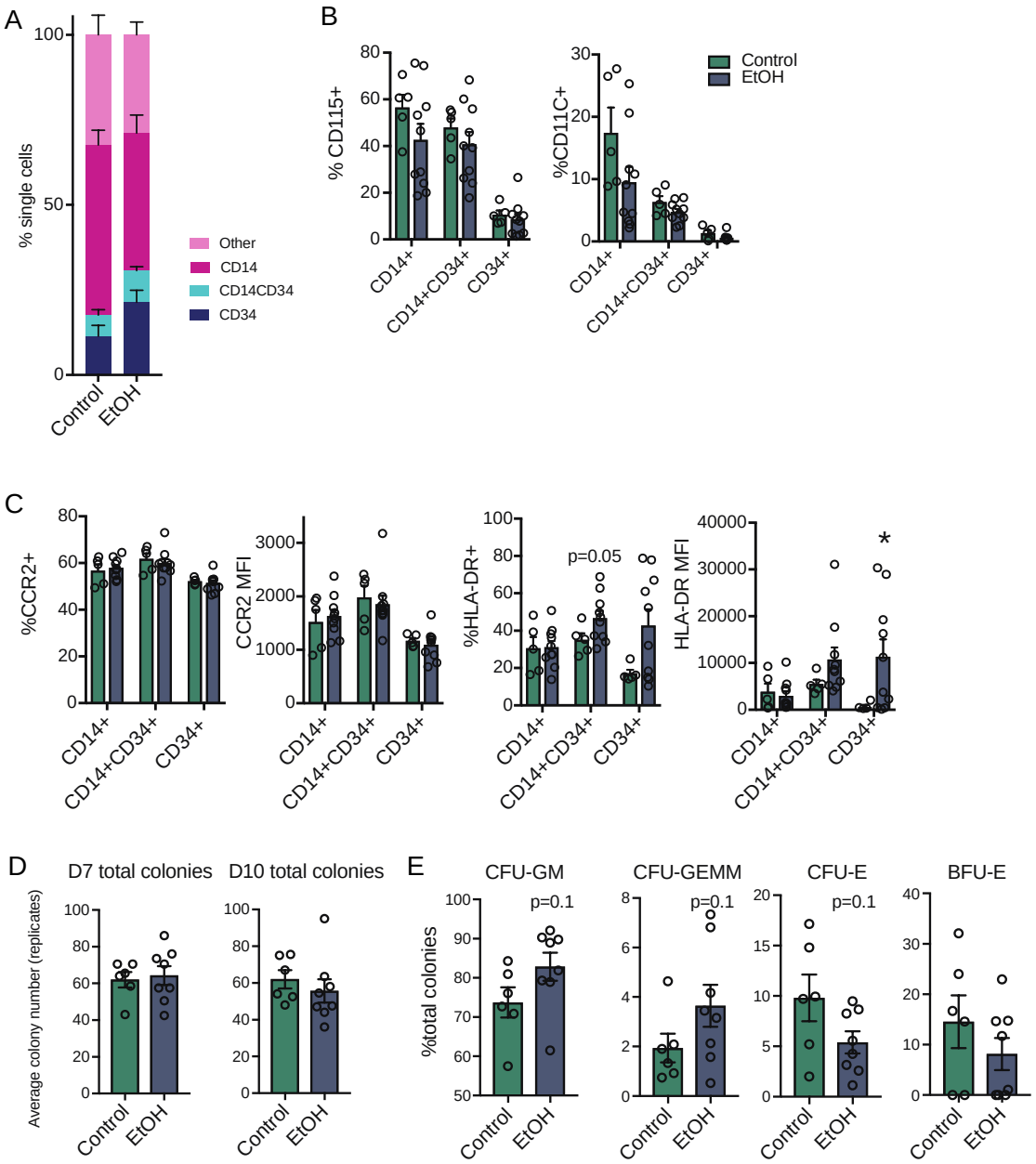

Supp. Figure 3.2: CD34+ progenitor differentiation assays

A) Bar plots showing distribution of CD14 and CD34 populations after monocyte culture assay. B) Bar plots showing %CD115+ (left) and %CD11C+ (right) quantification in culture populations from flow cytometry. C) Bar plots showing %CCR2+, CCR2 MFI, %HLA-DR+, and HLA-DR MFI quantification from flow cytometry. D) Bar graphs showing average colony numbers on day 7 and day 10 of culture. E) Bar plots showing percentage of each colony type calculated from total colony number. Statistical significance was tested by t-test with Welch's correction. *=$p<0.05$.

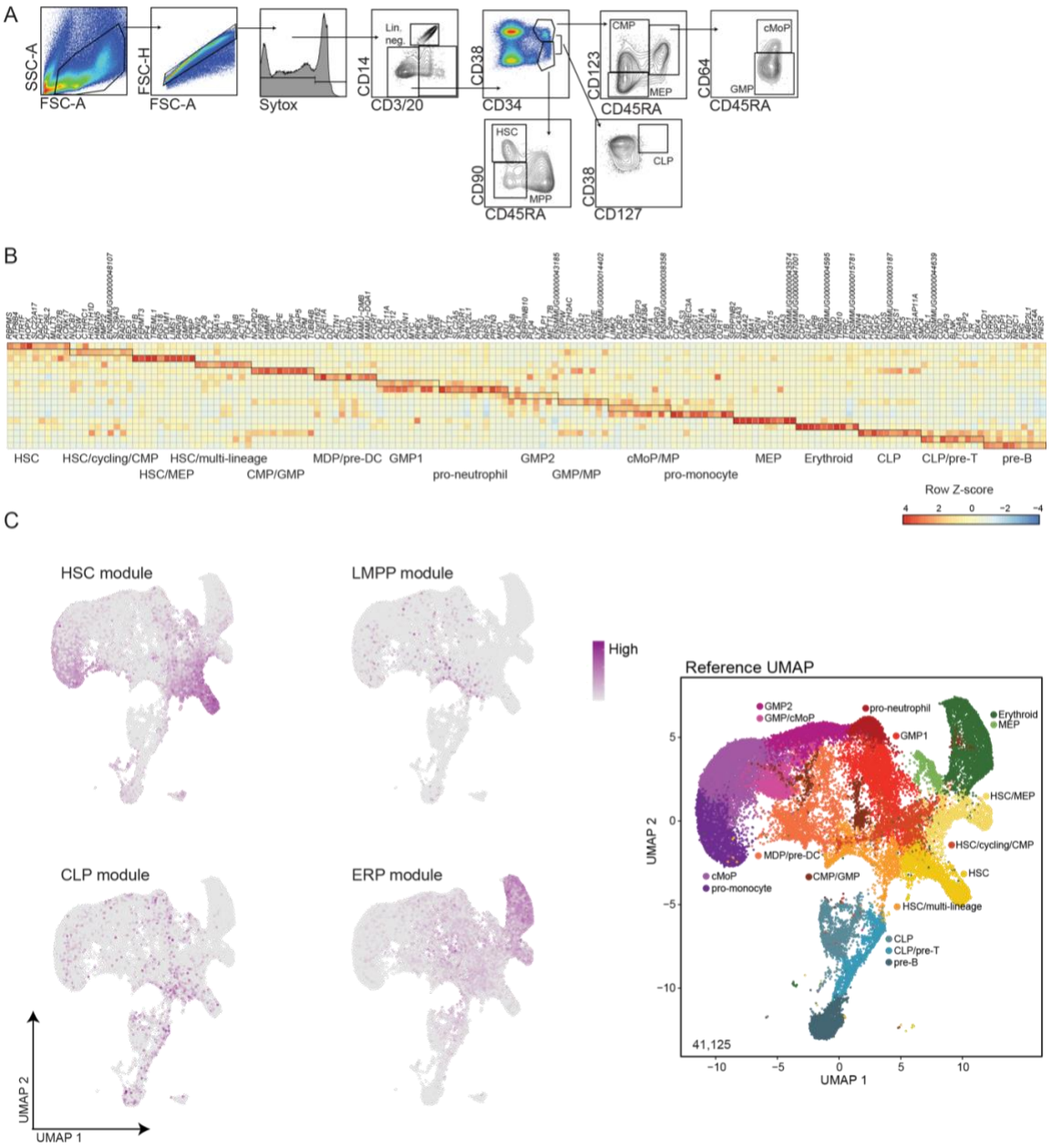

Supp. Figure 3.3: Flow cytometry and scRNA-Seq of CD34+ cells from the bone marrow

A) Gating strategy for bone marrow progenitor cells. B) Heatmap showing averaged gene expression of highly expressed genes from each progenitor cluster. C) Feature plots showing relative expression of module scores for HSC, lymphoid-primed multipotent progenitors (LMPP), CLP, and erythroid progenitors (ERP) in the myeloid lineage.

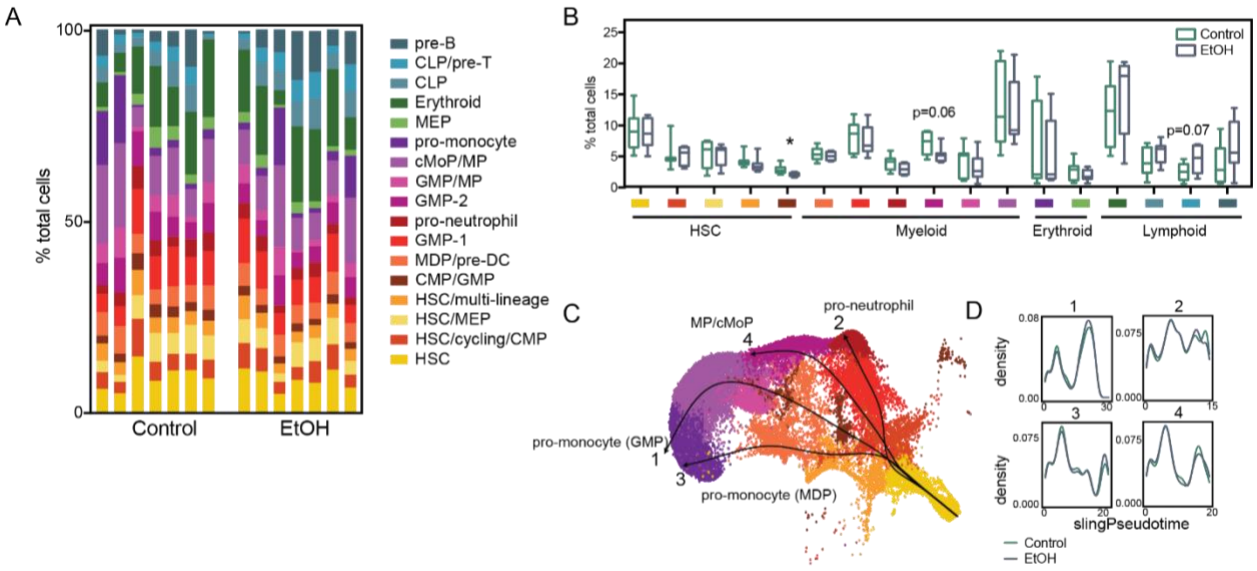

Supp. Figure 3.4: scRNA-Seq of CD34+ cells from the bone marrow

A) Relative distributions of progenitor populations across each scRNA-Seq sample. B) Box plots of percentages of each cluster across control and EtOH groups. C) Myeloid lineage UMAP with Slingshot lineage projection lines. D) Cell density plots for Control and EtOH groups across each trajectory lineage determined by Slingshot. Statistical significance was tested by t-test with Welch's correction. *=p<0.05.

SUPPLEMENTARY TABLES:

Supp. Table 3.1: Animal cohort characteristics

Supp. Table 3.2: FindAllMarkers (CD14+, Culture, CD34+)

Supp. Table 3.3: Module Score Gene Lists

Supp. Table 3.4: edgeR for sorted CMP-GMP bulk RNA-Seq

SUMMARY AND FUTURE DIRECTIONS

The immune system sits in a delicate balance; tipping too far in either direction can disrupt our ability to respond to microbial challenge and maintain tissue homeostasis. A connection between chronic heavy alcohol drinking and immune dysfunction is well established as indicated by higher susceptibility to viral and bacterial infections and diminished wound healing in patients with alcohol use disorders (14-17). A substantial body of work has reported disruptions to both innate and adaptive arms of immunity (4, 13). However, recapitulating the complex nature of human drinking behavior has thus far limited our ability to identify mechanisms of alcohol-induced immune dysfunction in a physiologically relevant way. In this work, we leveraged a non-human primate model of voluntary ethanol drinking to mirror the chronicity and complexity of human drinking behavior (34, 35). We specifically focused on animals that developed a heavy drinking phenotype defined as consuming more than 3g of ethanol per kg bodyweight per day, equating to more than 12 drinks per day in an average 60kg human. The advantages of this model include longitudinal access to samples before and along the drinking timeline, precise recording of ethanol consumption, control over other factors that influence immunity (diet, smoking, use of other drugs) and ability to collect samples such as bronchoalveolar lavage and bone marrow that are otherwise difficult to obtain from humans. This allows us to probe compartments that have previously been unexplored. Using this model, we aimed to characterize the impact of chronic alcohol drinking on immune cell populations in different compartments of the body. We specifically focused on tissue-resident macrophages from the alveolar space, monocytes from the blood, and progenitor cells from the bone marrow. Our studies identified similar epigenetic and transcriptional reprogramming events across these

cell populations, each with functional complications associated with the roles these cells play in homeostasis and response to microbial challenge. Broadly, chronic alcohol drinking induces stress and inflammation in these cells while dampening host-defense responses. These observations provide a mechanism for increased susceptibility of patients with alcohol use disorders to infection.

Chronic alcohol drinking and alveolar macrophages

Alveolar macrophages (AM) are the dominant immune population and first line of defense in the lung (86). They have roles in both pathogen clearance as well as resolving inflammation and repairing tissue (86). *In vitro* ethanol exposure has been shown to induce oxidative stress in AM resulting in reduced phagocytic clearance and altered cytokine production (92, 94). Similarly, we show that 12 months of daily alcohol drinking resulted in decreased phagocytosis ability accompanied by increased intracellular levels of ROS and increased mitochondrial activation in AM from non-human primates. These changes are likely due to epigenetic changes, identified by ATAC-Seq, that correlated with hyper-inflammatory responses to bacterial and viral antigens. Single cell RNA sequencing analysis allowed us to discover significant heterogeneity in monocyte-derived and tissue-resident macrophage populations and revealed heightened baseline activation states and of oxidative stress signatures with chronic ethanol drinking. Another key finding from this study was the increased cathepsin G (*CTSG*) expression in AM with alcohol at the transcriptomic and epigenetic levels. Future studies should aim to investigate the role cathepsin G activity plays in AM function and how this could contribute to alcohol-associate defects in host defense and inflammatory responses. Additionally, future studies should attempt to uncover

whether alcohol drinking rewires tissue resident macrophages and/or infiltrating monocyte/macrophage populations in the lung.

Chronic alcohol drinking and blood monocytes

Monocytes are short-lived cells that are constantly repopulated from the bone marrow, patrol the blood, and extravasate into tissue where they differentiate into macrophages (60). They respond to different stimuli in circulation and the regulation of their production and inflammatory responses is critical for effective pathogen clearance (61). Previous studies have shown that long-term alcohol exposure *in vivo* or *in vitro* led to heightened monocyte inflammatory responses to secondary bacterial stimulation (66, 70, 71). Similarly, we showed that 12 months of daily alcohol drinking led to increased frequency of circulating monocytes and heightened secondary response to bacterial stimulation in the NHP model. Single cell RNA sequencing of monocytes revealed increased signatures of oxidative stress and inflammation. Moreover, chromatin accessibility at promoter regions regulating genes involved in cytokine signaling pathways was increased with alcohol drinking. These data suggest, as summarized above for AM, that chronic alcohol drinking is priming monocytes towards heightened inflammatory responses. Future studies should aim to investigate alcohol-induced effects on monocyte migration, extravasation, and differentiation into tissue macrophages.

Chronic alcohol drinking and bone marrow progenitors

We next investigated whether alcohol-associated increases in monocyte percentage and inflammatory responses were resolved following a one-month abstinence period. We

found that increased abundance and heightened inflammatory responses persisted after the abstinence period, leading us to investigate bone marrow progenitor cells. Since monocytes are short-lived cells, these data strongly suggest that alcohol drinking disrupts monopoiesis in the bone marrow. Very little research exists on alcohol drinking and the bone marrow compartment, but disruptions to hematopoiesis have been observed in patients with alcohol use disorders (76, 173-177). Assessment of monocytes in the bone marrow revealed increased inflammatory and stress signatures similar to what we report in blood monocytes. Furthermore, CD34+ cells from alcohol drinking animals differentiated into monocytes that were skewed towards the granulocyte-monocyte lineage and that had heightened inflammatory responses to bacterial stimulation. Single cell RNA sequencing of CD34+ progenitors uncovered signatures of oxidative stress and inflammation throughout the myeloid lineages. This suggests that reprogramming events we have identified in tissue resident macrophages, and blood and bone marrow monocytes may originate from alcohol-induced changes in stem cell precursors. This study opens the door to many future directions examining the effects of alcohol on the bone marrow niche to alter hematopoiesis.

REFERENCES

1. NIAAA. (2019) SAMHSA, Center for Behavioral Health Statistics and Quality. 2019 National Survey on Drug Use and Health. Table 2.17B – Alcohol Use in Lifetime among Persons Aged 12 or Older, by Age Group and Demographic Characteristics: Percentages, 2018 and 2019.
2. CDC. (2015) Alcohol and Public Health: Alcohol-Related Disease Impact (ARDI). Annual Average for United States 2011–2015 Alcohol-Attributable Deaths Due to Excessive Alcohol Use, All Ages.
3. Romeo, J., Warnberg, J., Nova, E., Diaz, L. E., Gomez-Martinez, S., and Marcos, A. (2007) Moderate alcohol consumption and the immune system: a review. *Br J Nutr* **98 Suppl 1**, S111-115
4. Barr, T., Helms, C., Grant, K., and Messaoudi, I. (2016) Opposing effects of alcohol on the immune system. *Prog Neuropsychopharmacol Biol Psychiatry* **65**, 242-251
5. O'Keefe, J. H., Bhatti, S. K., Bajwa, A., DiNicolantonio, J. J., and Lavie, C. J. (2014) Alcohol and cardiovascular health: the dose makes the poison...or the remedy. *Mayo Clin Proc* **89**, 382-393
6. Mukamal, K. J., and Rimm, E. B. (2001) Alcohol's effects on the risk for coronary heart disease. *Alcohol Res Health* **25**, 255-261
7. Fedirko, V., Tramacere, I., Bagnardi, V., Rota, M., Scotti, L., Islami, F., Negri, E., Straif, K., Romieu, I., La Vecchia, C., Boffetta, P., and Jenab, M. (2011) Alcohol drinking and colorectal cancer risk: an overall and dose-response meta-analysis of published studies. *Ann Oncol* **22**, 1958-1972
8. Baan, R., Straif, K., Grosse, Y., Secretan, B., El Ghissassi, F., Bouvard, V., Altieri, A., Cogliano, V., and Group, W. H. O. I. A. f. R. o. C. M. W. (2007) Carcinogenicity of alcoholic beverages. *Lancet Oncol* **8**, 292-293
9. Grewal, P., and Viswanathen, V. A. (2012) Liver cancer and alcohol. *Clin Liver Dis* **16**, 839-850
10. Priddy, B. M., Carmack, S. A., Thomas, L. C., Vendruscolo, J. C., Koob, G. F., and Vendruscolo, L. F. (2017) Sex, strain, and estrous cycle influences on alcohol drinking in rats. *Pharmacol Biochem Behav* **152**, 61-67
11. Bruha, R., Dvorak, K., and Petrtyl, J. (2012) Alcoholic liver disease. *World J Hepatol* **4**, 81-90
12. O'Brien, J. M., Jr., Lu, B., Ali, N. A., Levine, D. A., Aberegg, S. K., and Lemeshow, S. (2011) Insurance type and sepsis-associated hospitalizations and sepsis-associated mortality among US adults: a retrospective cohort study. *Crit Care* **15**, R130
13. Szabo, G., and Saha, B. (2015) Alcohol's Effect on Host Defense. *Alcohol Res* **37**, 159-170
14. Delgado-Rodriguez, M., Mariscal-Ortiz, M., Gomez-Ortega, A., Martinez-Gallego, G., Palma-Perez, S., Sillero-Arenas, M., and Medina-Cuadros, M. (2003) Alcohol consumption and the risk of nosocomial infection in general surgery. *Br J Surg* **90**, 1287-1293
15. Saitz, R., Ghali, W. A., and Moskowitz, M. A. (1997) The impact of alcohol-related diagnoses on pneumonia outcomes. *Arch Intern Med* **157**, 1446-1452
16. Baum, M. K., Rafie, C., Lai, S., Sales, S., Page, J. B., and Campa, A. (2010) Alcohol use accelerates HIV disease progression. *AIDS Res Hum Retroviruses* **26**, 511-518
17. Bhattacharya, R., and Shuhart, M. C. (2003) Hepatitis C and alcohol: interactions, outcomes, and implications. *J Clin Gastroenterol* **36**, 242-252
18. Delgado-Rodriguez, M., Gomez-Ortega, A., Mariscal-Ortiz, M., Palma-Perez, S., and Sillero-Arenas, M. (2003) Alcohol drinking as a predictor of intensive care and hospital mortality in general surgery: a prospective study. *Addiction* **98**, 611-616
19. Jung, M. K., Callaci, J. J., Lauing, K. L., Otis, J. S., Radek, K. A., Jones, M. K., and Kovacs, E. J. (2011) Alcohol exposure and mechanisms of tissue injury and repair. *Alcohol Clin Exp Res* **35**, 392-399

20. Kenneth Murphy, C. W. (2017) *Janeway's Immunobiology*, Garland Science
21. Netea, M. G., Dominguez-Andres, J., Barreiro, L. B., Chavakis, T., Divangahi, M., Fuchs, E., Joosten, L. A. B., van der Meer, J. W. M., Mhlanga, M. M., Mulder, W. J. M., Riksen, N. P., Schlitzer, A., Schultze, J. L., Stabell Benn, C., Sun, J. C., Xavier, R. J., and Latz, E. (2020) Defining trained immunity and its role in health and disease. *Nat Rev Immunol* **20**, 375-388
22. Ifrim, D. C., Quintin, J., Joosten, L. A., Jacobs, C., Jansen, T., Jacobs, L., Gow, N. A., Williams, D. L., van der Meer, J. W., and Netea, M. G. (2014) Trained immunity or tolerance: opposing functional programs induced in human monocytes after engagement of various pattern recognition receptors. *Clin Vaccine Immunol* **21**, 534-545
23. Kar, U. K., and Joosten, L. A. B. (2020) Training the trainable cells of the immune system and beyond. *Nat Immunol* **21**, 115-119
24. Sureshchandra, S., Stull, C., Ligh, B. J. K., Nguyen, S. B., Grant, K. A., and Messaoudi, I. (2019) Chronic heavy drinking drives distinct transcriptional and epigenetic changes in splenic macrophages. *EBioMedicine* **43**, 594-606
25. Sureshchandra, S., Rais, M., Stull, C., Grant, K., and Messaoudi, I. (2016) Transcriptome Profiling Reveals Disruption of Innate Immunity in Chronic Heavy Ethanol Consuming Female Rhesus Macaques. *PLoS One* **11**, e0159295
26. Zisman, D. A., Strieter, R. M., Kunkel, S. L., Tsai, W. C., Wilkowski, J. M., Bucknell, K. A., and Standiford, T. J. (1998) Ethanol feeding impairs innate immunity and alters the expression of Th1- and Th2-phenotype cytokines in murine Klebsiella pneumonia. *Alcohol Clin Exp Res* **22**, 621-627
27. Sibley, D., and Jerrells, T. R. (2000) Alcohol consumption by C57BL/6 mice is associated with depletion of lymphoid cells from the gut-associated lymphoid tissues and altered resistance to oral infections with Salmonella typhimurium. *J Infect Dis* **182**, 482-489
28. Pruett, S. B., Zheng, Q., Fan, R. P., Matthews, K., and Schwab, C. (2004) Ethanol suppresses cytokine responses induced through Toll-like receptors as well as innate resistance to Escherichia coli in a mouse model for binge drinking. *Alcohol* **33**, 147-155
29. Heinz, R., and Waltenbaugh, C. (2007) Ethanol consumption modifies dendritic cell antigen presentation in mice. *Alcohol Clin Exp Res* **31**, 1759-1771
30. Lamas-Paz, A., Hao, F., Nelson, L. J., Vazquez, M. T., Canals, S., Gomez Del Moral, M., Martinez-Naves, E., Nevzorova, Y. A., and Cubero, F. J. (2018) Alcoholic liver disease: Utility of animal models. *World J Gastroenterol* **24**, 5063-5075
31. Liu, S. X., Du, Y. C., and Zeng, T. (2021) A mini-review of the rodent models for alcoholic liver disease: shortcomings, application, and future prospects. *Toxicol Res (Camb)* **10**, 523-530
32. Sengupta, M., Abuirqeba, S., Kameric, A., Cecile-Valfort, A., Chatterjee, A., Griffett, K., Burris, T. P., and Flaveny, C. A. (2021) A two-hit model of alcoholic liver disease that exhibits rapid, severe fibrosis. *PLoS One* **16**, e0249316
33. Stampfer, M. J., Colditz, G. A., Willett, W. C., Manson, J. E., Arky, R. A., Hennekens, C. H., and Speizer, F. E. (1988) A prospective study of moderate alcohol drinking and risk of diabetes in women. *Am J Epidemiol* **128**, 549-558
34. Baker, E. J., Farro, J., Gonzales, S., Helms, C., and Grant, K. A. (2014) Chronic alcohol self-administration in monkeys shows long-term quantity/frequency categorical stability. *Alcohol Clin Exp Res* **38**, 2835-2843
35. Grant, K. A., Leng, X., Green, H. L., Szeliga, K. T., Rogers, L. S., and Gonzales, S. W. (2008) Drinking typography established by scheduled induction predicts chronic heavy drinking in a monkey model of ethanol self-administration. *Alcohol Clin Exp Res* **32**, 1824-1838
36. Green, K. L., Szeliga, K. T., Bowen, C. A., Kautz, M. A., Azarov, A. V., and Grant, K. A. (1999) Comparison of ethanol metabolism in male and female cynomolgus macaques (Macaca fascicularis). *Alcohol Clin Exp Res* **23**, 611-616

37. Dufour, J., Ooms, T. G., Phillippi-Falkenstein, K. M., Penney, T., Doyle, L., Bagby, G. J., Nelson, S., Veazey, R. S., and Bohm, R. P., Jr. (2007) Complications of gastric catheters implanted in rhesus macaques (Macaca mulatta). *J Am Assoc Lab Anim Sci* **46**, 29-34
38. Davies, L. C., Jenkins, S. J., Allen, J. E., and Taylor, P. R. (2013) Tissue-resident macrophages. *Nat Immunol* **14**, 986-995
39. Jenkins, S. J., and Allen, J. E. (2021) The expanding world of tissue-resident macrophages. *Eur J Immunol* **51**, 1882-1896
40. Nobs, S. P., and Kopf, M. (2021) Tissue-resident macrophages: guardians of organ homeostasis. *Trends Immunol* **42**, 495-507
41. Watanabe, S., Alexander, M., Misharin, A. V., and Budinger, G. R. S. (2019) The role of macrophages in the resolution of inflammation. *J Clin Invest* **129**, 2619-2628
42. Okabe, Y. (2018) Molecular control of the identity of tissue-resident macrophages. *Int Immunol* **30**, 485-491
43. Jou, I. M., Lin, C. F., Tsai, K. J., and Wei, S. J. (2013) Macrophage-mediated inflammatory disorders. *Mediators Inflamm* **2013**, 316482
44. Gordon, S., and Pluddemann, A. (2017) Tissue macrophages: heterogeneity and functions. *BMC Biol* **15**, 53
45. Belchamber, K. B. R., and Donnelly, L. E. (2017) Macrophage Dysfunction in Respiratory Disease. *Results Probl Cell Differ* **62**, 299-313
46. Simet, S. M., and Sisson, J. H. (2015) Alcohol's Effects on Lung Health and Immunity. *Alcohol Res* **37**, 199-208
47. Jerrells, T. R., Pavlik, J. A., DeVasure, J., Vidlak, D., Costello, A., Strachota, J. M., and Wyatt, T. A. (2007) Association of chronic alcohol consumption and increased susceptibility to and pathogenic effects of pulmonary infection with respiratory syncytial virus in mice. *Alcohol* **41**, 357-369
48. Samokhvalov, A. V., Irving, H. M., and Rehm, J. (2010) Alcohol consumption as a risk factor for pneumonia: a systematic review and meta-analysis. *Epidemiol Infect* **138**, 1789-1795
49. Lujan, M., Gallego, M., Belmonte, Y., Fontanals, D., Valles, J., Lisboa, T., and Rello, J. (2010) Influence of pneumococcal serotype group on outcome in adults with bacteraemic pneumonia. *Eur Respir J* **36**, 1073-1079
50. Buskin, S. E., Gale, J. L., Weiss, N. S., and Nolan, C. M. (1994) Tuberculosis risk factors in adults in King County, Washington, 1988 through 1990. *Am J Public Health* **84**, 1750-1756
51. Narasimhan, P., Wood, J., Macintyre, C. R., and Mathai, D. (2013) Risk factors for tuberculosis. *Pulm Med* **2013**, 828939
52. Moss, M., Bucher, B., Moore, F. A., Moore, E. E., and Parsons, P. E. (1996) The role of chronic alcohol abuse in the development of acute respiratory distress syndrome in adults. *JAMA* **275**, 50-54
53. Moss, M., and Burnham, E. L. (2003) Chronic alcohol abuse, acute respiratory distress syndrome, and multiple organ dysfunction. *Crit Care Med* **31**, S207-212
54. Simou, E., Leonardi-Bee, J., and Britton, J. (2018) The Effect of Alcohol Consumption on the Risk of ARDS: A Systematic Review and Meta-Analysis. *Chest* **154**, 58-68
55. Karavitis, J., and Kovacs, E. J. (2011) Macrophage phagocytosis: effects of environmental pollutants, alcohol, cigarette smoke, and other external factors. *J Leukoc Biol* **90**, 1065-1078
56. Karavitis, J., Murdoch, E. L., Deburghgraeve, C., Ramirez, L., and Kovacs, E. J. (2012) Ethanol suppresses phagosomal adhesion maturation, Rac activation, and subsequent actin polymerization during FcgammaR-mediated phagocytosis. *Cell Immunol* **274**, 61-71
57. Yeligar, S. M., Harris, F. L., Hart, C. M., and Brown, L. A. (2012) Ethanol induces oxidative stress in alveolar macrophages via upregulation of NADPH oxidases. *J Immunol* **188**, 3648-3657

58. Yeligar, S. M., Harris, F. L., Hart, C. M., and Brown, L. A. (2014) Glutathione attenuates ethanol-induced alveolar macrophage oxidative stress and dysfunction by downregulating NADPH oxidases. *Am J Physiol Lung Cell Mol Physiol* **306**, L429-441
59. Yeligar, S. M., Mehta, A. J., Harris, F. L., Brown, L. A., and Hart, C. M. (2016) Peroxisome Proliferator-Activated Receptor gamma Regulates Chronic Alcohol-Induced Alveolar Macrophage Dysfunction. *Am J Respir Cell Mol Biol* **55**, 35-46
60. Teh, Y. C., Ding, J. L., Ng, L. G., and Chong, S. Z. (2019) Capturing the Fantastic Voyage of Monocytes Through Time and Space. *Front Immunol* **10**, 834
61. Guilliams, M., Mildner, A., and Yona, S. (2018) Developmental and Functional Heterogeneity of Monocytes. *Immunity* **49**, 595-613
62. Hoeksema, M. A., and de Winther, M. P. (2016) Epigenetic Regulation of Monocyte and Macrophage Function. *Antioxid Redox Signal* **25**, 758-774
63. Zakhari, S. (2013) Alcohol metabolism and epigenetics changes. *Alcohol Res* **35**, 6-16
64. Cederbaum, A. I. (2012) Alcohol metabolism. *Clin Liver Dis* **16**, 667-685
65. Norkina, O., Dolganiuc, A., Shapiro, T., Kodys, K., Mandrekar, P., and Szabo, G. (2007) Acute alcohol activates STAT3, AP-1, and Sp-1 transcription factors via the family of Src kinases to promote IL-10 production in human monocytes. *J Leukoc Biol* **82**, 752-762
66. Pang, M., Bala, S., Kodys, K., Catalano, D., and Szabo, G. (2011) Inhibition of TLR8- and TLR4-induced Type I IFN induction by alcohol is different from its effects on inflammatory cytokine production in monocytes. *BMC Immunol* **12**, 55
67. Bala, S., Tang, A., Catalano, D., Petrasek, J., Taha, O., Kodys, K., and Szabo, G. (2012) Induction of Bcl-3 by acute binge alcohol results in toll-like receptor 4/LPS tolerance. *J Leukoc Biol* **92**, 611-620
68. Pruett, S. B., Fan, R., Zheng, Q., and Schwab, C. (2005) Differences in IL-10 and IL-12 production patterns and differences in the effects of acute ethanol treatment on macrophages in vivo and in vitro. *Alcohol* **37**, 1-8
69. Afshar, M., Richards, S., Mann, D., Cross, A., Smith, G. B., Netzer, G., Kovacs, E., and Hasday, J. (2015) Acute immunomodulatory effects of binge alcohol ingestion. *Alcohol* **49**, 57-64
70. Zhang, Z., Bagby, G. J., Stoltz, D., Oliver, P., Schwarzenberger, P. O., and Kolls, J. K. (2001) Prolonged ethanol treatment enhances lipopolysaccharide/phorbol myristate acetate-induced tumor necrosis factor-alpha production in human monocytic cells. *Alcohol Clin Exp Res* **25**, 444-449
71. Mandrekar, P., Bala, S., Catalano, D., Kodys, K., and Szabo, G. (2009) The opposite effects of acute and chronic alcohol on lipopolysaccharide-induced inflammation are linked to IRAK-M in human monocytes. *J Immunol* **183**, 1320-1327
72. Wolf, A. A., Yanez, A., Barman, P. K., and Goodridge, H. S. (2019) The Ontogeny of Monocyte Subsets. *Front Immunol* **10**, 1642
73. Kawamura, S., and Ohteki, T. (2018) Monopoiesis in humans and mice. *Int Immunol* **30**, 503-509
74. Huber, R. (2017) Human monopoiesis is characterized by distinct and stage-specific gene expression profiles. *Br J Haematol* **176**, 341-342
75. Schultze, J. L., Mass, E., and Schlitzer, A. (2019) Emerging Principles in Myelopoiesis at Homeostasis and during Infection and Inflammation. *Immunity* **50**, 288-301
76. Smith, C., Gasparetto, M., Jordan, C., Pollyea, D. A., and Vasiliou, V. (2015) The effects of alcohol and aldehyde dehydrogenases on disorders of hematopoiesis. *Adv Exp Med Biol* **815**, 349-359
77. Yeung, K. Y., Klug, P. P., and Lessin, L. S. (1988) Alcohol-induced vacuolization in bone marrow cells: ultrastructure and mechanism of formation. *Blood Cells* **13**, 487-502
78. Heermans, E. H. (1998) Booze and blood: the effects of acute and chronic alcohol abuse on the hematopoietic system. *Clin Lab Sci* **11**, 229-232

79. Raasch, C. E., Zhang, P., Siggins, R. W., 2nd, LaMotte, L. R., Nelson, S., and Bagby, G. J. (2010) Acute alcohol intoxication impairs the hematopoietic precursor cell response to pneumococcal pneumonia. *Alcohol Clin Exp Res* **34**, 2035-2043
80. Shi, X., Lin, Y. P., Gao, B., and Zhang, P. (2017) Impairment of Hematopoietic Precursor Cell Activation during the Granulopoietic Response to Bacteremia in Mice with Chronic-Plus-Binge Alcohol Administration. *Infect Immun* **85**
81. Sisson, J. H. (1995) Ethanol stimulates apparent nitric oxide-dependent ciliary beat frequency in bovine airway epithelial cells. *Am J Physiol* **268**, L596-600
82. Sisson, J. H., Pavlik, J. A., and Wyatt, T. A. (2009) Alcohol stimulates ciliary motility of isolated airway axonemes through a nitric oxide, cyclase, and cyclic nucleotide-dependent kinase mechanism. *Alcohol Clin Exp Res* **33**, 610-616
83. Wyatt, T. A., and Sisson, J. H. (2001) Chronic ethanol downregulates PKA activation and ciliary beating in bovine bronchial epithelial cells. *Am J Physiol Lung Cell Mol Physiol* **281**, L575-581
84. Guidot, D. M., Modelska, K., Lois, M., Jain, L., Moss, I. M., Pittet, J. F., and Brown, L. A. (2000) Ethanol ingestion via glutathione depletion impairs alveolar epithelial barrier function in rats. *Am J Physiol Lung Cell Mol Physiol* **279**, L127-135
85. Simet, S. M., Wyatt, T. A., DeVasure, J., Yanov, D., Allen-Gipson, D., and Sisson, J. H. (2012) Alcohol increases the permeability of airway epithelial tight junctions in Beas-2B and NHBE cells. *Alcohol Clin Exp Res* **36**, 432-442
86. Rubins, J. B. (2003) Alveolar macrophages: wielding the double-edged sword of inflammation. *Am J Respir Crit Care Med* **167**, 103-104
87. D'Souza, N. B., Nelson, S., Summer, W. R., and Deaciuc, I. V. (1996) Alcohol modulates alveolar macrophage tumor necrosis factor-alpha, superoxide anion, and nitric oxide secretion in the rat. *Alcohol Clin Exp Res* **20**, 156-163
88. Craig, A., Mai, J., Cai, S., and Jeyaseelan, S. (2009) Neutrophil recruitment to the lungs during bacterial pneumonia. *Infect Immun* **77**, 568-575
89. Curry-McCoy, T. V., Venado, A., Guidot, D. M., and Joshi, P. C. (2013) Alcohol ingestion disrupts alveolar epithelial barrier function by activation of macrophage-derived transforming growth factor beta1. *Respir Res* **14**, 39
90. Mehta, A. J., Yeligar, S. M., Elon, L., Brown, L. A., and Guidot, D. M. (2013) Alcoholism causes alveolar macrophage zinc deficiency and immune dysfunction. *Am J Respir Crit Care Med* **188**, 716-723
91. Bhatty, M., Pruett, S. B., Swiatlo, E., and Nanduri, B. (2011) Alcohol abuse and Streptococcus pneumoniae infections: consideration of virulence factors and impaired immune responses. *Alcohol* **45**, 523-539
92. Joshi, P. C., Applewhite, L., Ritzenthaler, J. D., Roman, J., Fernandez, A. L., Eaton, D. C., Brown, L. A., and Guidot, D. M. (2005) Chronic ethanol ingestion in rats decreases granulocyte-macrophage colony-stimulating factor receptor expression and downstream signaling in the alveolar macrophage. *J Immunol* **175**, 6837-6845
93. Boe, D. M., Richens, T. R., Horstmann, S. A., Burnham, E. L., Janssen, W. J., Henson, P. M., Moss, M., and Vandivier, R. W. (2010) Acute and chronic alcohol exposure impair the phagocytosis of apoptotic cells and enhance the pulmonary inflammatory response. *Alcohol Clin Exp Res* **34**, 1723-1732
94. Liang, Y., Harris, F. L., and Brown, L. A. (2014) Alcohol induced mitochondrial oxidative stress and alveolar macrophage dysfunction. *Biomed Res Int* **2014**, 371593
95. Evren, E., Ringqvist, E., and Willinger, T. (2020) Origin and ontogeny of lung macrophages: from mice to humans. *Immunology* **160**, 126-138
96. Kopf, M., Schneider, C., and Nobs, S. P. (2015) The development and function of lung-resident macrophages and dendritic cells. *Nat Immunol* **16**, 36-44

97. Joshi, N., Walter, J. M., and Misharin, A. V. (2018) Alveolar Macrophages. *Cell Immunol* **330**, 86-90
98. Hussell, T., and Bell, T. J. (2014) Alveolar macrophages: plasticity in a tissue-specific context. *Nat Rev Immunol* **14**, 81-93
99. Hetzel, M., Ackermann, M., and Lachmann, N. (2021) Beyond "Big Eaters": The Versatile Role of Alveolar Macrophages in Health and Disease. *Int J Mol Sci* **22**
100. Garbi, N., and Lambrecht, B. N. (2017) Location, function, and ontogeny of pulmonary macrophages during the steady state. *Pflugers Arch* **469**, 561-572
101. Varol, C., Mildner, A., and Jung, S. (2015) Macrophages: development and tissue specialization. *Annu Rev Immunol* **33**, 643-675
102. Tan, S. Y., and Krasnow, M. A. (2016) Developmental origin of lung macrophage diversity. *Development* **143**, 1318-1327
103. Robinson, M. D., McCarthy, D. J., and Smyth, G. K. (2010) edgeR: a Bioconductor package for differential expression analysis of digital gene expression data. *Bioinformatics* **26**, 139-140
104. Zhou, Y., Zhou, B., Pache, L., Chang, M., Khodabakhshi, A. H., Tanaseichuk, O., Benner, C., and Chanda, S. K. (2019) Metascape provides a biologist-oriented resource for the analysis of systems-level datasets. *Nat Commun* **10**, 1523
105. Heinz, S., Benner, C., Spann, N., Bertolino, E., Lin, Y. C., Laslo, P., Cheng, J. X., Murre, C., Singh, H., and Glass, C. K. (2010) Simple combinations of lineage-determining transcription factors prime cis-regulatory elements required for macrophage and B cell identities. *Mol Cell* **38**, 576-589
106. Stuart, T., Butler, A., Hoffman, P., Hafemeister, C., Papalexi, E., Mauck, W. M., 3rd, Hao, Y., Stoeckius, M., Smibert, P., and Satija, R. (2019) Comprehensive Integration of Single-Cell Data. *Cell* **177**, 1888-1902 e1821
107. Street, K., Risso, D., Fletcher, R. B., Das, D., Ngai, J., Yosef, N., Purdom, E., and Dudoit, S. (2018) Slingshot: cell lineage and pseudotime inference for single-cell transcriptomics. *BMC Genomics* **19**, 477
108. Lewis, S. A., Sureshchandra, S., Doratt, B., Jimenez, V. A., Stull, C., Grant, K. A., and Messaoudi, I. (2021) Transcriptional, Epigenetic, and Functional Reprogramming of Monocytes From Non-Human Primates Following Chronic Alcohol Drinking. *Front Immunol* **12**, 724015
109. Bharat, A., Bhorade, S. M., Morales-Nebreda, L., McQuattie-Pimentel, A. C., Soberanes, S., Ridge, K., DeCamp, M. M., Mestan, K. K., Perlman, H., Budinger, G. R., and Misharin, A. V. (2016) Flow Cytometry Reveals Similarities Between Lung Macrophages in Humans and Mice. *Am J Respir Cell Mol Biol* **54**, 147-149
110. Cai, Y., Sugimoto, C., Arainga, M., Alvarez, X., Didier, E. S., and Kuroda, M. J. (2014) In vivo characterization of alveolar and interstitial lung macrophages in rhesus macaques: implications for understanding lung disease in humans. *J Immunol* **192**, 2821-2829
111. Hunegnaw, R., Mushtaq, Z., Enyindah-Asonye, G., Hoang, T., and Robert-Guroff, M. (2019) Alveolar Macrophage Dysfunction and Increased PD-1 Expression During Chronic SIV Infection of Rhesus Macaques. *Front Immunol* **10**, 1537
112. Makita, N., Hizukuri, Y., Yamashiro, K., Murakawa, M., and Hayashi, Y. (2014) IL-10 enhances the phenotype of M2 macrophages induced by IL-4 and confers the ability to increase eosinophil migration. *International Immunology* **27**, 131-141
113. Sureshchandra, S., Raus, A., Jankeel, A., Ligh, B. J. K., Walter, N. A. R., Newman, N., Grant, K. A., and Messaoudi, I. (2019) Dose-dependent effects of chronic alcohol drinking on peripheral immune responses. *Sci Rep* **9**, 7847
114. Keenan, A. B., Torre, D., Lachmann, A., Leong, A. K., Wojciechowicz, M. L., Utti, V., Jagodnik, K. M., Kropiwnicki, E., Wang, Z., and Ma'ayan, A. (2019) ChEA3: transcription factor enrichment analysis by orthogonal omics integration. *Nucleic Acids Res* **47**, W212-W224

115. Baharom, F., Rankin, G., Blomberg, A., and Smed-Sorensen, A. (2017) Human Lung Mononuclear Phagocytes in Health and Disease. *Front Immunol* **8**, 499
116. Patel, S., Homaei, A., El-Seedi, H. R., and Akhtar, N. (2018) Cathepsins: Proteases that are vital for survival but can also be fatal. *Biomed Pharmacother* **105**, 526-532
117. Burnham, E. L., Kovacs, E. J., and Davis, C. S. (2013) Pulmonary cytokine composition differs in the setting of alcohol use disorders and cigarette smoking. *Am J Physiol Lung Cell Mol Physiol* **304**, L873-882
118. O'Halloran, E. B., Curtis, B. J., Afshar, M., Chen, M. M., Kovacs, E. J., and Burnham, E. L. (2016) Alveolar macrophage inflammatory mediator expression is elevated in the setting of alcohol use disorders. *Alcohol* **50**, 43-50
119. Evans, B. J., Haskard, D. O., Sempowksi, G., and Landis, R. C. (2013) Evolution of the Macrophage CD163 Phenotype and Cytokine Profiles in a Human Model of Resolving Inflammation. *Int J Inflam* **2013**, 780502
120. Kwiecień, I., Polubiec-Kownacka, M., Dziedzic, D., Wołosz, D., Rzepecki, P., and Domagała-Kulawik, J. (2019) CD163 and CCR7 as markers for macrophage polarization in lung cancer microenvironment. *Cent Eur J Immunol* **44**, 395-402
121. Xiong, Z., Leme, A. S., Ray, P., Shapiro, S. D., and Lee, J. S. (2011) CX3CR1+ lung mononuclear phagocytes spatially confined to the interstitium produce TNF-alpha and IL-6 and promote cigarette smoke-induced emphysema. *J Immunol* **186**, 3206-3214
122. Aran, D., Looney, A. P., Liu, L., Wu, E., Fong, V., Hsu, A., Chak, S., Naikawadi, R. P., Wolters, P. J., Abate, A. R., Butte, A. J., and Bhattacharya, M. (2019) Reference-based analysis of lung single-cell sequencing reveals a transitional profibrotic macrophage. *Nat Immunol* **20**, 163-172
123. Lewis, S. A., Sureshchandra, S., Doratt, B., Jimenez, V. A., Stull, C., Grant, K. A., and Messaoudi, I. (2021) Transcriptional, epigenetic, and functional reprogramming of blood monocytes in non-human primates following chronic alcohol drinking. *bioRxiv*, 2021.2005.2012.443856
124. Chen, S., Yang, J., Wei, Y., and Wei, X. (2020) Epigenetic regulation of macrophages: from homeostasis maintenance to host defense. *Cell Mol Immunol* **17**, 36-49
125. Saeed, S., Quintin, J., Kerstens, H. H., Rao, N. A., Aghajanirefah, A., Matarese, F., Cheng, S. C., Ratter, J., Berentsen, K., van der Ent, M. A., Sharifi, N., Janssen-Megens, E. M., Ter Huurne, M., Mandoli, A., van Schaik, T., Ng, A., Burden, F., Downes, K., Frontini, M., Kumar, V., Giamarellos-Bourboulis, E. J., Ouwehand, W. H., van der Meer, J. W., Joosten, L. A., Wijmenga, C., Martens, J. H., Xavier, R. J., Logie, C., Netea, M. G., and Stunnenberg, H. G. (2014) Epigenetic programming of monocyte-to-macrophage differentiation and trained innate immunity. *Science* **345**, 1251086
126. Das, S. K., and Vasudevan, D. M. (2007) Alcohol-induced oxidative stress. *Life Sci* **81**, 177-187
127. Harijith, A., Ebenezer, D. L., and Natarajan, V. (2014) Reactive oxygen species at the crossroads of inflammasome and inflammation. *Front Physiol* **5**, 352
128. Morris, N. L., Harris, F. L., Brown, L. A. S., and Yeligar, S. M. (2021) Alcohol induces mitochondrial derangements in alveolar macrophages by upregulating NADPH oxidase 4. *Alcohol* **90**, 27-38
129. Mokdad, A. H., Marks, J. S., Stroup, D. F., and Gerberding, J. L. (2004) Actual causes of death in the United States, 2000. *JAMA* **291**, 1238-1245
130. Maraslioglu, M., Oppermann, E., Blattner, C., Weber, R., Henrich, D., Jobin, C., Schleucher, E., Marzi, I., and Lehnert, M. (2014) Chronic ethanol feeding modulates inflammatory mediators, activation of nuclear factor-kappaB, and responsiveness to endotoxin in murine Kupffer cells and circulating leukocytes. *Mediators Inflamm* **2014**, 808695
131. Coleman, L. G., Jr., and Crews, F. T. (2018) Innate Immune Signaling and Alcohol Use Disorders. *Handb Exp Pharmacol* **248**, 369-396

132. Zhu, X., Coleman, R. A., Alber, C., Ballas, Z. K., Waldschmidt, T. J., Ray, N. B., Krieg, A. M., and Cook, R. T. (2004) Chronic ethanol ingestion by mice increases expression of CD80 and CD86 by activated macrophages. *Alcohol* **32**, 91-100
133. McClain, C. J., and Cohen, D. A. (1989) Increased tumor necrosis factor production by monocytes in alcoholic hepatitis. *Hepatology* **9**, 349-351
134. Bird, G. L., Sheron, N., Goka, A. K., Alexander, G. J., and Williams, R. S. (1990) Increased plasma tumor necrosis factor in severe alcoholic hepatitis. *Ann Intern Med* **112**, 917-920
135. Bishehsari, F., Magno, E., Swanson, G., Desai, V., Voigt, R. M., Forsyth, C. B., and Keshavarzian, A. (2017) Alcohol and Gut-Derived Inflammation. *Alcohol Res* **38**, 163-171
136. Mukherjee, S. (2013) Alcoholism and its effects on the central nervous system. *Curr Neurovasc Res* **10**, 256-262
137. Szabo, G., and Lippai, D. (2014) Converging actions of alcohol on liver and brain immune signaling. *Int Rev Neurobiol* **118**, 359-380
138. Mehta, A. J., and Guidot, D. M. (2017) Alcohol and the Lung. *Alcohol Res* **38**, 243-254
139. Sureshchandra, S., Stull, C., Ligh, B. J. K., Nguyen, S. B., Grant, K. A., and Messaoudi, I. (2019) Chronic heavy drinking drives distinct transcriptional and epigenetic changes in splenic macrophages. *EBioMedicine*
140. Jimenez, V. A., Helms, C. M., Cornea, A., Meshul, C. K., and Grant, K. A. (2015) An ultrastructural analysis of the effects of ethanol self-administration on the hypothalamic paraventricular nucleus in rhesus macaques. *Front Cell Neurosci* **9**, 260
141. Barr, T., Sureshchandra, S., Ruegger, P., Zhang, J., Ma, W., Borneman, J., Grant, K., and Messaoudi, I. (2018) Concurrent gut transcriptome and microbiota profiling following chronic ethanol consumption in nonhuman primates. *Gut Microbes* **9**, 338-356
142. Trapnell, C., Pachter, L., and Salzberg, S. L. (2009) TopHat: discovering splice junctions with RNA-Seq. *Bioinformatics* **25**, 1105-1111
143. Langmead, B., and Salzberg, S. L. (2012) Fast gapped-read alignment with Bowtie 2. *Nat Methods* **9**, 357-359
144. Lawrence, M., Huber, W., Pages, H., Aboyoun, P., Carlson, M., Gentleman, R., Morgan, M. T., and Carey, V. J. (2013) Software for computing and annotating genomic ranges. *PLoS Comput Biol* **9**, e1003118
145. Huang, D. W., Sherman, B. T., Tan, Q., Collins, J. R., Alvord, W. G., Roayaei, J., Stephens, R., Baseler, M. W., Lane, H. C., and Lempicki, R. A. (2007) The DAVID Gene Functional Classification Tool: a novel biological module-centric algorithm to functionally analyze large gene lists. *Genome Biol* **8**, R183
146. Shannon, P., Markiel, A., Ozier, O., Baliga, N. S., Wang, J. T., Ramage, D., Amin, N., Schwikowski, B., and Ideker, T. (2003) Cytoscape: a software environment for integrated models of biomolecular interaction networks. *Genome Res* **13**, 2498-2504
147. Zheng, G. X., Terry, J. M., Belgrader, P., Ryvkin, P., Bent, Z. W., Wilson, R., Ziraldo, S. B., Wheeler, T. D., McDermott, G. P., Zhu, J., Gregory, M. T., Shuga, J., Montesclaros, L., Underwood, J. G., Masquelier, D. A., Nishimura, S. Y., Schnall-Levin, M., Wyatt, P. W., Hindson, C. M., Bharadwaj, R., Wong, A., Ness, K. D., Beppu, L. W., Deeg, H. J., McFarland, C., Loeb, K. R., Valente, W. J., Ericson, N. G., Stevens, E. A., Radich, J. P., Mikkelsen, T. S., Hindson, B. J., and Bielas, J. H. (2017) Massively parallel digital transcriptional profiling of single cells. *Nat Commun* **8**, 14049
148. Butler, A., Hoffman, P., Smibert, P., Papalexi, E., and Satija, R. (2018) Integrating single-cell transcriptomic data across different conditions, technologies, and species. *Nat Biotechnol* **36**, 411-420
149. Corces, M. R., Trevino, A. E., Hamilton, E. G., Greenside, P. G., Sinnott-Armstrong, N. A., Vesuna, S., Satpathy, A. T., Rubin, A. J., Montine, K. S., Wu, B., Kathiria, A., Cho, S. W., Mumbach, M. R., Carter, A. C., Kasowski, M., Orloff, L. A., Risca, V. I., Kundaje, A., Khavari, P.

A., Montine, T. J., Greenleaf, W. J., and Chang, H. Y. (2017) An improved ATAC-seq protocol reduces background and enables interrogation of frozen tissues. *Nat Methods* **14**, 959-962
150. Yu, G., Wang, L. G., and He, Q. Y. (2015) ChIPseeker: an R/Bioconductor package for ChIP peak annotation, comparison and visualization. *Bioinformatics* **31**, 2382-2383
151. Liao, Y., Smyth, G. K., and Shi, W. (2014) featureCounts: an efficient general purpose program for assigning sequence reads to genomic features. *Bioinformatics* **30**, 923-930
152. Fontana, M. F., Baccarella, A., Pancholi, N., Pufall, M. A., Herbert, D. R., and Kim, C. C. (2015) JUNB is a key transcriptional modulator of macrophage activation. *J Immunol* **194**, 177-186
153. Hannemann, N., Cao, S., Eriksson, D., Schnelzer, A., Jordan, J., Eberhardt, M., Schleicher, U., Rech, J., Ramming, A., Uebe, S., Ekici, A., Canete, J. D., Chen, X., Bauerle, T., Vera, J., Bogdan, C., Schett, G., and Bozec, A. (2019) Transcription factor Fra-1 targets arginase-1 to enhance macrophage-mediated inflammation in arthritis. *J Clin Invest* **129**, 2669-2684
154. Sadeghi, K., Wisgrill, L., Wessely, I., Diesner, S. C., Schuller, S., Durr, C., Heinle, A., Sachet, M., Pollak, A., Forster-Waldl, E., and Spittler, A. (2016) GM-CSF Down-Regulates TLR Expression via the Transcription Factor PU.1 in Human Monocytes. *PLoS One* **11**, e0162667
155. Sanchez-Martin, L., Estecha, A., Samaniego, R., Sanchez-Ramon, S., Vega, M. A., and Sanchez-Mateos, P. (2011) The chemokine CXCL12 regulates monocyte-macrophage differentiation and RUNX3 expression. *Blood* **117**, 88-97
156. Zhang, D. E., Hetherington, C. J., Chen, H. M., and Tenen, D. G. (1994) The macrophage transcription factor PU.1 directs tissue-specific expression of the macrophage colony-stimulating factor receptor. *Mol Cell Biol* **14**, 373-381
157. Zhu, X., Meyers, A., Long, D., Ingram, B., Liu, T., Yoza, B. K., Vachharajani, V., and McCall, C. E. (2019) Frontline Science: Monocytes sequentially rewire metabolism and bioenergetics during an acute inflammatory response. *J Leukoc Biol* **105**, 215-228
158. Messaoudi, I., Asquith, M., Engelmann, F., Park, B., Brown, M., Rau, A., Shaw, J., and Grant, K. A. (2013) Moderate alcohol consumption enhances vaccine-induced responses in rhesus macaques. *Vaccine* **32**, 54-61
159. Kawasaki, T., and Kawai, T. (2014) Toll-like receptor signaling pathways. *Front Immunol* **5**, 461
160. Huber, R., Bikker, R., Welz, B., Christmann, M., and Brand, K. (2017) TNF Tolerance in Monocytes and Macrophages: Characteristics and Molecular Mechanisms. *J Immunol Res* **2017**, 9570129
161. Seeley, J. J., and Ghosh, S. (2017) Molecular mechanisms of innate memory and tolerance to LPS. *J Leukoc Biol* **101**, 107-119
162. Widdrington, J. D., Gomez-Duran, A., Pyle, A., Ruchaud-Sparagano, M. H., Scott, J., Baudouin, S. V., Rostron, A. J., Lovat, P. E., Chinnery, P. F., and Simpson, A. J. (2018) Exposure of Monocytic Cells to Lipopolysaccharide Induces Coordinated Endotoxin Tolerance, Mitochondrial Biogenesis, Mitophagy, and Antioxidant Defenses. *Front Immunol* **9**, 2217
163. Netea, M. G., Quintin, J., and van der Meer, J. W. (2011) Trained immunity: a memory for innate host defense. *Cell Host Microbe* **9**, 355-361
164. de Diego, I., Muller-Eigner, A., and Peleg, S. (2020) The Brain Epigenome Goes Drunk: Alcohol Consumption Alters Histone Acetylation and Transcriptome. *Trends Biochem Sci* **45**, 93-95
165. Mews, P., Egervari, G., Nativio, R., Sidoli, S., Donahue, G., Lombroso, S. I., Alexander, D. C., Riesche, S. L., Heller, E. A., Nestler, E. J., Garcia, B. A., and Berger, S. L. (2019) Alcohol metabolism contributes to brain histone acetylation. *Nature* **574**, 717-721
166. Di Rocco, G., Baldari, S., Pani, G., and Toietta, G. (2019) Stem cells under the influence of alcohol: effects of ethanol consumption on stem/progenitor cells. *Cell Mol Life Sci* **76**, 231-244

167. (WHO), W. H. O. (2018) Global status report on alcohol and health 2018. World Health Organization.
168. Yanez, A., Coetzee, S. G., Olsson, A., Muench, D. E., Berman, B. P., Hazelett, D. J., Salomonis, N., Grimes, H. L., and Goodridge, H. S. (2017) Granulocyte-Monocyte Progenitors and Monocyte-Dendritic Cell Progenitors Independently Produce Functionally Distinct Monocytes. *Immunity* **47**, 890-902 e894
169. Kawamura, S., Onai, N., Miya, F., Sato, T., Tsunoda, T., Kurabayashi, K., Yotsumoto, S., Kuroda, S., Takenaka, K., Akashi, K., and Ohteki, T. (2017) Identification of a Human Clonogenic Progenitor with Strict Monocyte Differentiation Potential: A Counterpart of Mouse cMoPs. *Immunity* **46**, 835-848 e834
170. Lee, J., Breton, G., Oliveira, T. Y., Zhou, Y. J., Aljoufi, A., Puhr, S., Cameron, M. J., Sekaly, R. P., Nussenzweig, M. C., and Liu, K. (2015) Restricted dendritic cell and monocyte progenitors in human cord blood and bone marrow. *J Exp Med* **212**, 385-399
171. Takizawa, H., Boettcher, S., and Manz, M. G. (2012) Demand-adapted regulation of early hematopoiesis in infection and inflammation. *Blood* **119**, 2991-3002
172. Baldridge, M. T., King, K. Y., and Goodell, M. A. (2011) Inflammatory signals regulate hematopoietic stem cells. *Trends Immunol* **32**, 57-65
173. Shi, X., DeLucia, A. L., Bao, J., and Zhang, P. (2019) Alcohol abuse and disorder of granulopoiesis. *Pharmacol Ther* **198**, 206-219
174. Panasiuk, A., and Kemona, A. (2001) Bone marrow failure and hematological abnormalities in alcoholic liver cirrhosis. *Rocz Akad Med Bialymst* **46**, 100-105
175. Liu, Y. K. (1980) Effects of alcohol on granulocytes and lymphocytes. *Semin Hematol* **17**, 130-136
176. Latvala, J., Parkkila, S., and Niemela, O. (2004) Excess alcohol consumption is common in patients with cytopenia: studies in blood and bone marrow cells. *Alcohol Clin Exp Res* **28**, 619-624
177. Ballard, H. S. (1997) The hematological complications of alcoholism. *Alcohol Health Res World* **21**, 42-52
178. Varlamov, O., Bucher, M., Myatt, L., Newman, N., and Grant, K. A. (2020) Daily Ethanol Drinking Followed by an Abstinence Period Impairs Bone Marrow Niche and Mitochondrial Function of Hematopoietic Stem/Progenitor Cells in Rhesus Macaques. *Alcohol Clin Exp Res* **44**, 1088-1098
179. Siggins, R. W., Molina, P., Zhang, P., Bagby, G. J., Nelson, S., Dufour, J., LeCapitaine, N. J., Walsh, C., and Welsh, D. A. (2014) Dysregulation of myelopoiesis by chronic alcohol administration during early SIV infection of rhesus macaques. *Alcohol Clin Exp Res* **38**, 1993-2000
180. Hafemeister, C., and Satija, R. (2019) Normalization and variance stabilization of single-cell RNA-seq data using regularized negative binomial regression. *Genome Biol* **20**, 296
181. Hay, S. B., Ferchen, K., Chetal, K., Grimes, H. L., and Salomonis, N. (2018) The Human Cell Atlas bone marrow single-cell interactive web portal. *Exp Hematol* **68**, 51-61
182. Chong, S. Z., Evrard, M., Devi, S., Chen, J., Lim, J. Y., See, P., Zhang, Y., Adrover, J. M., Lee, B., Tan, L., Li, J. L., Liong, K. H., Phua, C., Balachander, A., Boey, A., Liebl, D., Tan, S. M., Chan, J. K., Balabanian, K., Harris, J. E., Bianchini, M., Weber, C., Duchene, J., Lum, J., Poidinger, M., Chen, Q., Renia, L., Wang, C. I., Larbi, A., Randolph, G. J., Weninger, W., Looney, M. R., Krummel, M. F., Biswas, S. K., Ginhoux, F., Hidalgo, A., Bachelerie, F., and Ng, L. G. (2016) CXCR4 identifies transitional bone marrow premonocytes that replenish the mature monocyte pool for peripheral responses. *J Exp Med* **213**, 2293-2314
183. Tsou, C. L., Peters, W., Si, Y., Slaymaker, S., Aslanian, A. M., Weisberg, S. P., Mack, M., and Charo, I. F. (2007) Critical roles for CCR2 and MCP-3 in monocyte mobilization from bone marrow and recruitment to inflammatory sites. *J Clin Invest* **117**, 902-909

184. Winkler, I. G., Sims, N. A., Pettit, A. R., Barbier, V., Nowlan, B., Helwani, F., Poulton, I. J., van Rooijen, N., Alexander, K. A., Raggatt, L. J., and Levesque, J. P. (2010) Bone marrow macrophages maintain hematopoietic stem cell (HSC) niches and their depletion mobilizes HSCs. *Blood* **116**, 4815-4828
185. Mitroulis, I., Kalafati, L., Bornhauser, M., Hajishengallis, G., and Chavakis, T. (2020) Regulation of the Bone Marrow Niche by Inflammation. *Front Immunol* **11**, 1540
186. Garaycoechea, J. I., Crossan, G. P., Langevin, F., Daly, M., Arends, M. J., and Patel, K. J. (2012) Genotoxic consequences of endogenous aldehydes on mouse haematopoietic stem cell function. *Nature* **489**, 571-575